Intention Reading and Sensory Substitution for Improving Walking Quality of Paraplegia Wearing An Exoskeleton

Mengze LI

Acknowledgements

I am very lucky that many people gave me great help and encouragement during my PhD. Here, I want to express my sincere gratitude and high respect.

First of all, I would like to thank Professor Fukuda Toshio and Professor Hasegawa Yasuhisa. Professor Fukuda brought me to Nagoya University and introduced me to Professor Hasegawa. So I had the opportunity to study and research in this world-renowned University, to grow and finish my doctoral thesis. Professor Hasegawa accepted me as his student and led me to the door of exoskeleton research. Exoskeleton research was a completely new field for me. When I didn't have any results yet, Professor Hasegawa brought me to the IROS conference, and helped me made a presentation. What I learned in the conference is also a valuable enlightenment for my own research. In addition, He gave me great care and encouragement as well as academic guidance during my PhD.

I would like to thank the current and past members of Hasegawa Lab: Professor Aoyama gave me great help in determining research topics and revising papers. Senior Pei Di let me stayed in his home when I had no place to live. Professor Jian Huang in Huazhong University of Science and Technology and Professor Chaoyang Shi in Tianjin University helped me when I submit my third journal paper. Itadera-sensei helped me to prepare the paper files for this thesis. Noel taught me how to understand and write code for algorithm. Zhaofan Yuan and Xufeng Wang who were my group members have contributed to my achievements today. Yaonan Zhu helped me revise my paper and cared about my health when I am sick. Rubens played guitar for me when I'm in a bad mood.

I would like to thank the Otsuka Toshimi Scholarship foundation for their support for my one-year study and living expenses. Thanks to JSPS KAKENHI, I can have funds to complete my research projects.

Furthermore, I want to thank my family and friends, especially my parents. During the more than two years of postponement of graduation, I often lost my confidence. Since I still need the support from my family at the age that a person should be independent, I was full of self-blame and guilt. My parents gave me great understanding and encouragement

so that I can finish my studies.

Finally, thank you to everyone who gave me help and care. For all the people who once entered my life, I'm sorry if I forgot to mention your name, but you should know that you are also an important person who helped me through this process.

April 2020
Mengze LI

Contents

List of Figures

List of Tables

Chapter 1

Introduction

1.1 Background

1.1.1 Paralysis statistic

In 2013, the Christopher & Dana Reeve Foundation in the United States surveyed the prevalence of paralysis in the United States, as shown in Figure 1.1, and released shocking statistics.

The researchers conducted a detailed investigation including more than 70,000 families in United States. More than 30 paralysis and statistics experts from the Centers for Disease Control and Prevention (CDC), leading universities and medical centers helped design the parameters of this investigation.

This investigation shows that approximately 5.4 million people in the United States suffer from paralysis. On average, nearly 1 in 50 people suffer from paralysis. This population accounts for a large proportion of the US population, and is nearly 40% higher than previous estimates.

This investigation reveals some important findings: paralysis is much broader than people think. About 1.7% of the US population reported that they live in some form of paralysis. The study defined it as a disease of the central nervous system. According to the statistics of this research, the upper or lower limbs cannot move or cannot move. The two main causes of paralysis are stroke and spinal cord injury, accounting for more than 50% of the total. The family income of the paralysis is low. In terms of employment, the employment rate of paralyzed persons is 15.5%, while that of non-disabled persons is 63.1%. Besides, 41.8% of the paralysis said they could not work.

Spinal cord injury and its related diseases not only affect the patients, but also impose a

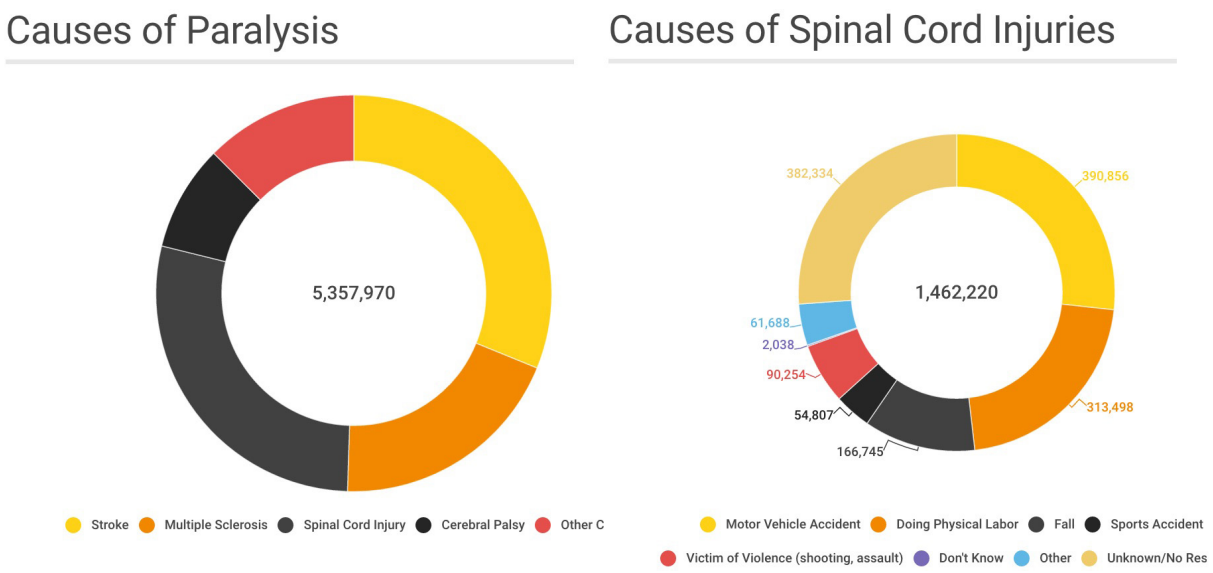

Figure 1.1: Paralysis statistics of US in 2013 [1].

great burden on the patient's family, friends, relatives, medical care workers and employers.

As the number of people suffering from paralysis and spinal cord injury increases day by day, the cost of treatment associated with it is also staggering. Billions of dollars are spent on paralysis and spinal cord injury each year.

Paralyzed patients often cannot afford these costs, and health insurance is not sufficient to cover the complex complications associated with these diseases. Like many patients with chronic diseases, they often rely on the care of friends or family members to maintain a normal life.

To ensure that millions of paralyzed patients can get the medical care, quality work and education they need, they need to find effective treatments and therapies and more support. The development and research of the exoskeleton has brought hope to the medical treatment and rehabilitation of patients with paralysis.

1.1.2 Paralysis and spinal cord injury

Paralysis is the loss of function of one or more body muscles. There may also be a loss of sensation in the affected area. The main causes of paralysis include injury to the nervous system, especially spinal cord injury, stroke, trauma, polio, Parkinson's disease, amyotrophic lateral sclerosis (ALS), botulism, and multiple sclerosis.

Paralysis can be divided into 4 types: (1) Monoplegia, which usually refers to the loss of motor and sensory function of one arm or one leg. (2) Hemiplegia, which usually refers

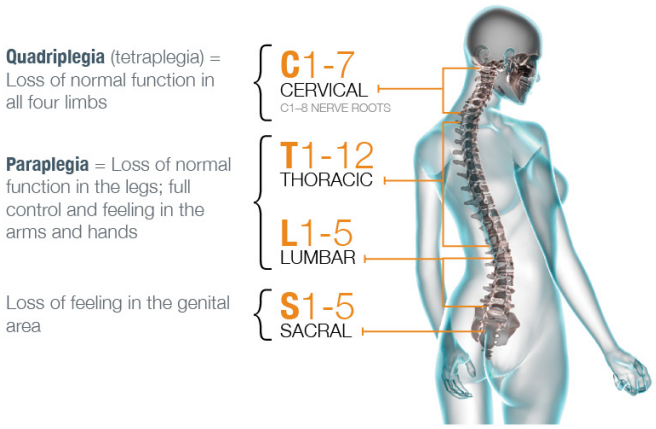

Figure 1.2: Levels of spinal cord injury [2].

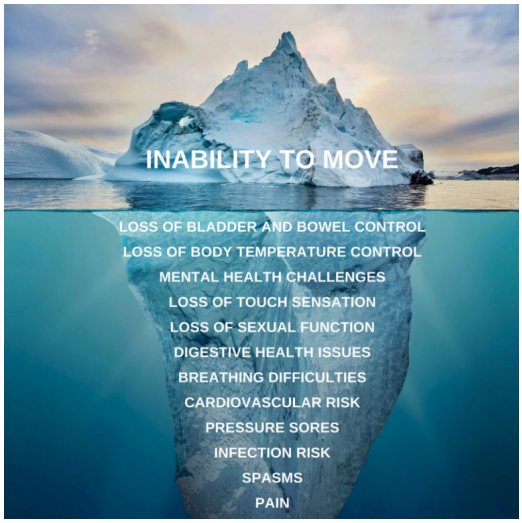

Figure 1.3: SCI iceberg [2].

to the loss of motor and sensory function of one arm and one leg on the same side of the body. (3) Paraplegia, which usually refers to the loss of motor and sensory function of both legs. (4) Quadriplegia, or tetraplegia, which usually refers to the loss of motor and sensory function both of arms and both of legs.

Figure 1.2 shows that the paralysis caused by spinal injury, it can be generally divided into two types according to the injury level: quadriplegia and paraplegia. The paraplegia lost the motor and sensory function of the lower body but has full control and feeling in the arms and hands. Figure 1.3 is known as the SCI iceberg where the loss of motor and sensory function is just the tip of the iceberg, the paralysis patient also suffers from mental health challenges, breathing difficulties, cardiovascular risk, pressure sores and so on. Spinal injuries are often caused by daily activities, such as vehicle accidents, sporting injuries, falls and others. That makes the spinal cord injury difficult to predict and entirely prevent.

1.1.3 Paraplegic patient

As mentioned above, paraplegic is a form of paralysis; it refers to the person who lost the motor and sensory of the lower body. Paraplegic patients are unable to move their legs and feel no sensations there, making it difficult for them to walk on their own. Paralysis or paraplegic is mainly caused by spinal cord injury, stroke and cerebral palsy. Among them, paralysis caused by spinal cord injury is the most common. After spinal cord injury, motor and sensory signals are difficult to transmit between the brain and limbs through

the central nervous system.

When an able-bodied person performs a voluntary movement, such as upright walking, the brain sends contraction commands along the efferent nerves to skeletal muscles. Upon receiving the contraction commands, the skeletal muscles drive the body joints to flex or extend. Simultaneously, the kinesthetic receptors distributed in the muscles and tendons release nerve impulses. Those nerve impulses are transferred along the afferent nerves to the cerebral cortex to generate kinesthesia. Employing loop establishment, the human voluntarily controls their body movements and perceives the continuously updated status of their body dynamics. However, paraplegic patients cannot perform voluntary movements of their lower limbs and suffer from loss of the function of somatic senses due to the impairment of efferent and afferent nerves. Consequently, they suffer from long-term complications, such as muscular dystrophy, poor blood circulation, bone loss, etc. Fortunately, powered exoskeletons have been developed to enhance the load capacity and increase the exercise durability of SCI patients as a way to help them restore their physical functionality through rehabilitation [3, 4], or to help paraplegic patients walk again [5].

1.2 Powered exoskeleton

The powered exoskeleton, also known as a powered suit or a powered armor, is a machine that consists of an exoskeleton-like frame and can be worn by people. The powered exoskeleton is driven by a system of electric motors, pneumatics, lever or hydraulics for providing extra energy that enhances strength and endurance for limb movement. The exoskeleton is designed to provide back support, sense user movement and send signals to motors that manage gears. The exoskeleton supports shoulders, waist, and thighs and assists in the movement to lift and hold heavy weights while reducing the pressure on back.

The powered exoskeleton, classified according to the application domain, it can be divided into rehabilitation, daily life assistance, power augmentation, impairment evaluation, and resistance exercises. The powered exoskeleton, classified according to the applied segment, it can be divided into upper limb exoskeleton, lower limb exoskeleton and whole body exoskeleton. The powered exoskeleton, classified according to the actuation, it can be divided into electric actuation, hydraulic actuation, pneumatic actuation and hybrid method. The powered exoskeleton, classified according to the power transmission, it can be divided into gear drives, cable drives, belt drives, screw drives and hybrid method.

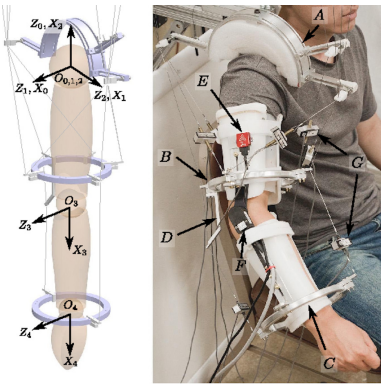

Figure 1.4: CAREX [6].

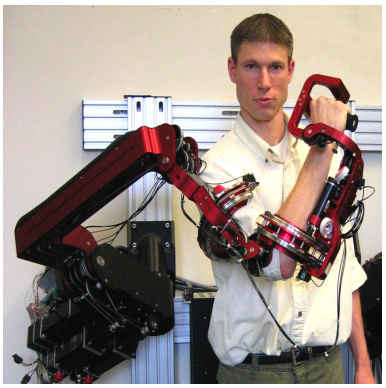

Figure 1.5: EXO-7 [7].

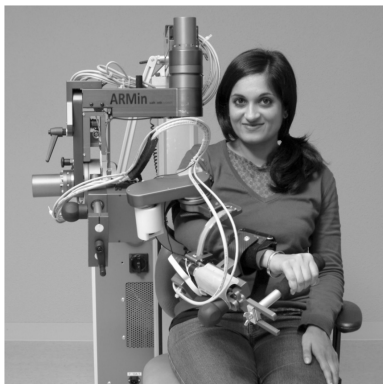

Figure 1.6: ARMin [8–12].

1.2.1 Upper limb exoskeleton

Figure 1.4 shows CAREX. CAREX [6] is designed for neurorehabilitation. This exoskeleton consists of three cuffs, which act on the shoulder, upper arm and forearm, respectively. The cuff link directly corresponds to the limbs and joints of the human body, this makes the alignment of the rotation axis of the human joint and the joint axis of the robot no longer a problem. Wearing this exoskeleton does not constrain the inherent freedom of the human arm. In addition, this exoskeleton is lighter than conventional exoskeletons.

Figure 1.5 shows EXO-7. EXO-7 [7] uses an anthropomorphic design approach. This exoskeleton allows shoulder internal and external rotation and forearm supination and pronation The connection between the exoskeleton and the person is non-closed, which allows the user to easily wear and remove the exoskeleton.

Figure 1.6 shows ARMin-III. ARMin-III [8–12] is an exoskeleton for rehabilitation. It has three active joints on the shoulder and one active joint on the elbow, and one passive joint on the forearm and one passive joint on wrist. The three active joints on the shoulder correspond to shoulder flexion and extension, shoulder abduction and adduction, and shoulder internal and external rotation, respectively. The active joint on the elbow corresponds to elbow flexion and extension. The passive joint on the forearm corresponds to forearm inward and outward rotation. The passive joints of the wrist correspond to wrist flexion and extension. ARMin III is an exoskeleton with adjustable size to suit different patients.

Figure 1.7 shows L-EXOS. L-EXOS [13] exoskeleton robots is used for tactile interaction in virtual environments. The robot supports shoulder rotation and elbow bending and extension. With open round components instead of closed round bearings, users can easily insert and remove arms without having to insert the arms through a closed loop structure..

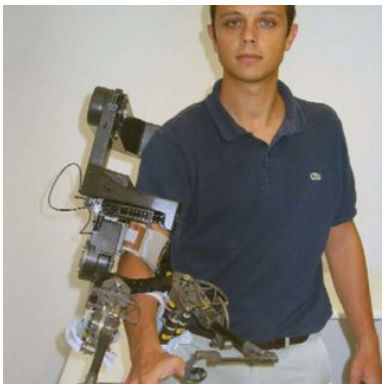

Figure 1.7: L-EXOS [13].

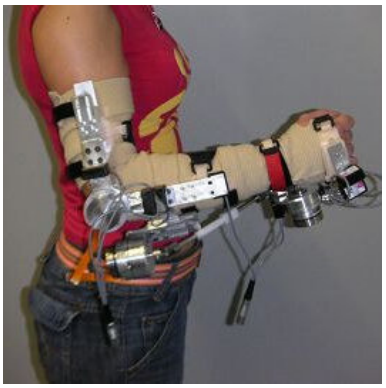

Figure 1.8: WOTAS [14,15].

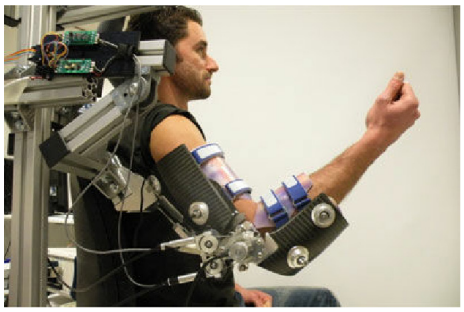

Figure 1.9: NEUROExos [16, 17].

Figure 1.8 shows WOTAS. WOTAS [14,15] is an exoskeleton with a function of measuring and suppressing tremor. Motors drive the exoskeleton on the wrist and elbow. WOTAS supports elbow flexion and extension, forearm external rotation and internal rotation, and wrist bending and extension. The sensor system of WOTAS consists of encoders and chip-type gyroscopes, which can continuously measure tremor force. WOTAS applies compensation force on the arm to suppress tremors.

Figure 1.9 shows NEUROExos. NEUROExos [16, 17] is a biologically inspired elbow exoskeleton used for rehabilitation. NEUROExos uses a double-shell link structure to reduce the presure between skin and exoskeleton. In addition, NEUROExos uses a mechanism to automatically align the rotation axis of the drive joint with the human joint. It is worth noting that the position and stiffness of the actuated joint can be adjusted individually to suit the control requirements. NEUROExos uses hydraulic pressure to power the joints through wire ropes and Bowden cables, ensuring kinematic compatibility between the human and exoskeleton without overloading the patient's joints..

1.2.2 Lower limb exoskeleton

Figure 1.10 shows BLEEX. BLEEX [18,19] is the first exoskeleton to provide load-carrying. It adopts anthropomorphic design, and the three segments of the exoskeleton leg correspond to users thigh, shank and feet, respectively. BLEEX has seven degrees of freedom on each leg: Where the active joints correspond to hip flexion and extension, hip abduction and adduction, knee flexion and extension as well as ankle dorsiflexion and plantar flexion. Where the passive joints correspond to hip intra and extra rotation, ankle inversion and eversion as well as ankle abduction and adduction. The ankle joint is equipped with springs to realize passive mechanical impedances.

Figure 1.10: BLEEX [18, 19].

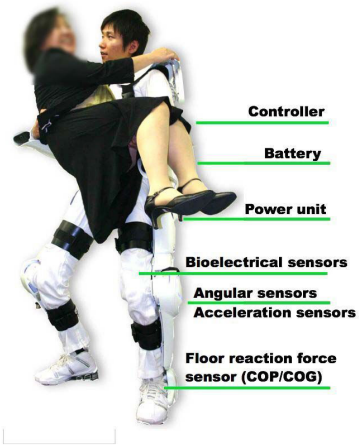

Figure 1.11: HAL [20, 21].

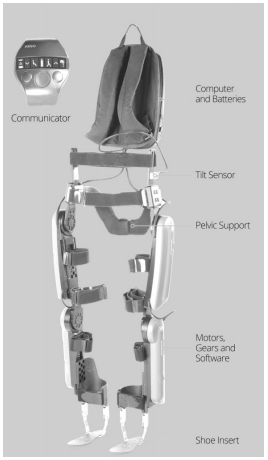

Figure 1.12: ReWalk [22, 23].

Figure 1.11 shows HAL. HAL [20, 21] can be used to enhance the joint strength of healthy people, or to help patients with gait disorders move and perform daily life work like healthy individuals. There are three types of HAL: orthosis, whole body exoskeleton and single leg exoskeleton. HAL mainly provide assistance on the sagittal plane motion, which is flexion and extension as well as dorsiflexion and plantar flexion. When the goal of HAL is to help people with walking difficulties, the hip and knee joints actively provide kinematic support, while the ankle joint passively provides kinematic support through springs. HAL divides the walking into swing phase and support phase. Its walking trajectory is pre-recorded from able-bodied subjects and relies on ground reaction forces and torso angles to control the user's walking phase.

Figure 1.12 shows ReWalk. ReWalk [22, 23] is a powered exoskeleton that helps person with nervous system injury to walk without outside help [7]. Its hip and knee joints follow a predetermined trajectory. The user can use the controller at the wrist pad to start the robot's standing, sitting, and walking assistance. By using the body tilt sensor, the user can achieve a gradual transition in gait while walking. ReWalk has been tested with twelve SCI patients. Through eight weeks of training, the patients can independently walk at a speed of 0.03 m/s to 0.45 m/s in a substantially symmetrical gait for 5-10 minutes.

Figure 1.13 shows eLEGS. The eLEGS [24] exoskeleton supports patients with lower extremities paralysis who have difficulty in sitting, standing and walking. The hips and knees flexion and extension are actuated. The ankles dorsiflexion and plantar flexion are passively actuated by springs. The exoskeleton uses a finite state machine as the control center and divides the walking cycle into four stages: left swing stage, left double

support stage, right swing stage and right double support stage. Moving canes triggers the transition between swing and stance and shifting body weight as well as heel strike detection.

Figure 1.14 shows soft Exosuit. Soft Exosuit [25, 26] is not strictly an exoskeleton. The suit does not include any rigid material, but consists of soft webbing. The suit uses a gear motor to pull a cable connected to the ankle joint as a driver. When the cable is activated, the tension on the clothes increases, which will raise the heel and increase the torque that acts on the hip and knee joints to help walking. Preliminary test results show that the torque provided by Exosuit for hips and ankles is about 18% of the torque required for normal people to walk.

Figure 1.15 shows IHMC Mobility Assist Exoskeleton [27, 28]. IHMC has three active joints, which are used for hip abduction and adduction, hip flexion and extension, and knee flexion and extension. IHMC has two passive joints, which are used for hip rotation and ankle dorsiflexion and plantar flexion. IHMC adopts user-friendly design concept and uses series elastic actuators (SEA) as the driving device [29], which enables accurate and stable force control. IHMC has three working modes, of which zero assistance mode is used to record the joint trajectory from able-bodied people during walking and rehabilitation mode is used to assist the patient to walk. During walking, the patient needs to adjust the torso inclination to match the swing of the leg.

1.3 Related researches

1.3.1 Assistive strategy of exoskeleton

Tingfang Yan *et al.* classify the assistive strategy of exoskeletons into Predefined gait trajectory control, Model-based control, Adaptive oscillators-based control, Fuzzy control, Predefined action based on gait pattern and Hybrid assistive strategy [30]. The following introduces some assistive strategy that is often mentioned and used in rehabilitation or have a tendency to use for paralysis.

Model-based control

Y. Yu *et al.* Proposed a bilateral hip exoskeleton [31], as shown in Figure 1.16. The bilateral hip exoskeleton is arranged around user's hip joint in a parallel kinematic chain form. It consisting of 6 degrees of freedom, with three universal-prism-shaped series connected on each side. This exoskeleton uses pseudo-compliant control [32]. Based on the force

Figure 1.13: eLEGS [24].

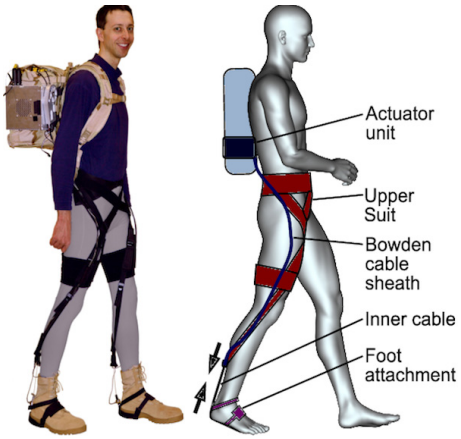

Figure 1.14: Exosuit [25, 26].

Figure 1.15: IHMC [27, 28].

information provided by a force sensor that detects the force between the human thigh and the exoskeleton, pseudo-compliant control can predict the expected end effector velocity, and then use the predicted end effector velocity to determine the exporting velocity of the actuator. Among them, the velocity relationship between the active joint and the end effector is determined using direct kinematic Jacobian. They have validated this controller in simulation and experiment; the result shows the error is small.

G. Aguirre-Ollinger *et al*. proposed a one DOF exoskeleton [33], as shown in Figure 1.17. They proposed a control approach based on the admittance model between user and exoskeleton, which performs inertial compensation on the movement of the exoskeleton according to the joint angular acceleration. This method adds a feedback loop to the controller. The angular acceleration is obtained from this loop with a low-pass filter. The inertial compensation torque is obtained by multiplying this angular acceleration by a negative gain. The controller after inertia compensation can achieve two effects: reduce the energy consumption of walking and increase the agility of the user's leg movements.

RoboKnee [34], as shown in Figure 1.18, is a knee exoskeleton used to assist people carrying heavy objects up and down stairs and squats. RoboKnee consists of thighs and shank two parts, which are connected by linear SEA joints at the knee joint. RoboKnee's control algorithm is not complicated. The algorithm assumes that the ground reaction force is completely vertical and can be obtained by a force sensor on the sole plate. A position sensor on the knee joint used to obtain the knee axis. The actuation torque can be obtained by multiplying the ground reaction force and the moment arm. In RoboKnee's evaluation experiment, the subjects repeated the squat motion with and without wearing RoboKnee.

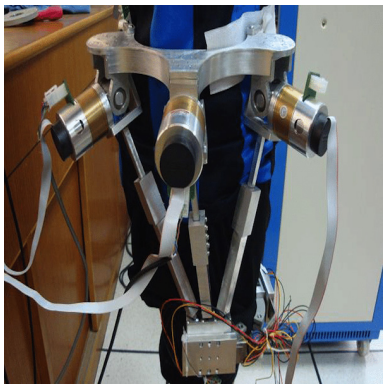

Figure 1.16: Parallel mechanism exoskeleton [31].

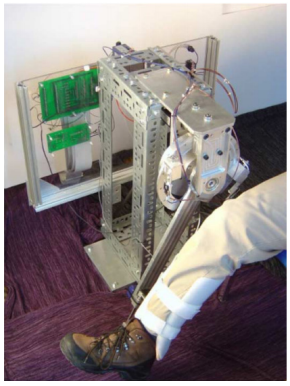

Figure 1.17: 1-Dof lower-limb exoskeleton [33].

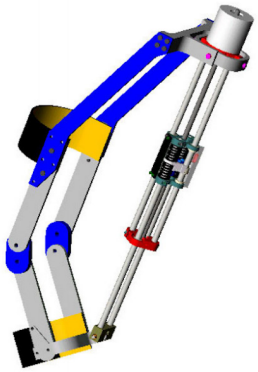

Figure 1.18: Roboknee [34].

The experimental results prove that Roboknee exoskeleton enhances the wearer's strength and endurance.

Polinkovsky *et al.* proposed a prototype of a active ankle-foot orthosis (AFO) called IPEC AFO [35], as shown in Figure 1.19. Most AFOs are passive assist devices that lock the ankle or restrict the movement of the ankle. However, IPEC AFO integrates SEA with a standard passive AFO to form an active assistive device. The assistive effect mainly comes from the pre-tensioned spring. The spring is connected to the linear slider through a moment arm. The spring releases elastic potential energy as an assistive thrust. IPEC AFO uses a kinematic model to predict the required torque, which is equal to the spring force times the displacement of the slider.

Andrej gams *et al.* proposed a Robotic knee exoskeleton [36], as shown in Figure 1.20. It is a prototype knee exoskeleton that acts on the legs to provide support for users. Each exoskeleton leg has an active rotation joint at the knee and a passive ball joint at the ankle. In their study, they investigated the effect of a prototype knee exoskeleton on the metabolism of healthy users during regular squat exercises. They compared the effects of three different control methods: gravity compensation control method, position control method and oscillator-based control method. The gravity compensation controller calculates the required torque by introducing a simplified knee joint model. The torque is directly related to the extension angle of the joint. The position controller calculates the required torque according to the difference between the current joint angle and the target joint angle. The oscillator-based controller synchronize its frequency with the knee joint, and then calculates the torque according to the simplified model. Seven healthy subjects wore exoskeletons for a five-minute squat exercise. Experimental results show that the metabolism under the three control methods is reduced, and the oscillator-based control

Figure 1.19: Ankle-foot orthosis [35].

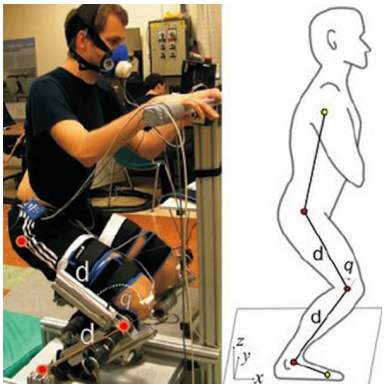

Figure 1.20: Robotic knee exoskeleton [36].

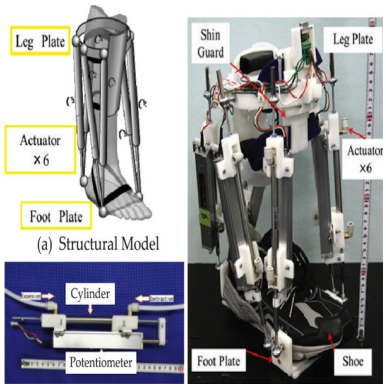

Figure 1.21: Platform-type ankle-foot assistive device [37].

method has the best effect on reducing metabolism.

Takemura *et al*. proposed a Wearable Stewart Platform-Type AFO [37], as shown in Figure 1.21. This AFO is a wearable and portable walking assistance device for rehabilitation. This AFO has a foot plate and a leg ring, the foot plate is used to fix the sole of the foot, and the leg ring is used to cover the lower leg. From top to bottom, six linear actuators are connected between the leg ring and the foot plate. Two linear actuators are installed behind the heel, and the other four linear actuators are installed on both sides of the foot. This AFO uses forward and reverse robot kinematics models to calculate the torque for the ankle joint.

Predefined gait pattern

B. G. Do Nascimento *et al*. proposed a hip orthosis [38], as shown in Figure 1.22 to help step transition during walking. This orthosis is composed of a pelvic support and thigh support, and is connected by a hinged beam at the hip joint. There are two artificial pneumatic muscles on the front of the orthosis, which connect the thigh support and the pelvic support to provide torque. This orthosis uses a threshold to control muscle contraction and release. When the hip joint reaches the minimum, the pneumatic muscles contract. When the hip joint reaches its maximum, the pneumatic muscles release. This orthosis was tested with polio patients. Clinical trials have shown that this orthosis can help patients complete the step transition during walking.

C. Lewis *et al*. proposed a hip exoskeleton [39], as shown in Figure 1.23. The exoskeleton is composed of a pelvis and a thigh cuff, powered by a pair of pneumatic muscles

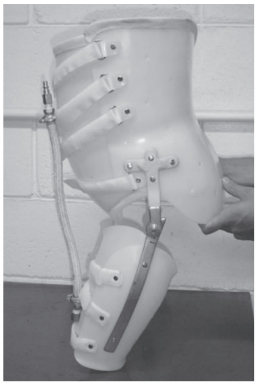

Figure 1.22: Pneumatically actuated hip orthosis [38].

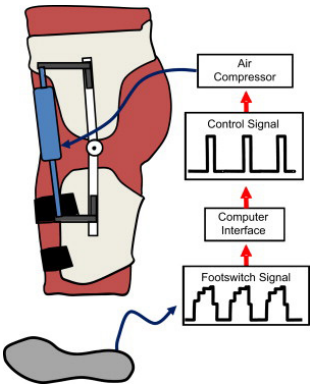

Figure 1.23: Robotic hip exoskeleton: invariant hip moment pattern [39].

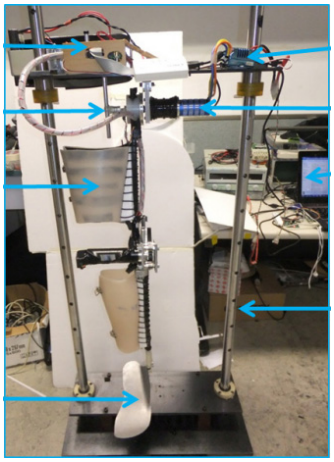

Figure 1.24: Knee orthosis: Hip-knee control for gait assistance [40].

outside the cuff. This exoskeleton applied a foot-switch control approach that based on a predetermined portion of the gait cycle. Each gait cycle starts from heel strike, the hip exoskeleton provides 30% to 50% hip flexion assistance.

Lai *et al*. proposed a powered knee orthosis (KPO) [40], as shown in Figure 1.24. This KPO was developed for the elderly and patients with walking disorder to regain a regular gait. This KPO analyzes the gait model and provides support for walking by controlling the motion of the knee joint. It assumes that the trajectory of the hip joint and knee joint are similar during the swing phase. The target knee joint angle can be estimated from the measured hip joint angle. During the standing phase, the knee joint is fully stretched. The subjects wearing the KPO and walking on a treadmill verified this control strategy.

In article [41], a knee extension device, as shown in Figure 1.25, for transition between standing-up and sitting-down has been introduced. The device relies on the torque provided by the spring and pneumatic actuator to help the wearer complete the transition. During sitting-down process, the user sinks and compresses the spring. In order to make the sitting-down process smooth, the pneumatic actuator provides a small resistance torque to mitigate the impact caused by inertia and body sink. After sitting-down, both pneumatic actuator and spring are locked. During standing-up process, the spring is released, the pre-stored spring potential energy is converted into thrust, and the actuator is activated to provide knee extension torque to help the user stand.

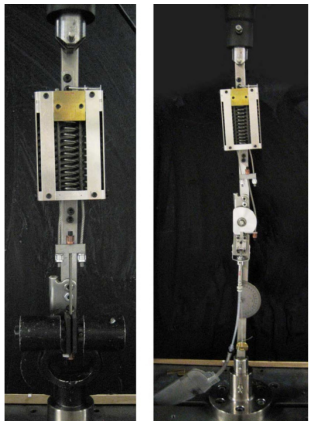

Figure 1.25: Evaluation of orthotic knee-extension assist [41].

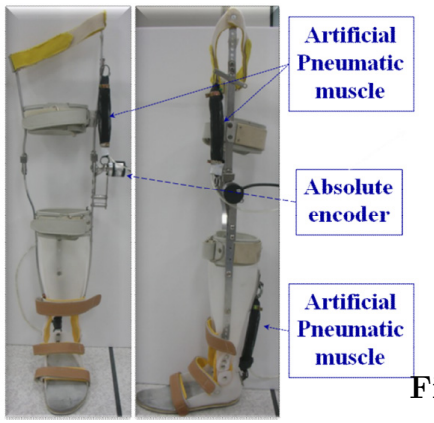

Figure 1.26: Knee orthosis using muscular force feedback [42].

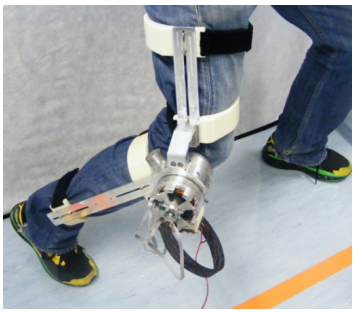

Figure 1.27: Knee exoskeleton for motion augmentation based on tele- impedance [43].

Muscle stiffness control

K. Kim *et al*. proposed a knee orthosis [42], as shown in Figure 1.26. This orthosis has a cuff for fixing the thigh, a cuff for fixing the shank, and a foot plate for fixing the sole of the foot. Two metal frames on the left and right sides of the leg connect the cuff-cuff-plate structure. An encoder is installed at the knee joint. Two pneumatic artificial muscles are installed on the outside of the thigh and on the back of shank. The position of the pneumatic artificial muscle corresponds to the position of the active muscle of the knee joint, which provides assistance for the joint extension. The orthosis uses the muscle stiffness control strategies. The Muscle Stiffness Sensor (MSFS) consists of a pressure sensor and a jig used to quantify muscle tension. Based on the muscle tension, the user's knee extension intention is inferred, and the contraction of the pneumatic muscle is controlled.

N. Karavas *et al*. proposed a knee orthosis [43], as shown in Figure 1.27. The exoskeleton is composed of cuffs of thighs and shanks. A frame connects the two cuffs with an actuating joint. The control strategy of the exoskeleton is increasing the actuation joint stiffness to enhance the user's knee strength. The study uses EMG to speculate on user intentions and determine joint stiffness. In order to improve control accuracy, a detailed musculoskeletal model was introduced to determine the nonlinear relationship between muscle activity and joint torque. A healthy subject demonstrated the effectiveness of the knee exoskeleton and its supporting strategies through a standing experiment.

EMG&EEG-based control

The Technical University of Berlin has proposed a unilateral knee exoskeleton (TUPLEE) [44]. A linear actuator actuates the knee flexion and extension. TUPLEE controller uses a biomechanical model, which combines the results of different biomechanics and biomedical research teams, and is reasonably simplified. The controller using EMG signals to calculate the torque of knee joint basing on the biomechanical model. Because the controller relies heavily on EMG activity, this control method is only suitable for able-bodied people or subjects with residual voluntary muscle control.

Kiguchi *et al.* developed a hierarchical neuro-fuzzy controller that analyze the EMG signals the to understand the user's intention to move robotic exoskeleton [45]. Yin *et al.* also used a neirao-fuzzy controller with EMG signal, joint angle, and interaction force as input to speculate the stroke patient's intention of walking [46]. Nam *et al.* designed a GOM-Face interface that detects tongue, eye and teeth movements for persons with motor disability to perform daily task and tested the interface on a user controlled humanoid robot to perform pre-defined tasks [47]. McMullen *et al.* combined EEG to initialing the motion and eye tracking to control the end effector for the use of a robotic upper limb prosthetic [48]. Ma *et al.* proposed a EOG/EEG hybrid human machine interface for motor disability persons, in which the EOG is for low-level control and the EEG is for menu-selection [49].

1.3.2 Sensory substitution

The four commonly used sensory substitution are visual stimulation, auditory stimulation, electro-tactile stimulation and vibration stimulation [50], Electro-tactile and vibro-tictile stimulation have been investigated the most effective and the most common used among the four modalities. For example, the cell phone use vibration to remind the user that a new message or a phone call is coming. However, only a few researches applied sensory substitution for the information feedback of the lower limb exoskeleton or protheses control system.

Pamungkas *et al.* proposed a electro-tactile feedback system to enhance virtual reality [51]. The electro-tactile feedback system consists of a glove and Transcutaneous Electro Neural Stimulation (TENS) unit. The electrode is mounted on the back of a glove. The wearer wears the glove and control a hand for touching task in a virtual environment, he/she receives the stimulus on the wrist when the hand is in contact with an object. Four tactile sensations were regulated according to four different textures by changing the

frequency and intensity of the stimuli.

Daniel S. Pamungkas *et al.* used electro-tactile feedback for tele-operation of a robot arm [52–54]. In this research, obstacle avoidance experiment and peg in hole experiment are conducted to test the effect of electro-tactile feedback. The subject wears gloves to control the movement and grasping of the robotic arm, and at the same time receives the status information of the robotic gripper transmitted by electrical stimulation feedback. These information includes the closed state of the gripper and its distance from the environment. These information is obtained by the pressure sensor on the griper and the distance sensor at the front of the robotic arm.

There are several researched attempts to compensate for impaired afferent nerves: Arai *et al.* applied electrical stimulation as pressure feedback when an amputee controlled a prosthesis to touch an object [55, 56]. Fan *et al.* developed a pneumatic cuff to indicate the contact force of the soles for lower-limb prostheses users [57]. Cheng *et al.* mapped the vibration and complex hand configurations for prosthesis users [58, 59]. Tsukahara *et al.* use a display screen to indicate the angle of the joint and the change in CoG for rehabilitation training [60].

1.4 Remaining problem and research purpose

It can be seen from the above related research that the the powered exoskeleton has achieved certain achievements in hardware design and control algorithms. However, there are still deficiencies that can be classified into three aspects: assistive strategies, sensory feedback, as well as balance keeping during walking.

For assistive strategy: Although there are a large number of assistive strategies, there are still few suitable for people with lower limb paralysis. For the paraplegia has lost motor function due to spinal cord injury, the control method based on muscle stiffness is not applicable. Also, since there are no control signals transmitted from the brain to the lower limbs, the control method based on EMG is not applicable. Exoskeletons specifically designed for paraplegic patient usually use a pre-programed walking trajectory to assist the walking. Note that all that exoskeletons only allow the user to control the timing of initialing and stopping the walking. Exoskeletons drive the patients leg to track a pre-programmed walking trajectory, rather than walking in accordance with the patients intention of detailed leg movement. Although walking support systems without the gait control are effective on a flat terrain, gait control is required when the users want to land their foot at a specified position or climb stairs. It is desirable for exoskeleton wearers to be

able to voluntarily control their leg movements, such as stride and foot height. Therefore, we propose an easy-to-use walking control interface that mounted on the handle of a cane that used for keeping balance. The use of the interface does not affect the use of cane and does not increase the burden of user.

For sensory feedback: Currently the exoskeleton does not provide any form of sensory feedback. However, feedback signals from exoskeletons are important when the exoskeletons are applied to paraplegic patients because the patients typically look down at their lower limbs to confirm their position owing to the loss of lower-limb sensation. Therefore, we applied electro-tactile stimulation feedback to make up for this deficiency. The electro-tactile feedback has four advantages: First, it can be made into a thin electrode substrate, compact and miniaturized. Secondly, it has the potential to present high-resolution haptic information and can be used to present shapes and trajectories. Third, because it can be miniaturized, it is easy to carry and wear, and it does not increase the burden on the wearer when wearing. Fourth, electrical stimulation can be naturally used for multi-touch sensing.

For balance keeping: The powered lower limb exoskeleton does not participate in balance control, patients often rely on canes to maintain balance during walking. The balance in walking is extremely important. If the exoskeleton can participate in balance control, it will greatly reduce the burden on patients. We propose a trajectory optimization method based on a zero moment point and a nonlinear inverted pendulum model to improve walking stability.

In view of the above existing problems, the purpose of this research is to improve the powered lower-limb exoskeleton system from gait control, sensory feedback and walking stability aspects, so that the paraplegic patient wearing exoskeleton can walk better. This improvement can be achieved by compensating the impaired efferent and afferent nerves of the paraplegic patient using a wearable walking control interface with electric stimulation for the upper limbs, so that the patient can voluntarily control the gait and receive the the walking state while walking. A paraplegic patient wears an exoskeleton to walk, and holds a pair of crutches to maintain their balance. The walking intention is conveyed from the brain to the lower extremities using the finger as a medium. The lower limb movements are also transmitted back to the brain with the finger as a medium to form a closed loop of control and feedback. We propose a wearable walking control interface that enables a user to voluntarily control their gait instead of following a programmed walking trajectory. We also propose the use of electric stimulation that informs the user regarding their foot position [50], meaning the exoskeleton user does not have to rely on vision to check the

spatial location and posture of their legs. For safety concerns, we developed a walking robot to simulate a paraplegic patient wearing an exoskeleton [61]. The robot simulates a paraplegic patient wearing an exoskeleton and holding a pair of crutches to keep their balance. The robot is used in this study to implement the proposed control interface and electric stimulation feedback device instead of a real patient for safety concerns.

1.5 Thesis Organization

The organization of this thesis is shown in figure 1.28. In chapter 1, We introduced the statistics and life status of people with lower limb paralysis. This leads to the importance of exoskeletons that supports the paralysis fro walking. This chapter focuses on the powered lower limb exoskeleton and related research, which leads to the existing problems and explains the purpose of this work.

In chapter 2, we introduce the waking control interface with electro-tactile feedback. The interface can be used to control the step length during walking, and the electrical stimulation feedback conveys the position information of the foot to the user. The proposed interface was verified through a robot walking experiment, in which the subject control a robot to walking using the interface while receiving the electro-tactile feedback.

In chapter 3, we introduce the second generation of the waking control interface with electro-tactile feedback. Difference from the interface in chapter two, the interface introduced in chapter 3 does not only control stride of walking, but also the foot height. The design of the interface fits with the palm, and the user controls the movement trajectory of the lower limbs while walking with index finger. In order to adapt to the 2 degrees of freedom control, electrical stimulation divides the motion space of the foot into three planes by changing the stimulation interval, and feeds back position information to the user. Through experiments, we investigated the human skin's ability to feel electrical stimulation and the accuracy of controlling the foot position with the help of electrical stimulation.

In chapter 4, we first introduce a method for generating lower limb movement trajectories through human walking synergy. According to the zero moment point and the nonlinear inverted pendulum model, we modify the generated trajectory. The modified trajectory is close to people's walking habits, and increases the balance of walking.

In chapter 5, we summarize the contributions of the control interface, electrical stimulation feedback and gait modification based on the ZMP algorithm. Then analyzed the shortcomings in the current work, and finally discussed the future research direction,

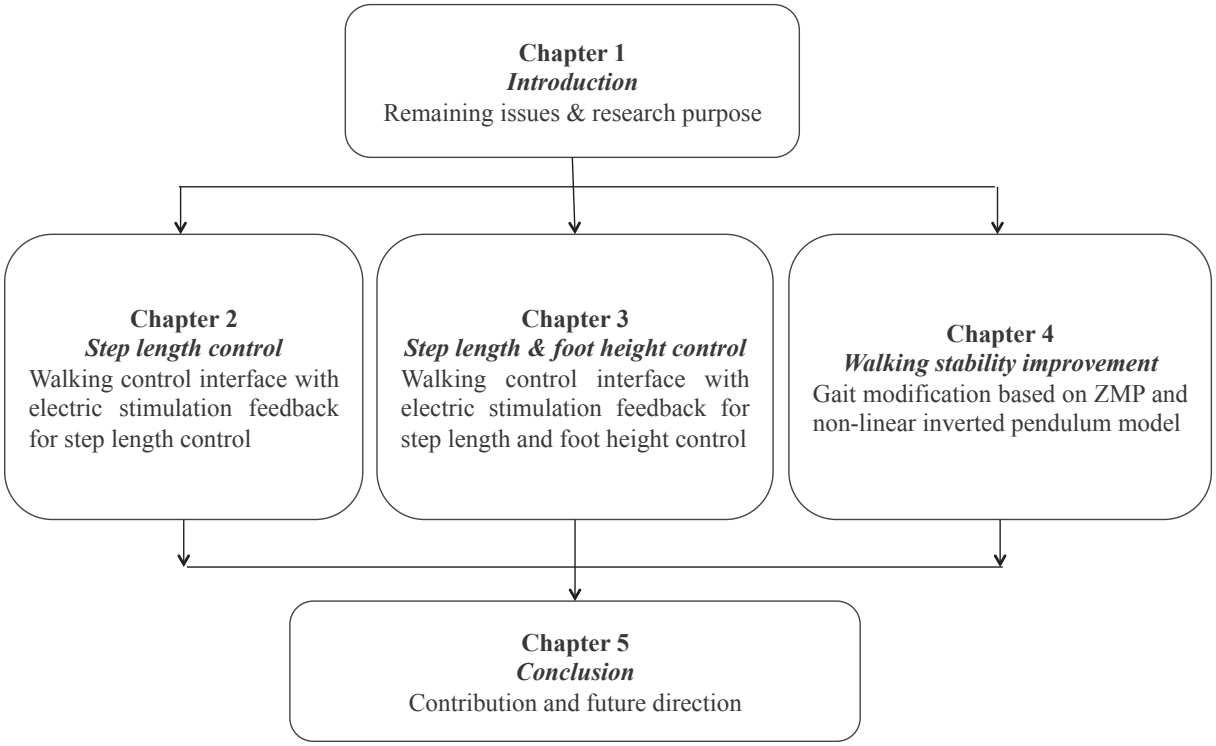

Figure 1.28: Thesis Organization.

Chapter 2

Walking control interface with electro-tactile feedback for stride control

This chapter introduces the wearable walking control interface and an electric stimulation pattern for a paraplegic patient wearing a powered exoskeleton. The wearable interface allows the paraplegic patient to voluntarily control their own stride while they walk with the aid of an exoskeleton. The electric stimulation equipment provides the wearer with tactile feedback regarding their foot position. For security reasons, a humanoid walking robot was used to replace the patient during the experiments. The robot simulates a paraplegic patient that walks with the aid of an exoskeleton. A series of robot walking experiments were implemented to validate the feasibility of the wearable walking control interface and to evaluate the contribution of the electric stimulation pattern. The experiments to confirm the effectiveness of electric stimulation were implemented under three feedback conditions: visual feedback, electric stimulation feedback, and no feedback. The experimental results indicate that the wearable walking controller enables an operator to voluntarily control their stride while walking. The experimental results also indicate that the electric stimulation provides helpful information to assist in walking at nearly the same level as visual feedback.

2.1 Concept of interface with feedback

When an able-bodied person performs a voluntary movement, such as upright walking, the brain sends contraction commands along the efferent nerves to skeletal muscles. Upon receiving the contraction commands, the skeletal muscles drive the body joints to flex or

extend. Simultaneously, the kinesthetic receptors distributed in the muscles and tendons release nerve impulses. Those nerve impulses are transferred along the afferent nerves to the cerebral cortex to generate kinesthesia. By means of loop establishment, the human voluntarily controls their body movements and perceives the continuously updated status of their body dynamics. However, paraplegic patients cannot perform voluntary movements of their lower limbs and suffer from loss of the function of somatic senses due to the impairment of efferent and afferent nerves. Consequently, they suffer from long-term complications, such as muscular dystrophy, poor blood circulation, bone loss, etc.

As one solution, the proposition and the application of exoskeletons enable paraplegic patients to regain their walking ability. These exoskeletons, such as BLEEX [62], HAL [63], Ekso [64], Rewalk [5], Rex [65] etc., physically support the wearer's weight and augment the wearer's joint torque. Exoskeletons have undeniably enhanced the efficiency of rehabilitation therapy for paraplegic patients and lightened the workload for nurses and physicians [4, 66–68]. Furthermore, EEG and EMG approaches have been extensively studied to assist the physically-challenged person to control exoskeletons and prostheses [69–73]. EEG signals can be analyzed as a high-level command. However, it is difficult to extract action details, such as joint angular trajectory, from EEG signals. EMG signals are difficult to capture from paraplegic patient's lower limbs due to spinal cord injuries.

In rehabilitation, the powered exoskeleton drives the patient's leg to track a preprogramed walking trajectory, rather than walking in accordance with the patient's intentions. In the case of daily life, we consider that walking habits and gait characteristics are individualized. It is desirable for exoskeleton wearers to be able to voluntarily control their leg movements, such as stride length and foot height. Additionally, the patients rely on their vision to check leg posture and leg spatial locations due to the lack of lower limb sensation.

In order to compensate for impaired efferent nerves, researchers detect variations in posture and contact force in order to speculate user movement intentions. Tsukahara *et al*. [3] [74] detected the timing of leg swing based on the center of ground reaction force and adjusted walking speed based on the walking velocity of a paraplegic patient wearing a HAL suit. The Ekso bionics system [64] takes a step when the exoskeleton senses that the posture of the user has reached a balance point. The REX bionics system [65] uses a joy stick to control flat surface walking and stair climbing. However, exoskeleton wearers are still unable to control stride length and step height while walking.

In order to compensate for impaired afferent nerves, researchers apply tactile feedback systems to represent the posture of the extremities [57, 75, 76]. Kawanishi *et al*. [60] de-

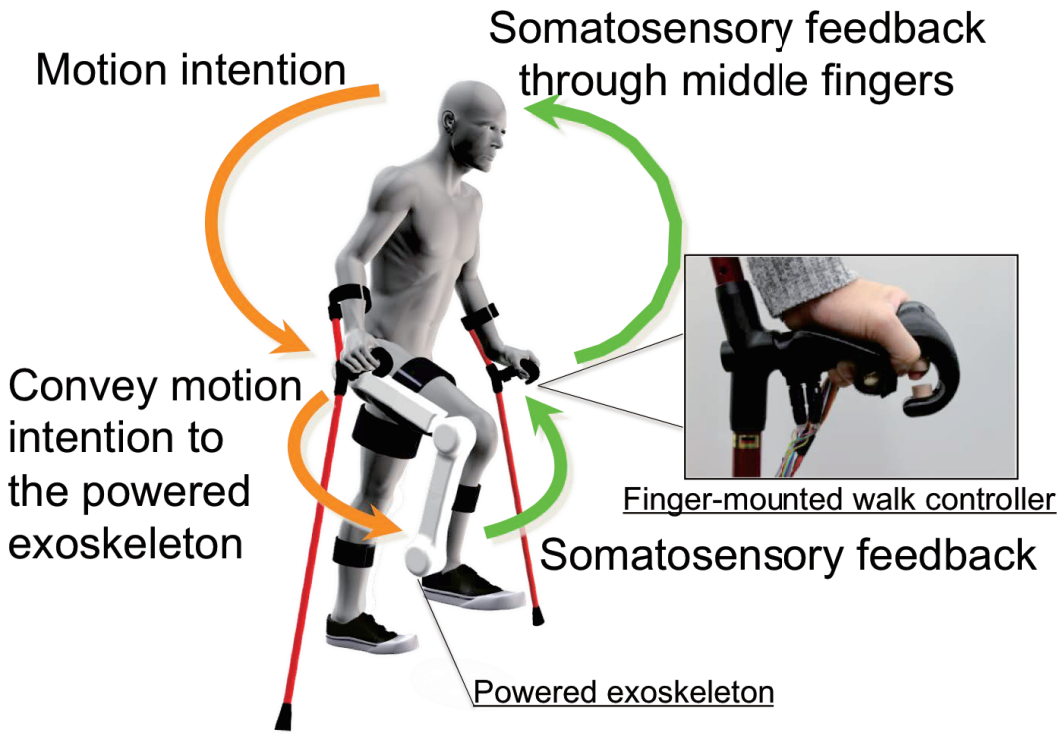

Figure 2.1: Concept of powered exoskeleton with a wearable walking controller.

veloped a visual feedback system to display joint angles and center of mass of the patient in rehabilitation. Arai *et al.* [55, 56] applied electrical stimulation as pressure feedback when an amputee controlled a prosthesis to touch an object. Cheng *et al.* [58, 59] applied vibration to represent complex hand configurations for prosthesis users. All of these studies use sensory substitutions to suggest the posture of the limbs. Among them, we prefer the tactile feedback method, because it does require visual concentration. This allows vision to be used to detect changes in the environment and ensure the safety of walking.

The purpose of this research is to compensate for the impaired efferent and afferent nerves of the paraplegic patient by using a wearable walking controller and an electric stimulation device for the upper limbs. The concept of our research is shown in Figure 2.1. We propose a wearable walking interface that enables a user to voluntarily control their gait instead of following a programmed walking trajectory. We also propose an electric stimulation pattern that conveys foot position to the wearer, meaning the wearer does not have to rely on vision to check the spatial location and posture of their legs. For safety concerns, we use a walking robot to replace a patient for preliminary experimental implementation. The robot simulates a paraplegic patient wearing an exoskeleton and holding a pair of crutches to keep their balance.

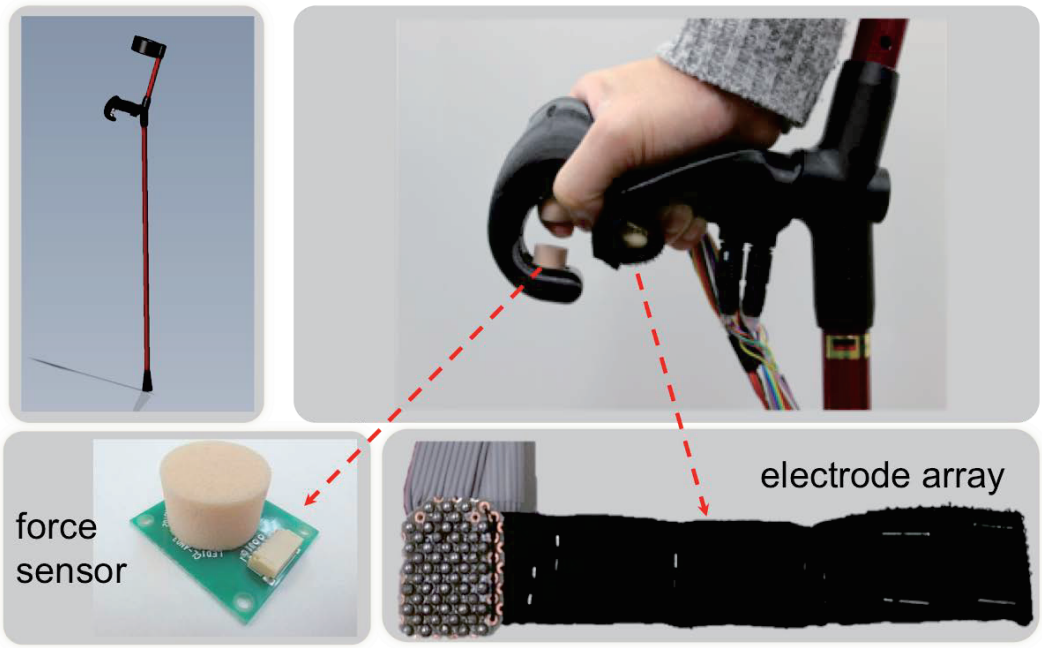

Figure 2.2: Configuration of the wearable walking controller and the electrode array.

2.2 Wearable walking controller and cooperative control

2.2.1 Finger-mounted walking controller

Figure 2.2 shows the wearable walking controller. It is a pair of crutches that each have two force sensors mounted on the front of the gripper. A paw sensor is used in this research. The sensor measures pressure by using an infrared ray to detect the deformation of the sensor's sponge. When the force reaches 0.715 Newton, the sensor begins to deform. When the force reaches 2.558 Newton, the deformation reaches its maximum. Paraplegic patients are able to apply sufficient pressure to operate the interface. The upper sensor is used for flexion and the lower sensor is used for extension. An operator inserts the distal phalanx of their index finger between two pressure sensors. The operator pushes on these sensors to control hip joint torque in order to express their walking intentions. The specifications of the wearable walking controller are listed in Table 2.1.

Table 2.1: Specifications of the developed finger-mounted walking controller.

Size	89 × 140 × 54[mm]
Weight	0.162 [kg] × 2
Sensor	RT corporation PAW sensor × 2

2.2.2 Gait control

When a paraplegic patient wears an exoskeleton and walks, they can use the wearable walking controller to intentionally control their gait. The forces acting on the upper and lower sensors correspond to the extension and flexion torques of the exoskeleton's hip joints, respectively. An exoskeleton wearer directly controls the torque of the hip joints by pressing on the upper or lower sensors of the wearable walking controller. When the wearer presses the upper sensor, the exoskeleton drives the leg swing forward. When the wearer presses the lower sensor, the exoskeleton drives the leg swing backward. In this manner, the finger's muscle tensions are directly transmitted to hip joint's muscle tensions through the wearable walking controller.

Because we used a robot instead of a patient to conduct experiments, the following explanation uses the robot as the controlled object. The forces acting on the upper and lower sensors correspond to the extension and flexion torques of the robot's hip joint. The flexion torque τ_{flx} and extension torque τ_{ext} are calculated as:

$$\tau_{flx} = k_1 p_{lower}, \tag{2.1}$$

$$\tau_{ext} = k_2 p_{upper}, \tag{2.2}$$

where k_1 and k_2 are proportional gains, and p_{lower} and p_{upper} are the outputs of the lower and upper force sensors. The proportional gains were determined empirically through trails to make sure that the hip joint can generate enough torque to reach the limitations of the rotation range. In the case of a patient wearing an exoskeleton, the proportional gains should be decided individually based on patients body size and weight. The operator cannot press the upper and lower sensor at the same time. At any moment, one of the outputs should be zero. The difference between the flexion torque and the extension torque is the total torque of the hip joint, τ_{hip}, which is calculated as follows:

$$\tau_{hip} = \tau_{flx} - \tau_{ext}. \tag{2.3}$$

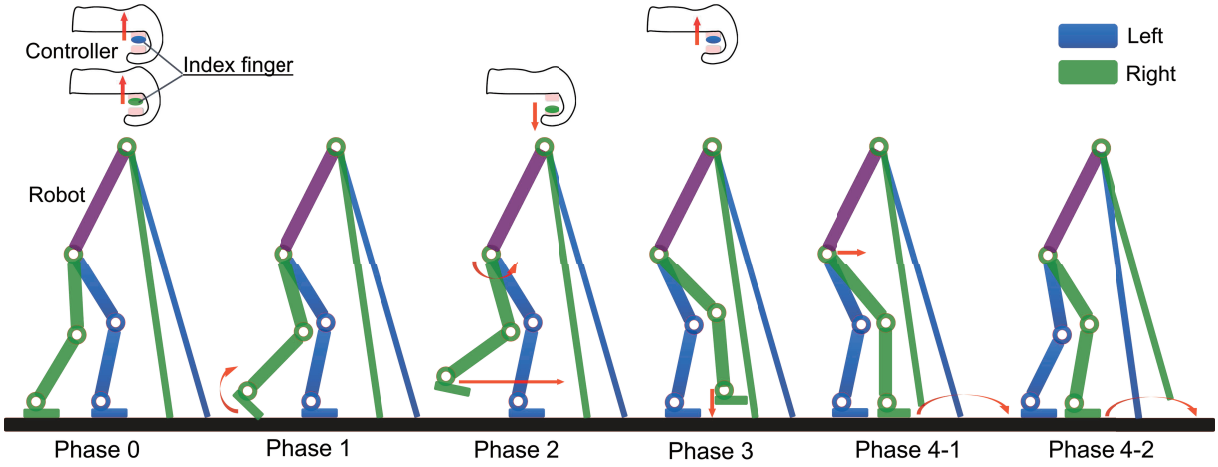

Figure 2.3: Robot walking sequence and operations of the wearable walking controller during cooperative control.

2.2.3 Cooperative control

The conventional wearable powered exoskeleton completely controls the actions of each step. The patients legs are driven by the exoskeleton. Our method gives the operator the authority to control leg swing motion. The operator controls the swing leg for the next step and the exoskeleton controls the stance leg for weight support. The patient decides both the foot landing timing and position. The exoskeleton then plants the foot on the ground and lifts the other foot for the next step. In this manner, each step is completed through cooperation between the exoskeleton and the patient. In the case of a patient wearing an exoskeleton, the patient controls the crutches for balance. In this research, a control program automatically controls the crutches to ensure that the center of gravity provides proper balance and the operator concentrates on stride control.

The walking process is divided into the four phases depicted in Figure 2.3: Phase zero is a preparation phase. Phase one, phase three, and phase four are performed automatically. Phase two is controlled by the operator through the wearable walking controller. The robot walks by repeating phases one through four.

Phase 0:

The robot assumes a prepared posture.

This phase ends when the operator presses both hands against the upper sensors at the same time as hard as they can.

Phase 1:

The robot transfers its center of mass to the side of the stance leg and lifts its rear leg to

assume a pre-swing posture.
This action finishes in 1.2 seconds.
Phase 2:
The operator voluntarily controls the rear leg to swing forward. During control, the operator adjusts the leg's position by adjusting the hip joint's torque with the wearable walking controller on the side of the swing leg.
This phase ends when the operator presses the upper sensor on the side of the stance leg as hard as they can.
Phase 3:
The foot of the swing leg is planted on the floor.
This action finishes in 0.4 seconds.
Phase 4:
The robot swings the crutch on the side of the planted foot forward by the same distance as the stride taken in phase 2, then plants it on the floor.
These actions require 1.2 seconds.

2.3 Electric stimulation for somatosensory feedback

Conventionally, exoskeleton wearers rely on their vision to confirm leg posture, leg spatial location, and ground contact while walking, because somatosensory feedback such as tendon length and the weight distribution of the sole is lost due to afferent nerve injuries. However, vision should be used for observing the surrounding environment to ensure safety. Therefore, this study applies electric stimulation to the fingers to inform the patient regarding foot position. Electric stimulation in the form of a 50Hz pulse stimulates the tactile corpuscles, also known as the Meissner corpuscles, in the skin as a cue. This electric stimulation enables the operator to control their stride without visual confirmation.

Figure 2.4 shows the electrode array. The electric stimulation device has an electrode array with a bandage, as shown in Figure 2.2. The bandage mounts the electrode array on the user's finger. This device is lightweight and portable. Therefore, using the device does not hinder hand movements, such as holding the gripper of the crutch and pressing on the force sensors. The electrode array has 22 stimulation points and 33 ground points. One can find the details of the electric stimulation equipment in our previous works [77], [78].

The electric stimulation pattern is shown in Figure 2.4. The movable range of the robotic foot in the horizontal direction is 44 cm. Along the red line, from the initial point to the final point, the 22 stimulation points divide the 44 cm into 22 sections. Each

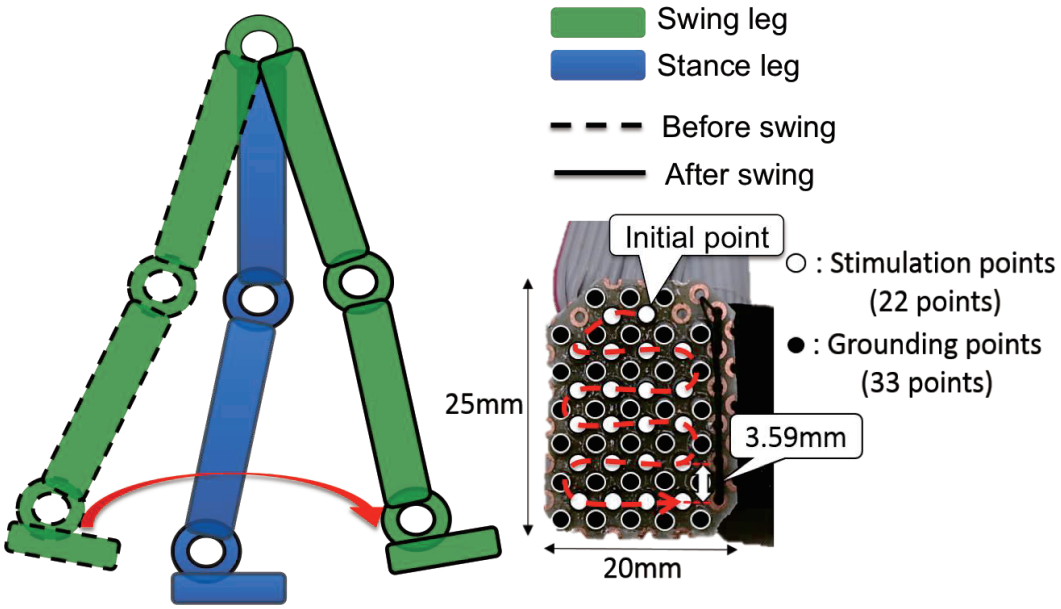

Figure 2.4: Stimulation pattern for presenting the relative distance between the stance and swing legs.

stimulation point represents a 2 cm distance in the range of the foot in the horizontal direction. When the robotic foot moves forward, the stimulation position transfers along the red line. At any moment, only one stimulation point is energized. When the right leg swings, the electrode array on the right side generates electric stimulation, while the array on the left side activates when the left leg swings.

2.4 Walking robot simulating a paraplegic patient

It is dangerous to apply this walking control interface to a paraplegic patient before validating its feasibility. Furthermore, an able-bodied subject cannot wear an exoskeleton to replace a patient for validation experiments. Although able-bodied subjects can consciously try to imitate paraplegic patients, they subconsciously put force into their lower limbs to keep their balance when the risk of falling is high. Therefore, a walking robot was developed to simulate a paraplegic patient wearing an exoskeleton in order to conduct walking experiments for safety reasons. Through the experiments, we confirm that a robot can walk stably under the control of an operator by using the wearable walking control interface.

As show in Figure 2.5, the weight of the walking robot is 25 kilograms and it has 10

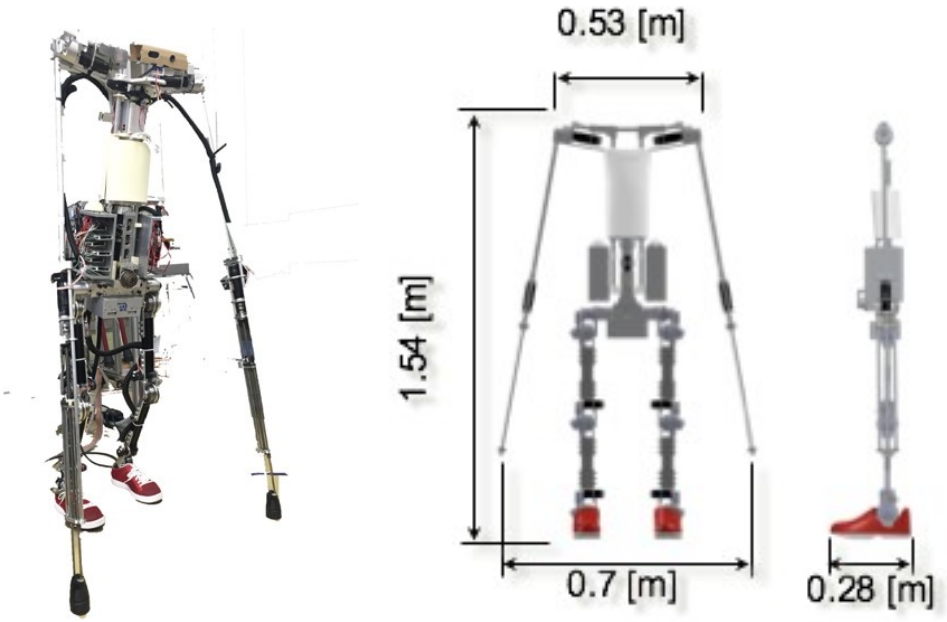

Figure 2.5: The walking robot simulating a paraplegic patients body and a walking support system.

Table 2.2: Exoskeleton parameters of walking robot.

Parameter/Part	Thigh	Lower	Foot
Mass[kg]	1.742	1.774	0.592
Length[cm]	33.3	32.75	20

degrees of freedom. Each joint is equipped with an encoder, which measures the joint angle during experiments. The movable joints are the shoulder joints, hip joints, knee joints, and ankle joints. The inertia and link lengths of the lower body are shown in Table 2.2. Additional details regarding the walking robot are provided in our previous works [61, 79].

2.5 Robot walking experiment

Four subjects participated in our experiments. They are all able-bodied, male, and aged between 20 and 30 years old.

Table 2.3: Stimulation parameters for all subjects (1).

Subject/Intensity/Point	1	2	3	4	5	6	7	8	9	10	11
A	116	114	125	119	110	69	118	140	140	82	110
B	125	120	100	135	135	100	115	155	145	105	135
C	70	70	80	80	70	60	65	80	80	80	65
D	137	127	213	122	120	240	112	239	199	175	98

Table 2.4: Stimulation parameters for all subjects (2).

Subject/Intensity/Point	12	13	14	15	16	17	18	19	20	21	22
A	127	125	95	90	117	130	65	65	90	90	75
B	205	145	115	130	145	130	110	85	120	100	70
C	80	80	75	65	65	65	72	65	65	65	65
D	137	197	120	110	143	250	120	128	145	155	165

2.5.1 Preparation stage

Finger skin has different sensitivity in different areas. The electric current for electric stimulation (stimulation intensity) should be decided on a point-by-point to fit each subject's characteristics. We find the proper electric current for each stimulation point for each individual by increasing the target electric current from zero until the subject says that they can clearly feel the electric stimulation. The stimulation intensity is equally divided into 255 gradients for precise adjustment.

$$C = I \times 10/255. \tag{2.4}$$

where C is the electric current for electrical stimulation and I is the stimulation intensity. Table 2.3 and 2.4 shows the stimulation parameters for all subjects.

2.5.2 Learning stage

The learning stage is implemented with two goals:

1) To enable the subject to learn stride control by using the wearable walking controller.

2) To enable the subject to convert the electric stimulation into foot position information.

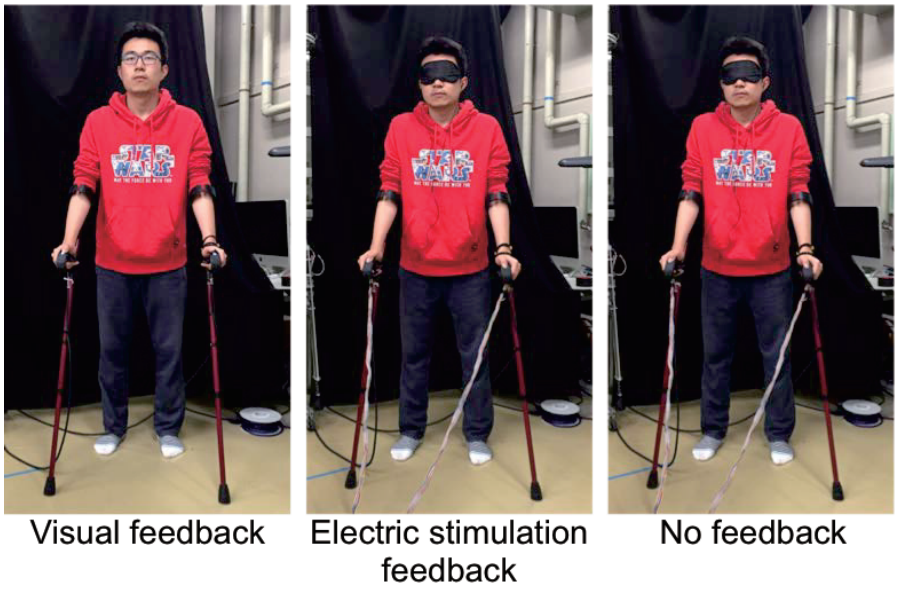

Figure 2.6: Image of a subject under three feedback conditions.

The subject controls the robot to walk through the interface while looking at the robot. Simultaneously, the subject receives the electric stimulation and intentionally establishes a connection between the electric stimulation and the foot position of the robot. This training ends when the following conditions are satisfied: 1) The robot walks three meters in the absence of a tendency to fall. 2) The subject indicates that they can understand the foot position from the electric stimulation. The duration of the training varied from person to person, but all subjects completed training within one hour.

2.5.3 Testing stage

In testing stage, the subjects controls the robot to walk three meters under the three feedback conditions: visual feedback, electric stimulation, and no feedback. Figure 2.6 describes the three feedback conditions. A subject holds a pair of crutches and voluntarily controls the stride of each step during the robot walking experiment. Under the visual feedback condition, the subject visually confirms the posture and spatial location of the robot's legs. Under the electric stimulation and no feedback conditions, an eyepatch was used to shields the subject's eyes. Under the electric stimulation condition, a pair of electrode arrays was banded to the subject's left and right middle fingers. The electrode array generates electric stimulation with a pattern to present the relative distance between the right and left foot. Under the no feedback condition, the subject also wears electrode

arrays. However, they only receive a pulse signal when they should take a step.

The main purpose of the three meter walking experiment is to evaluate the accuracy of the electric stimulation. In order to achieve this purpose, a task was assigned to each subject during the walking control experiment. Two steps, one left step and one right step, are considered to be one step group. The subject is asked to control the stride on one side without significant attention, but is then asked to control the stride on the other side to make the two strides in each step group equal. The subject follows this rule to control the robot during experiments under all three feedback conditions. In this manner, the accuracy of electric stimulation could be evaluated by comparing the error between the left and right stride with electric stimulation with that under the other feedback conditions. Additionally, the subject was asked to attempt to move the robot faster on the basis of ensuring the walking stability.

The robot walking tests were repeated 3 times for each subject under each feedback condition. The order of the experimental conditions was randomized in order to avoid practice effects. During walking, the encoder measures each joint angle of the robot. The relative distance between the feet and the spatial location of the robot, as well as the walking time, were calculated and recorded by a program. If the subject controlled the robot's leg swing too quickly or the relative distance between the left and right foot become too large, the robot fell down and failed the experiment. Success rates were recorded in order to evaluate the walking control interface and electric stimulation.

2.6 Result and discussion

2.6.1 Performance of wearable walking controller

Figure 2.7 presents images of one subject during two steps in the robot walking experiment with visual feedback. Corresponding to Figure 2.7, Figure 2.8 shows the experimental data corresponding to the two steps. The foot position, hip joint angle, and hip joint angular velocity are calculated from encoder data. The torque is calculated by multiplying output current by a torque constant. The shaded area indicates the stride control portion of the walking process.

When the left foot swings, the right foot position becomes the original. Here, the position of the foot represents the relative distance between the feet. The variation of foot position in figure 2.8 matches the stride range represented by electric stimulation, which ranges from -20cm to 24cm. During stride control, the operator controls the hip

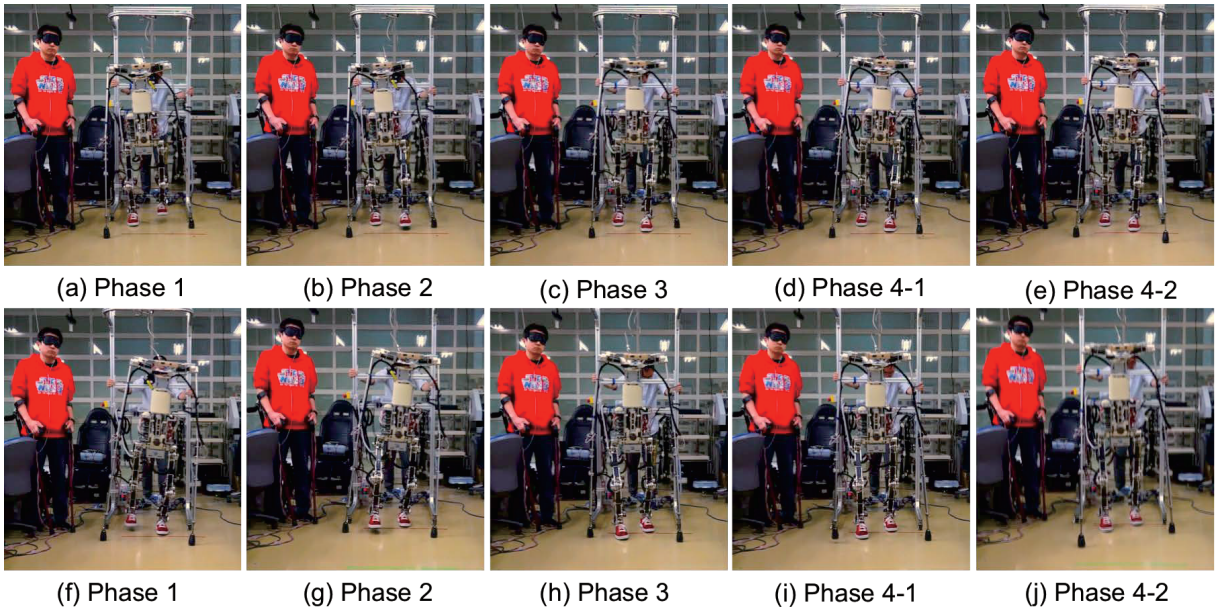

Figure 2.7: Snapshots of a 3-meter walk on a flat floor.

Table 2.5: Success rate.

Subject	Vision feedback	Electric stimulation feedback	No feedback
A	3/3	3/3	2/3
B	3/3	3/3	1/3
C	3/3	3/3	2/3
D	3/3	3/3	3/3

joint torque of the swing leg through the wearable walking controller. When the operator presses the lower force sensor, the hip joint angle increases and the foot moves forward.

2.6.2 Success rates and walking speed

Table 2.5 contains the success rates of the subjects under different experimental conditions. Among the experiments, only subject D was able to complete the walk with no feedback. Although the robot can typically automatically maintain balance, the robot will fall if the stride is too long or the leg swings too fast. This result proves that both visual feedback and electric stimulation assist the user in locating the foot landing positions and controlling swing velocity.

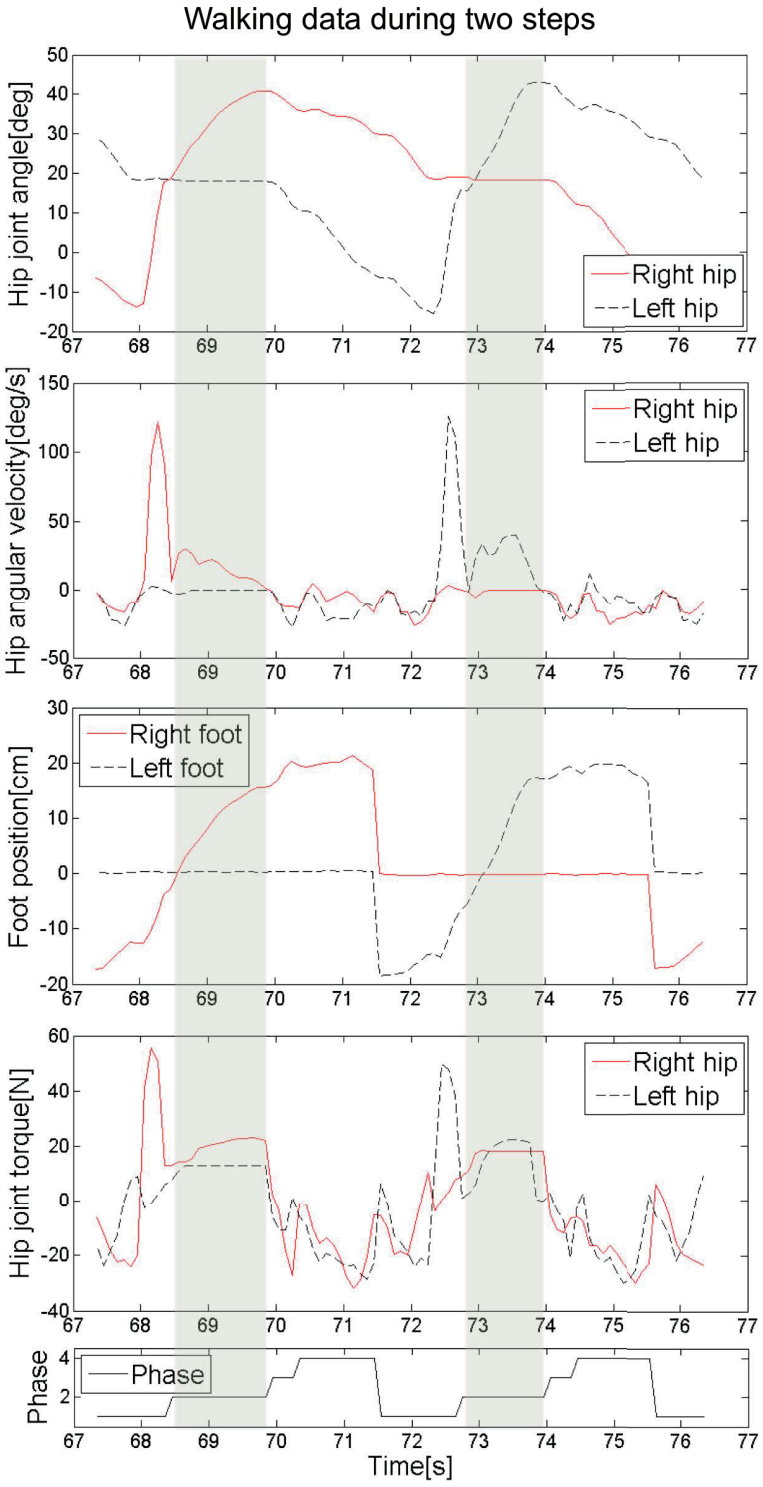

Figure 2.8: Hip joint angles, hip joint angular velocities, foot positions, and hip joint torques of each phase during two steps.

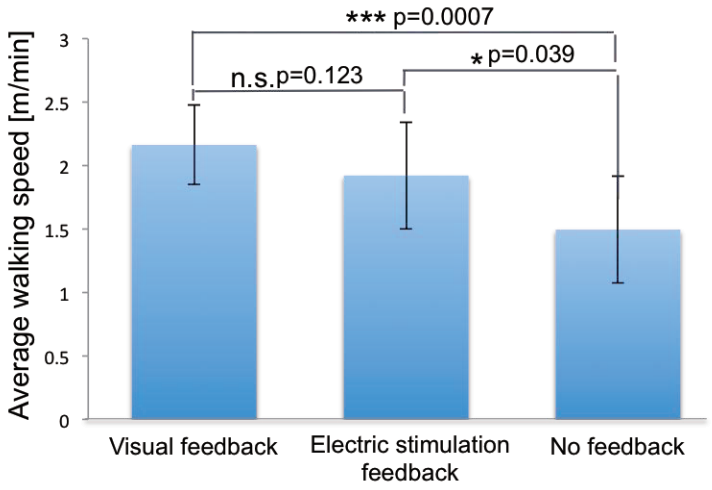

Figure 2.9: Average walking speed under visual feedback, electric stimulation feedback, and no feedback.

Figure 2.9 shows average walking speed under visual feedback, electric stimulation feedback, and no feedback. As shown in Figure 2.9, the walking speed is compared based on two-way ANOVA. Differences in mean values were assessed using the Bonferroni multiple comparison procedure (significance level: 5%) by using IBM SPSS Statistics. There is a significant difference between visual feedback and no feedback, and between electric stimulation feedback and no feedback in the experimental results. However, there is no significant difference between visual feedback and electric stimulation feedback in the experimental results. The average walking speed was relatively slow compared to complete SCI (spinal cord injury) patients walking with a powered exoskeleton, who walk at a speed of 6.67 [m/min] [63].

We consider three main reasons for this:

1) Control proficiency

The walking speed in these experiments is already improved compared to previous experimental results [80] where the subject was not well trained. The walking speed was 1.82 [m/min]. With a short training time prior to evaluation, the subject can better use the controller and understand the electrical stimulation feedback. However, subjects have not yet controlled the robot legs as if they were their own legs. More training is necessary in order to improve walking quality.

2) Feedback proficiency

The subject takes time to make the left and right stride equal. The time spent is

highly related to the subject's familiarity with the feedback. Subjects are most familiar with frequently used visual feedback and comparatively unfamiliar with the new electric stimulation feedback. Walking takes even more time if there is no feedback. Prior to the experiment, we expected that the no feedback condition would have the fastest walking speed. However, the robot falls if the step is too long or the leg swings too fast. Here, we use the data only if the experiment was successfully completed.

3) Man-machine difference

In the robot walking experiment, each action is executed sequentially and the stance leg stays still while the swing leg moves forward. However, when a paraplegic patient walks with the aid of an exoskeleton, sometimes the patient will move the leg and the crutch at the same time and the movement of the center of mass continues. The challenge for our cooperative walking system is to plan the trajectory of the center of gravity in real time in order to adapt to a walking motion that may vary with every step. The walking algorithm must be improved in order to speed up walking. Additionally, a smooth gait transition method should be considered to handle situations where a patient changes their speed and gait while walking.

2.6.3 Error of electric stimulation

Figure 2.10 shows the average differences between left and right stride in the cases of visual feedback, electric stimulation feedback, and no feedback during the robot walking experiment. As shown in Figure 2.10, the effectiveness of the electric stimulation feedback was evaluated based on two-way ANOVA. Differences in mean values were assessed using the Bonferroni multiple comparison procedure (significance level: 5%) by using IBM SPSS Statistics. There is a significant difference between visual feedback and no feedback, and between electric stimulation feedback and no feedback in the experimental results. However, there is no significant difference between visual feedback and electric stimulation feedback in the experimental results.

The standard deviations of average stride differences under each feedback condition illustrate a greater degree of dispersion. The reasons we considered are as follows:

Under the visual feedback experimental condition, the subject relies on visual memory to control robot stride in order to make each step the same length. During the walking experiment, the movement of the robot causes a change in the relative position between the subject and the robot. This change in relative position affects the accuracy of stride control and causes the large dispersion of stride differences under the visual feedback condition.

Under the electric stimulation feedback experimental condition, the subject memorizes

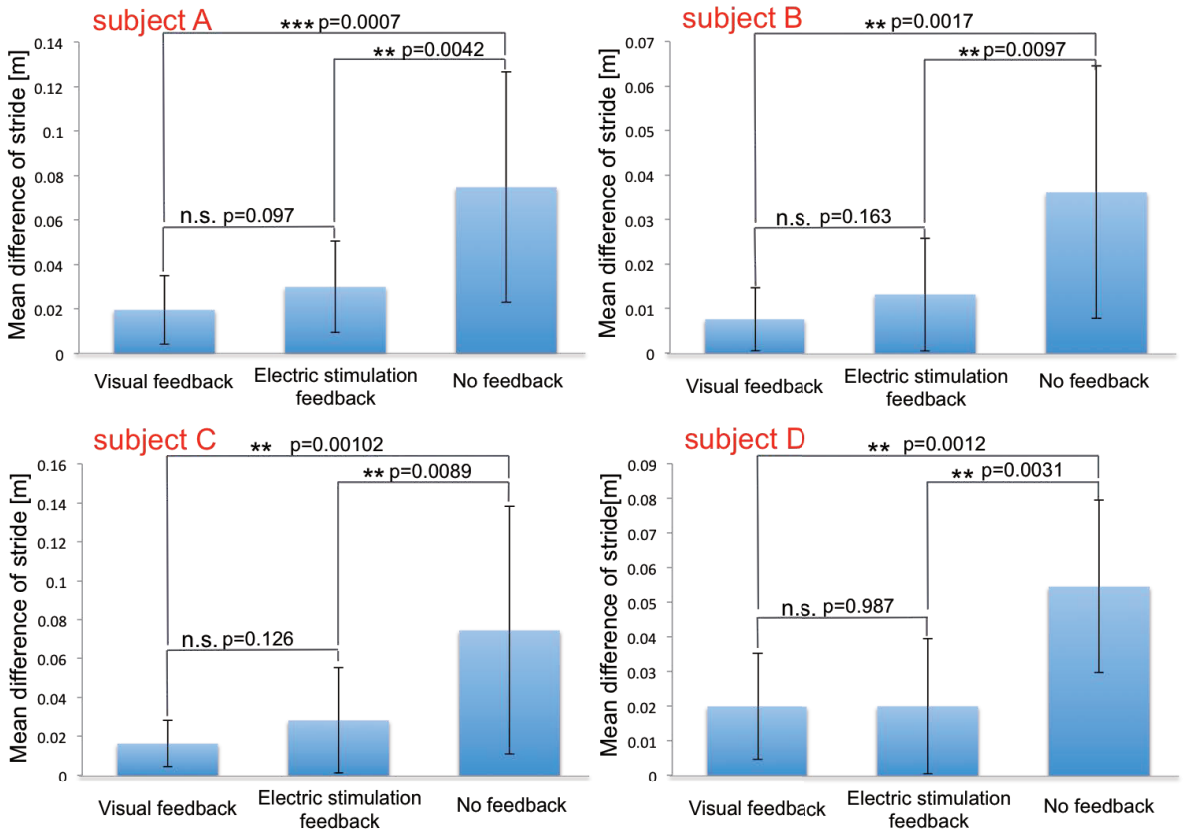

Figure 2.10: Mean stride error of each subject under visual feedback, electric stimulation feedback, and no feedback conditions.

the stimulation points in the electrode array when they control the leg landing on the floor. They then control the other to land when they feel the stimulation transfer to the same position as they felt for the first leg. One reason for dispersion is the resolution of the electrode array. The 22 stimulation points correspond to a 44cm stride with an inherent error of 2 cm. Another reason is that the subject can confuse adjacent stimulation points due to finger sweat or a weak slip between the electrode array and the finger.

Under the no feedback experimental condition, two subjects claimed that they relied on finger pressure sensation to control stride when they applied force on the pressure sensors of the walking interface. However, this feeling is ambiguous and uncertain. The paw sensor we used is soft and the reaction force is small. Short-term training is not sufficient to allow subjects to differentiate between subtle pressure changes.

In summary, the experimental results indicate that the accuracy of electric stimulation feedback is at nearly the same level as visual feedback. In other words, electric stimulation could replace vision to assist paraplegic patients walking with an exoskeleton. The results

also indicate that subjects have difficulties in expressing their intention to walk without feedback.

2.7 Summary

We have proposed a wearable walking interface, a cooperative control method, and an electric stimulation system to provide somatosensory feedback for lower limb paralysis while wearing a powered exoskeleton, with the goal of compensating for impaired afferent and efferent nerves via healthy fingers. This chapter also introduced a walking robot that walks with the aid of crutches to emulate paraplegic patients, with the goal of executing preliminary investigations safely prior to clinical trials. The wearable walking interface allows its users to voluntarily control their stride while walking. The cooperative control system enables users with partial control competence to control their stride instead of forcing them to follow a predefined walking trajectory when they wear exoskeletons. The electric stimulation equipment is lightweight, portable, and banded to the finger to provide the wearer with feedback regarding the relative distance between their stance foot and swing foot.

A series of robot walking experiments, which aimed to determine the effectiveness of the wearable walking controller and the electric stimulation device, were implemented under three conditions: visual feedback, electric stimulation feedback, and no feedback. The experimental results indicate that: 1) The wearable walking controller enables the user to control the stride based on their will while walking. 2) The electric stimulation provides helpful information related to stride control and could replace vision for assisting paraplegic patients walking with an exoskeleton.

Chapter 3

Walking control interface with electro-tactile feedback for gait control

The research and development of powered exoskeletons is expected to support the walking of paraplegic patients. At the current stage, exoskeletons do not allow patients to voluntarily control their gait, nor do they provide sensory feedback to compensate for the loss of lower-body sensation. This chapter proposes a wearable walking control interface to achieve voluntary gait control, and an electrical stimulation method to inform the patients about their foot position for voluntary gait control. In this study, a walking robot that simulated a paraplegic patient wearing an exoskeleton was used to investigate the performance of the proposed interface and stimulation method. We confirmed that, by using the interface, the subjects were able to control the robot gait for a distance of 3 m. Moreover, the accuracy of the electrical stimulation feedback was confirmed to approximate the visual feedback achieved through the human eyes. The experimental results revealed that the proposed interface and electrical stimulation feedback could be applied to a walking support system for patients with complete paraplegia.

3.1 Concept of interface with feedback

Exoskeletons generally use electromyography (EMG) [45–47] or electroencephalogram (EEG) signals [48, 49, 81] to estimate the movement intention of the users. EMG-based exoskeletons are not applicable to paraplegic patients because the bioelectric signals cannot be transferred to the lower limbs, owing to the impairment of the patients' nerves. On the

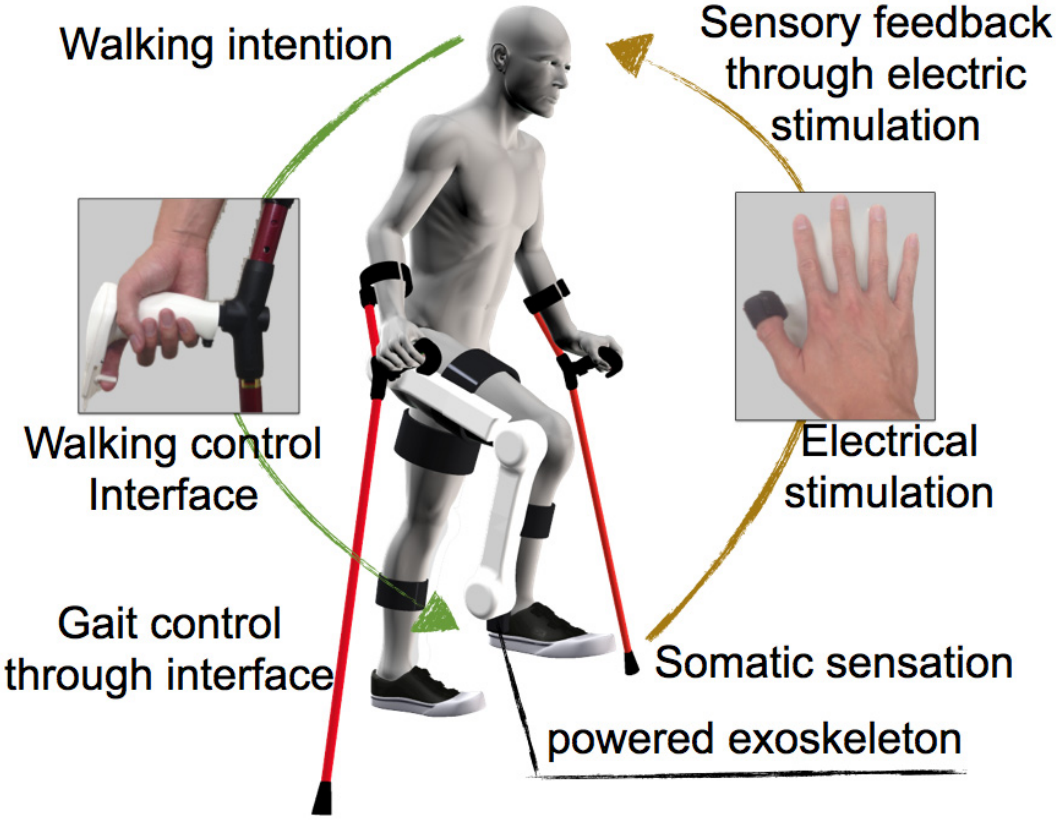

Figure 3.1: Concept of powered exoskeleton with wearable walking control interface and electrical stimulation feedback.

contrary, although EEG signals are obtainable from the head part of paraplegic patients, it is difficult to infer the details of the generated actions.

Ekso is an exoskeleton, which was developed by Ekso Bionics, and estimates the walking intention of paraplegic patients by detecting the center of gravity (CoG) transfer, when their upper body leans forward [64]. Additionally, Sankai's group developed HAL, which estimates the walking intention of paraplegic patients by detecting the changes in the contact force between the soles of the feet and the ground [63,74]. These power exoskeletons assist users with the start and end of their walking motion. However, the gait itself cannot be controlled.

Walking support systems without voluntary gait control are effective on a flat terrain. However, control is required when the users want to land their foot in a specified position or climb stairs. Additionally, feedback signals from exoskeletons are important when the exoskeletons are applied to paraplegic patients, because the patients typically look down at their lower limbs to confirm their position, owing to the loss of lower-limb sensation.

Tsukahara *et al.* used a display screen to indicate the angle of the joint and the change in the CoG for rehabilitation training [60]. Although the visual feedback system is feasible for rehabilitation purposes, vision should also be used to carry out daily activities, since the patient's visual sense will be occupied by the display.

Some research groups use tactile feedback to compensate for the lack of feedback sensation for paraplegic patients. Fan *et al.* developed a pneumatic cuff to indicate the contact force of the soles for lower-limb prostheses users [57]. Cheng *et al.* applied vibration to represent complex hand configurations [82]. Yokoi *et al.* investigated electrical stimulation as a type of biofeedback in order to control the use of a prosthesis [55, 56]. Although these tactile feedback approaches are effective in compensating for the lack of a feedback sensation, feedback systems have not yet been considered for paraplegic patients.

This study proposes a wearable walking control interface and an electrical stimulation feedback method for power exoskeletons, which allows paraplegic patients to control their gait and compensate for the loss of physical sensation at their lower limbs. Figure 3.1 shows the concept and objective of this study. A paraplegic patient wears the exoskeleton in order to walk, and uses a pair of crutches to maintain balance. A walking control interface is mounted onto the handle of a crutch. The interface allows the user to voluntarily control their footsteps and foot height during walking, with the assistance of an exoskeleton. Correspondingly, the user receives transcutaneous electrical stimulation, which informs them about their foot position [50].

We previously developed a walking robot in order to simulate a paraplegic patient wearing an exoskeleton [61]. In this study, owing to safety concerns, a robot was used to implement the proposed control interface and electrical stimulation feedback device, instead of a real patient. The preliminary contribution of this study was partially presented in [80], where an interface was used to achieve foot position control and generate a feedback signal. In comparison with our previous work [83], the new contributions of the present study are as follows: 1) The degrees-of-freedom (DoF) of the foot position control and feedback signal were increased from 1-DoF to 2-DoF. 2) The control interface design was modified to adjust to the newly applied 2-DoF system. 3) The stimulation-relaxation of the electrical stimulation was modulated to represent the foot position. 4) The response time and recognition rate of the single point stimulation was investigated.

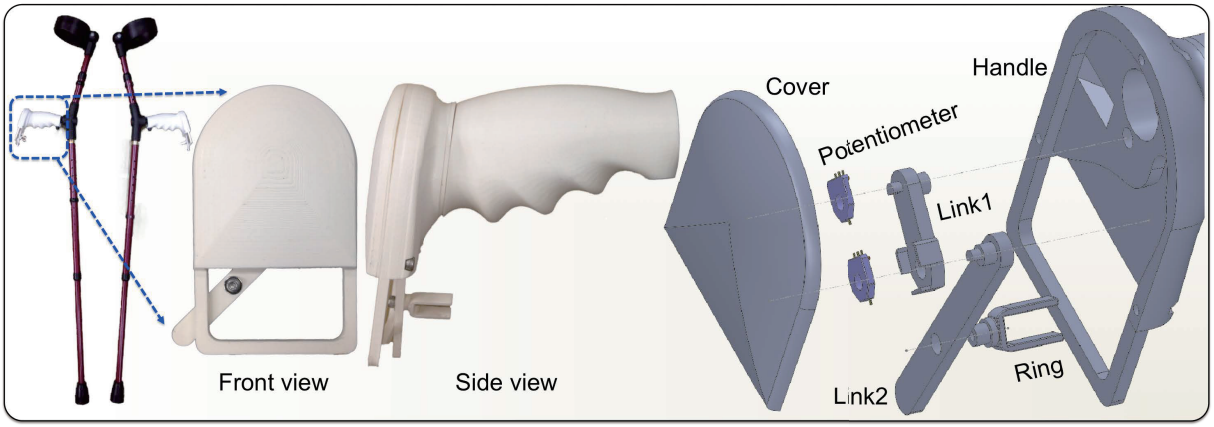

Figure 3.2: Exterior and assembly drawing of wearable walking control interface.

3.2 Gait control using wearable walking control interface

3.2.1 Wearable walking control interface

Figure 3.2 shows an exterior and assembly drawing of the wearable walking control interface developed in this study. The handles attached to a pair of crutches were designed with consideration to ergonomic principles, and allow the user to grasp them comfortably. The interface and handle were integrally connected in front of the handle. A group of connecting rods consisting of two rotatable links and a rotatable ring was installed inside the interface. The center of rotation of the connecting rod was fixed to the inner wall of the interface. Two potentiometers were installed at the junction between the link and the inner wall and at the junction between the two links, in order to measure the joint angles, respectively. The user can grasp the handle and insert their index finger into the ring in order to control their walking gait. The interface of the left crutch was used to control the left leg, while the interface of the right crutch was used to control the right leg.

3.2.2 Gait control

In this study, a walking robot was used instead of a paraplegic patient. Figure 3.3 shows an overview and schematic of the walking robot used in this study. The coordinate system is also described in Figure 3.3. The vertical projection of the middle of the connection between the two hip joints on the ground is the origin of this coordinate system.

The exoskeleton user can control their gait by using the ring of the control interface.

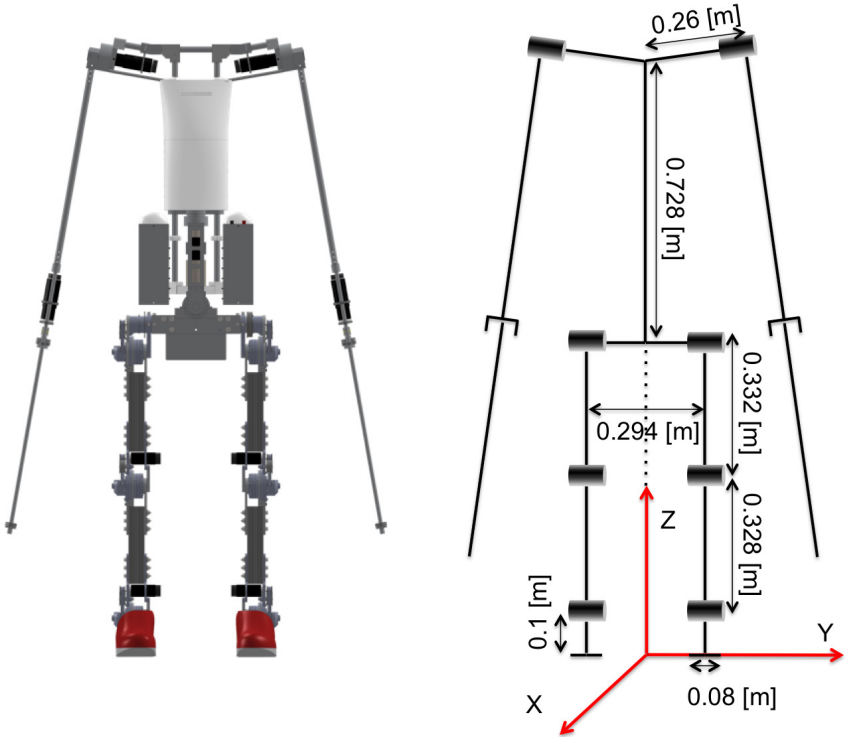

Figure 3.3: Robot schematic and coordinate system.

Figure 3.4 shows an overview of the gait control that is achieved through the interface. The vertical projection of the rotation center of the connecting rod at the lower edge of the cover is the origin of the interface coordinate system. The foot position of the robot and the ring position of the interface are associated. A paraplegic patient can use their index finger to control one of the robots legs. We considered the interface and swinging leg of the robot as a dual-articulated manipulator with only two revolute joints. Then, the position of the end-effector can be calculated as follows:

$$\begin{bmatrix} X_c \\ Y_c \\ Z_c \end{bmatrix} = \begin{bmatrix} L_0 \cos\Theta_0 + L_1 \cos(\Theta_0 + \Theta_1) \\ 0 \\ d_s - L_0 \sin\Theta_0 - L_1 \sin(\Theta_0 + \Theta_1) \end{bmatrix}, \tag{3.1}$$

$$\begin{bmatrix} x_c \\ y_c \\ z_c \end{bmatrix} = \begin{bmatrix} l_0 \cos\theta_0 + l_1 \cos(\theta_0 + \theta_1) \\ 0 \\ l_0 \sin\theta_0 + l_1 \sin(\theta_0 + \theta_1) - d_i \end{bmatrix}, \tag{3.2}$$

where X_c, Y_c, and Z_c are the current foot position of the swing-leg, and d_s is the vertical distance from the hip joint to the ground. x_c, y_c, and z_c are the current positions of the

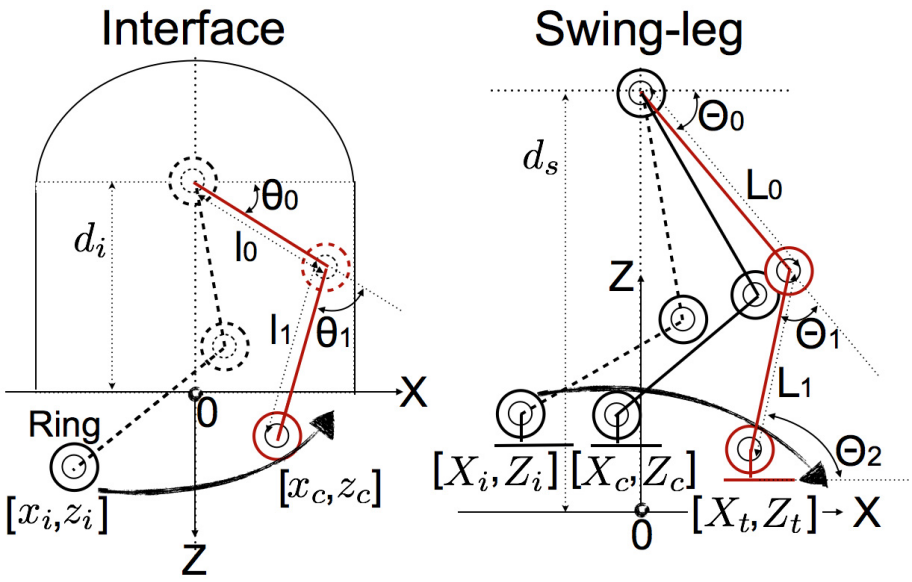

Figure 3.4: Gait control through wearable walking control interface.

interface ring, and d_i is the vertical distance from the rotation center to the lower edge of the interface cover. Additionally, Θ and θ are the joint angles of the leg and interface, respectively. The robot leg is controlled within the track of the reference trajectories, which are represented by X_t and Z_t, as shown in Figure 3.4. The target foot position, X_t and Z_t are derived as follows:

$$X_t = X_i + k_1\delta_x, \tag{3.3}$$

$$Z_t = Z_i + k_2\delta_z, \tag{3.4}$$

$$\delta_x = x_c - x_i, \tag{3.5}$$

$$\delta_z = z_c - z_i, \tag{3.6}$$

where X_i and Z_i are the initial foot positions, and k_1 and k_2 are the proportional gains. x_c and z_c are obtained from equation (3.2), and x_i and z_i are the initial position of the interface ring. The reference trajectory of each joint is derived from the reference foot trajectory by using the damped least squares method [84], as follows:

$$\delta\boldsymbol{\Theta} = \boldsymbol{J}^T(\boldsymbol{J}\boldsymbol{J}^T + \lambda^2\boldsymbol{I})^{-1}\boldsymbol{e}, \tag{3.7}$$

where $\boldsymbol{J}$ is a Jacobian matrix, $\boldsymbol{J}^T$ is the transpose of $\boldsymbol{J}$, and λ is the non-zero damping constant. In this study, the value of λ was considered as 2.24. Through simulation, a leg

with the same kinematic as the robot was decided to follow the target position. $\boldsymbol{I}$ is a unit matrix, and $\boldsymbol{e}$ is the vector pointing from the current foot position to the target foot position. Because the leg was composed of revolute joints, the Jacobian matrix can be simply written as follows:

$$\boldsymbol{J} = \begin{bmatrix} -L_0 \sin\Theta_0 - L_1 \sin(\Theta_0 + \Theta_1) & -L_1 \sin(\Theta_0 + \Theta_1) \\ 0 & 0 \\ -L_0 \cos\Theta_0 - L_1 \cos(\Theta_0 + \Theta_1) & -L_1 \cos(\Theta_0 + \Theta_1) \end{bmatrix}, \tag{3.8}$$

$$\boldsymbol{e} = [\delta_X, 0, \delta_Z]^T, \tag{3.9}$$

$$\delta_X = X_t - X_c, \tag{3.10}$$

$$\delta_Z = Z_t - Z_c. \tag{3.11}$$

where X_c, Z_c, X_t, and Z_t, can be obtained from equations (3.1), (3.3), and (3.4), respectively. To avoid an issue where the foot and ring positions do not coincide initially, the interface determines the relative distance between the initial robot foot position and the current foot position, rather than simply determining the corresponding ring and foot positions. Additionally, this interface has low control impedance, and a 20-order finite impulse response (FIR) low-pass filter was employed to deal with erroneous finger movement. The sample rate of the control signal was 50 [Hz]. The passband frequency of the filter was 3 [Hz], and the stopband frequency was 9 [Hz]. We used Matlab's signal processing toolbox and offline collected data to build the filter and apply it to the interface.

3.2.3 Walking control

Conventional exoskeletons allow a paraplegic patient to follow an pre-programed walking trajectory. In contrast, our walking control interface provides the users with partial control, which allows them to voluntarily control the foot position of their swinging leg. Walking is achieved through cooperation between the subject and the robot. The robot controller uses three of the four extremities, two legs, and two crutches, to automatically maintain stability, whereas, the swinging leg is operated by the subject through the wearable walking control interface. The robot's CoG is controlled to remain within the support polygon by adjusting the length of the extremities. The cooperative control method enables the subject to concentrate on the gait control while walking.

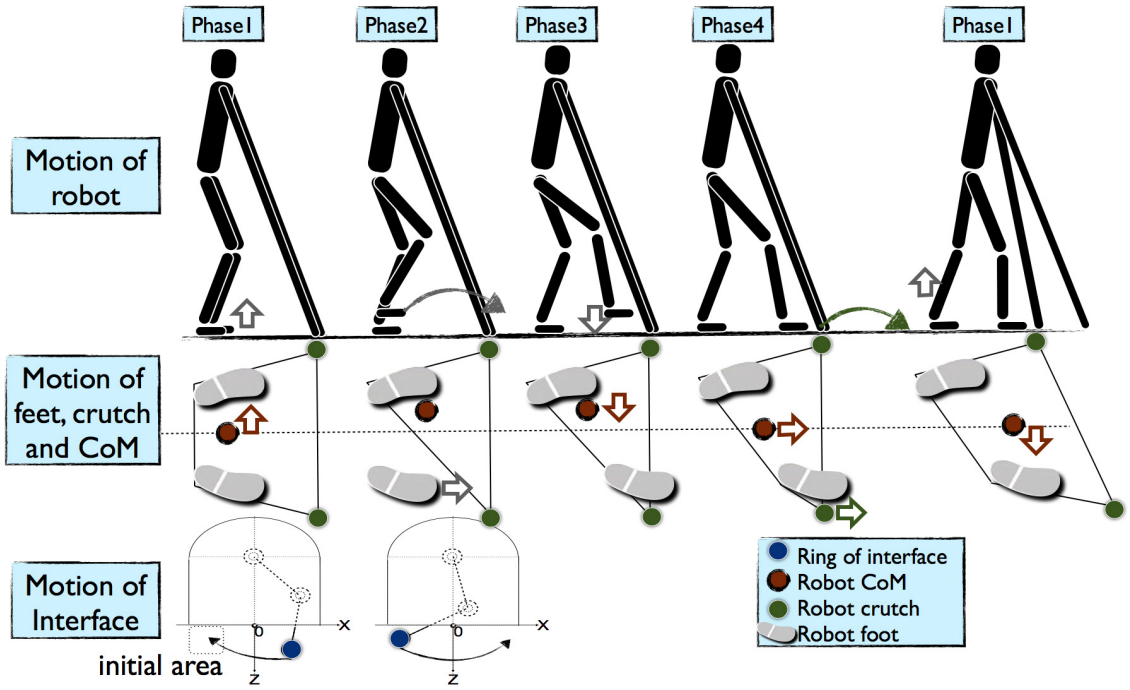

Figure 3.5: Four phases of robot walking control.

The safety distance d is used before the robot swings its leg forward to avoid contact between the foot and the ground, and to avoid impact when the robot lands its foot on the ground. Here, d was set to 2 [cm], which is the vertical distance between the foot and ground. Figure 3.5 shows the walking sequence and motion of each phase. The gait control explained in the previous subsection corresponds only to phase 2 of the entire walking process. In phase 1, the controller initiates the walking as a switch. In phase 2, the robot foot moves along with the user's finger movement. In phases 3 and 4, the robot automatically controls the foot landing, crutch swing, and transfer of the CoG. The robot walks on a flat floor by applying a right leg swing, right crutch swing, left leg swing, and left crutch swing, in sequence.

Phase 1: The subject places their index finger with the ring inside the initial area, as shown in Figure 3.5, in order to start the gait control. This start motion is detected by calculating the ring's position from the potentiometer signals embedded into the interface. Afterwards, the robot transfers its CoG to the side of the stance leg and vertically lifts the foot of the swinging leg upward at a distance d away from the ground in order to prepare for the leg swing. The prepared action lasts for 0.8 s.

Phase 2: As explained in subsection 3.2.2, the subject sends motion instructions, including step length and step height, by using the walking control interface. The robot's foot moves

along with the control signal. When the horizontal position of the swing-foot exceeds the horizontal position of the support-foot, and the distance between the sole of robot's foot and the ground becomes less than the distance d, the control mode proceeds to phase 3.

Phase 3: The robot lands the foot of its swing leg on the ground. The foot landing action lasts for 0.4 s.

Phase 4: The robot swings the crutch forward on the same side as the landing foot, lands it on the ground, and simultaneously moves its CoG forward. The crutch-swing action lasts for 1.2 s.

3.2.4 Robot walking experiments

Robot walking control experiments were conducted to evaluate the performance of the gait control by using our wearable walking control interface. Five subjects participated in these experiments, operated the robot's gait, and walked a distance of 3 m by visually confirming their walking motion through the control interface. The subjects controlled the left leg of the robot by operating the control interface with their left hand, and controlled the right leg of the robot by operating the control interface with their right hand. All subjects were able to master the robot walking control skills with guidance and after five practice attempts.

Figure 3.6 shows the sequential photographs of the two steps in the robot walking control experiments. The red dotted circles in the figure highlight the main movement part of the robot during each phase. Figure 3.7 shows the trajectory of the robot's foot and the control signal from the interface in an experiment with one subject. The robot's step length and step height were calculated by using data from each joint encoder. The target stride and target foot height were calculated by using signals from the interface potentiometers. The target positions were indicated by the black dotted lines, while the actual positions were indicated through the red solid lines, with a sampling frequency of 10 [Hz]. For stride control, the initial position was set to zero. The max error was 3.86 cm, while the mean error was 1.16 cm. For foot height control, the floor plane was set to zero, the max error was 2.48 cm, and the mean error was 0.88 cm.

Although some errors occurred between the target foot position and the actual foot position, the robot foot followed the control signal from the control interface. This indicates that the users were able to control the step length and step height, while walking according to their own intention by using the developed walking control interface.

Figure 3.6: Snapshot of two steps during robot walking experiment.

3.3 Electrical stimulation for sensory compensation

3.3.1 Structure of electrical stimulation device

Figure 3.8 shows the electrical stimulation device, which is an electrode array placed on the tip of a thumb finger and wrapped with a bandage. Although the electrode array of the device had 22 stimulation points, and each one could produce an electrical stimulation, two or more points could not produce an electrical stimulation concurrently. These stimulation points were in contact with the finger pulp in order to provide information regarding the foot position through electrical stimulation. The overall circuit structure of the electrical stimulation device has been described in detail in a previously published paper [78], where the finger skin resolution was investigated to determine the distance between each point and allow the users to selectively identify the stimulation position.

3.3.2 Stimulation-relaxation modulation

The stimulation sensation varied depending on the stimulation frequency, electric current intensity, and stimulation-relaxation modulation. Each stimulation point could generate

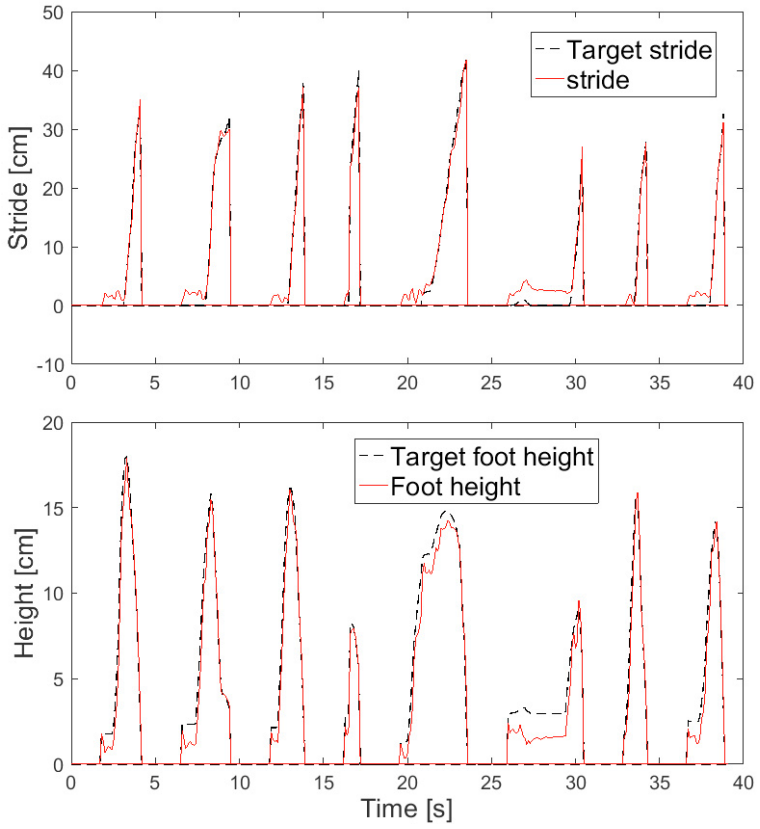

Figure 3.7: Step length and step height of robot walking experiment.

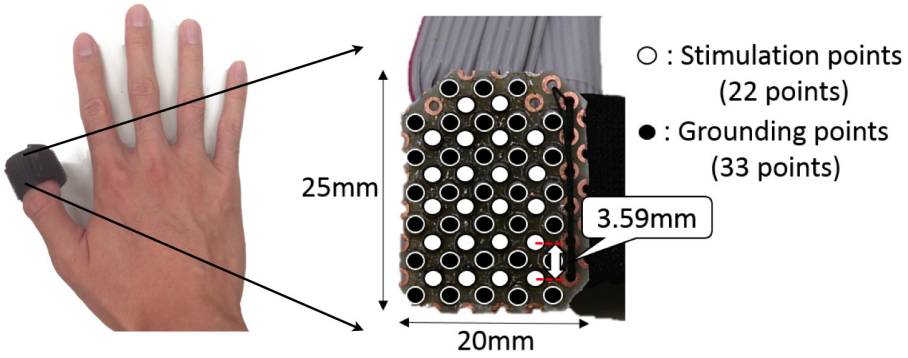

Figure 3.8: Appearance and size of electrical stimulation device.

several different stimulation sensations by changing the above parameters. Electrical stimulation was applied to the tactile corpuscles (Meissner's corpuscles) on the fingertip, which were sensitive to a stimulation of 50 [Hz]. We regulated the electrical stimulation frequency to 50 [Hz] such that all subjects could clearly sense the stimulation. The resistance of the electrical stimulation varied within and across each individual. The stimulation intens-

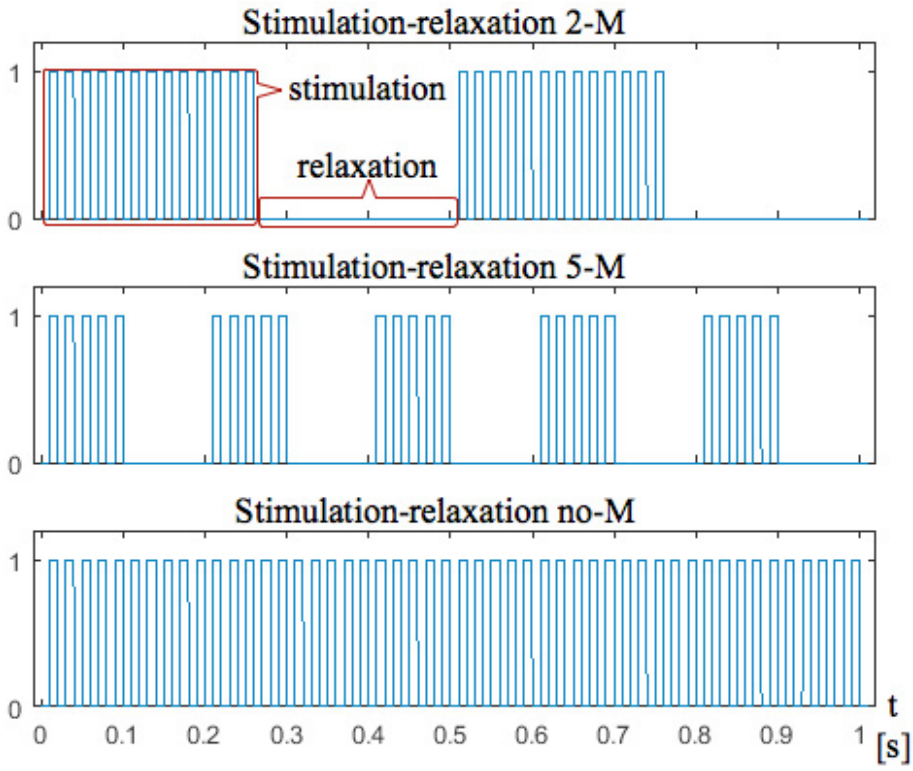

Figure 3.9: Examples of stimulation-relaxation modulation.

ity was adjusted point-by-point in order to fit each subject's characteristics. Figure 3.9 shows three examples of stimulation-relaxation modulation. The electrical stimulation was modulated in order to generate a different stimulation sensation by using a single point through cutting and recovering the stimulation during a single stimulation cycle. In this study, the stimulation and relaxation durations were equal. The "n-modulation" or "n-M" means that the stimulation-relaxation occurred "n" times in 1 s, where n is a scalar. The "no-modulation" or "no-M" means that the electrical stimulation was not modulated.

This study investigated three types of stimulation sensations by stimulation-relaxation modulation and used one stimulation point. During the experiment, the stimulation varied from 2-M to no-M. Five subjects participated in this experiment. Their thumbs were pressed against the surface of the electrode array in order to receive an electrical stimulation. The experimental procedure was carried out as follows:

a) 2-M was selected as the reference, and a higher modulation was selected as the comparison.

b) Each subject received electrical stimulation at a reference modulation and comparison modulation for 2 s.

Table 3.1: Recognition of stimulation-relaxation modulation.

M	2	3	4	5	6	7	8	10	20	no
2	×	×	△	√	√	√	√	√	√	√
3		×	×	×	△	√	√	√	√	√
4			×	×	×	×	×	△	√	√
5				×	×	×	×	△	√	√
6					×	×	×	×	×	△
7						×	×	×	×	△
8							×	×	×	△
10								×	×	×
20									×	×
no										×

c) The subjects were asked to answer whether they could clearly distinguish the two modulations.

d) The experimenter increased the comparison modulation and iterated through steps **a)** to **c)** until the stimulation-relaxation modulation reached the no-modulation state.

e) The experimenter increased the reference modulation and repeated steps **a)** through **d)** until the reference modulation reached the no-modulation state.

This experiment was repeated twice for each subject. Table 3.1 presents the experimental results, which are the minimal values of all subjects. Each row indicates the results of comparing the current reference modulation with the different comparison modulation. The √ indicates a stimulation applied to the comparison modulation that could also be clearly differentiated at the reference modulation. The △ indicates a stimulation applied to the comparison modulation that could be ambiguously differentiated at the reference modulation. Finally, the × indicates a stimulation applied to the comparison modulation that could not be differentiated at the reference modulation. In this study, we selected 2-M, 5-M, and no-M to represent the position of the robot's feet, based on the results shown in Table 3.1.

3.3.3 Response time and accuracy

The response time and accuracy at the selected stimulation-relaxation modulation were verified experimentally. Five subjects participated in this experiment. The subject sat in front of a table, with one hand on the electrode array and the other hand on a small keyboard, where three buttons were labeled 2-M, 5-M, and no-M. The experimenter controlled the electrical stimulation through the computer, including the stimulation position, stimulation-relaxation modulation, and starting and stopping of the stimulation. The computer recorded the time interval from the commencement of the electrical stimulation until a keyboard button was pressed, and the accuracy of the pressed button. The experimental procedure can be described as follows:

a) The experimenter arbitrarily selected a stimulation position and one of the three stimulation-relaxation modulations, and then started the stimulation.

b) The subject pressed the button corresponding to the proper modulation as soon as they identified the stimulation position and stimulation-relaxation modulation. At the same time, the subject verbally reported the stimulation position as a row and column.

c) The computer recorded the duration. The experimenter recorded the reported stimulation position and the actual stimulation position.

Each subject repeated the process from **a)** to **c)** 30 times, after 30 practice attempts. During the practice period, the subjects were informed of the correct answer. During the actual test, each stimulation-relaxation modulation was selected 10 times, and the stimulation positions were evenly distributed. Figures 3.10 and 3.11 show the variation of the response time of the stimulation-relaxation modulation. Figure 3.10 shows the experimental results of all subjects, and Figure 3.11 shows the experimental results of each subject. The mean response time of no-M was 1,208 [ms], that of 5-M was 1,151 [ms], and that of 2-M was 1,232 [ms]. Table 3.2 shows the correct modulation rate and position recognition. This table was presents data from all subjects.

Table 3.2: Recognition rate of electrical stimulation.

Position	Stimulation-relaxation		
	no-M	5-M	2-M
84.4%	100%	93.3%	96.6%

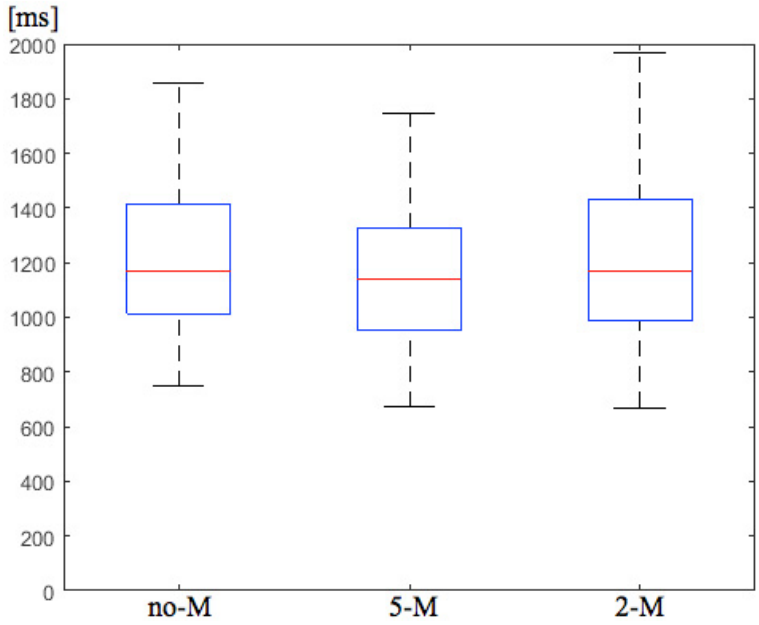

Figure 3.10: Reaction time of three stimuli types (overall).

3.3.4 Electrical stimulation pattern

Figure 3.12 shows the electrical stimulation pattern. A coordinate system was used to express the foot position. The electrical stimulation points were projected onto a two-dimensional space. By modulating the electrical stimulation, a single electrode array was used to represent the space normally represented by a three-electrode array. When the stimulation-relaxation was 2-M, 5-M, or no-M, this indicated that the stimulation position was in area A, B, or C of the coordinate system, respectively.

An electrical stimulation corresponding to the walking control interface was proposed to express the foot position in the sagittal plane. For the interface, the maximum controllable range of the horizontal direction was 42 cm, and the maximum controllable range of the vertical direction was 20 cm. Because the interface controls the relative position between the initial and target positions, the user needs a reference to understand the electrical stimulation. The hip joint and ground were set to zero in the horizontal and vertical directions, respectively. The X-axis had 12 stimulation points, which represented the positions in the forward direction from -30 to 12 [cm]. Each stimulation point represented a range of 3.5 [cm]. The Y-axis had five stimulation points, which represented the positions in the vertical direction from 0 to 20 [cm]. Each stimulation point represented a range of 4 [cm].

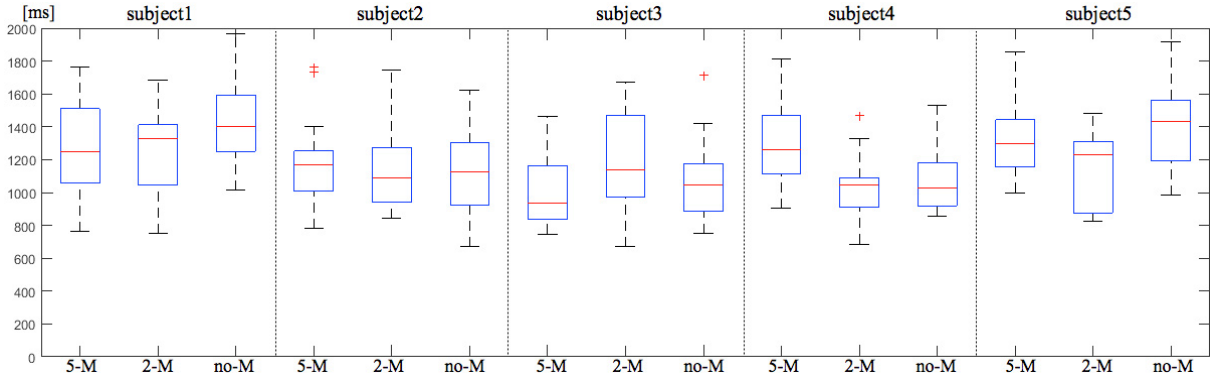

Figure 3.11: Reaction time of three stimuli types (each subject).

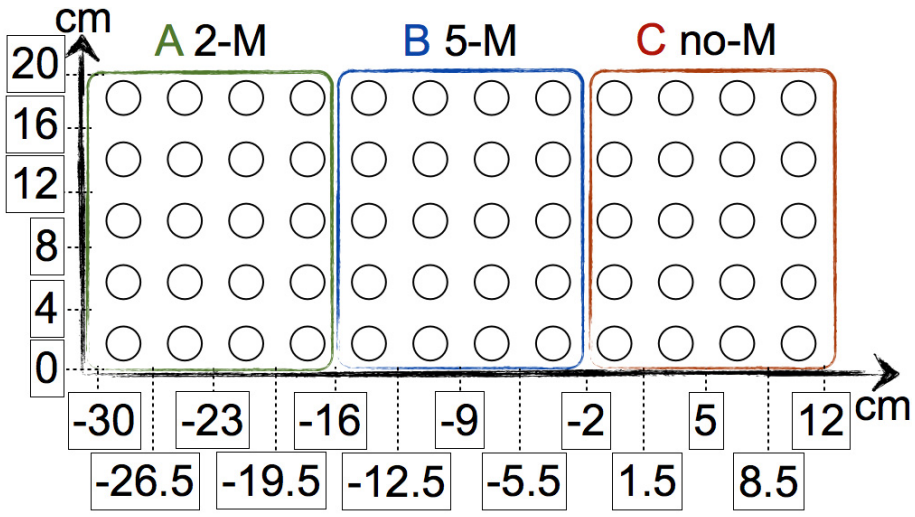

Figure 3.12: Coordinate system for representing foot position.

3.4 Foot position control with electric stimulation feedback

3.4.1 Experiment protocol

Generally, a human confirms their body posture and spatial location by using visual information and their somatosensory feedback. This experiment evaluates the foot position control with electrical stimulation feedback both in the horizontal and vertical direction. Five subjects participated in this experiment. The subjects conducted the experiment by using three different types of feedback: I) visual feedback, II) electrical stimulation feedback, and III) no feedback. For I), the subject looked at the robot's right foot. For II),

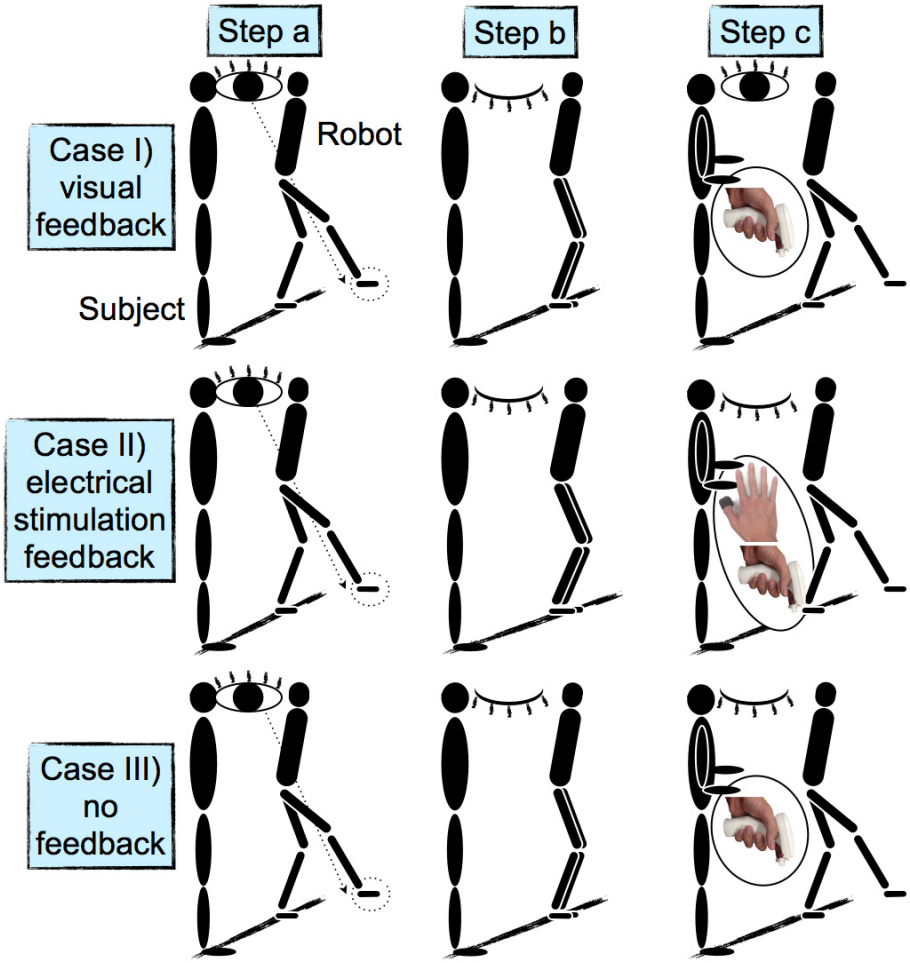

Figure 3.13: Procedures of target reaching experiment.

the subject wore an electrode array and received an electrical stimulation feedback. For III), the subject did not receive any form of feedback. The experimental procedure can be described as follows:

a) The robot lifted its right foot to a random position (random step length and random step height). The subject observed this process and memorized the foot position without electrical stimulation feedback.

b) The experimenter covered the subject's eyes with an eye mask. The robot returned its right foot to the initial position. The subject did not receive an electrical stimulation feedback.

c) The subject controlled the robot's right foot by using the walking control interface in order to reach the target position based on memory and one of the three feedback types.

Figure 3.13 shows the procedure of the target reaching experiment. The target position

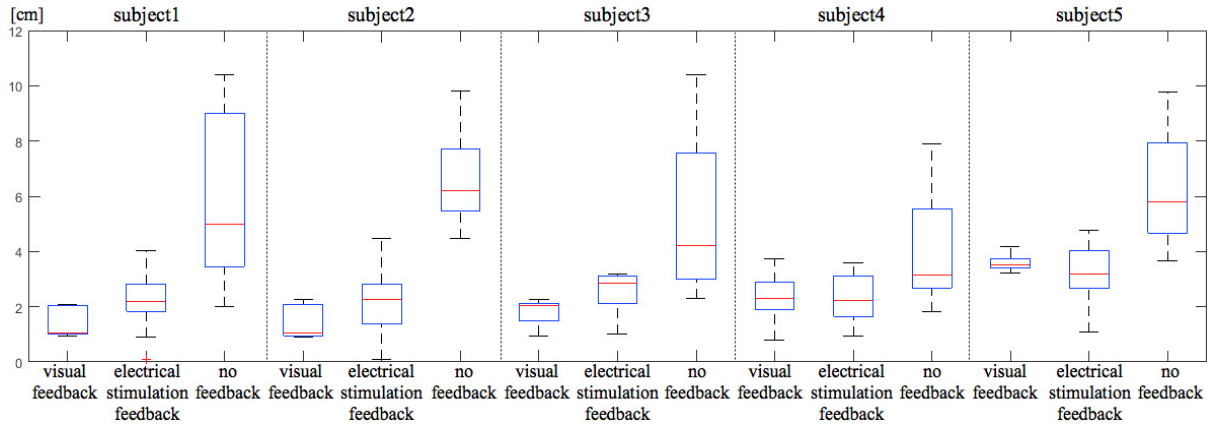

Figure 3.14: Distance error of target reaching experiment (each subject).

and reached position were recorded based on the encoder information of the robot. The Euclidean distance between the target position and the reached position was considered as the error. Each subject repeated the process from **a)** to **c)** 10 times after 20 practice attempts. Procedures **a)** through **c)** were conducted for cases I), II), and III), in this order.

3.4.2 Experiment results

Figures 3.14 and 3.15 show the distance errors when the subjects controlled the robot foot to reach the target position under each feedback condition in cases I), II), and III), respectively. Figure 3.14 shows the experimental results of each subject and Figure 3.15 shows the experimental results of all subjects. The experimental results of all subjects were analyzed by two-way ANOVA. The difference values were assessed by the Bonferroni multiple comparison procedure (significance level of 5%) using the IBM SPSS Statistics software. The mean distance errors in cases I), II), and III) were 2.11, 2.48, and 5.62 [cm], respectively. There were significant differences between the cases of visual feedback and no feedback, and between the cases of electrical stimulation feedback and no feedback. In contrast, there was no significant difference between the cases of visual feedback and electrical stimulation feedback. The least error fluctuation shown in the results indicates that the visual feedback was the most stable, followed by the electrical stimulation feedback. The experimental results revealed that the foot position control using the electrical stimulation feedback obtained almost the same accuracy as the foot position control with visual feedback, but with higher accuracy than the foot position control without any feedback.

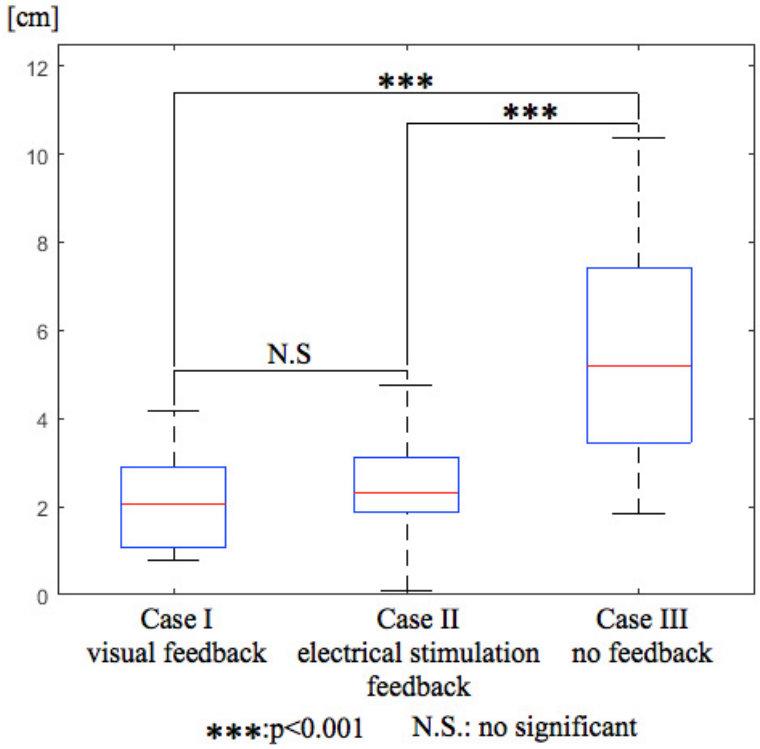

Figure 3.15: Distance error of target reaching experiment (overall).

3.5 Discussion

In this chapter, all of the experiments were conducted with a robot. To perform gait control through the interface, the entire body had to remain stable during the leg movements. To increase the walking stability, the robot moved only one crutch or one leg at each time. The robot did not move the CoG while the leg was moving, but adjusted the CoG while the crutch was moving.

Given the differences between the robot and a paraplegic patient wearing an exoskeleton, we considered two issues that will inevitably emerge when the experiment is conducted with an actual patient wearing an exoskeleton.

1) Weight distribution. The exoskeleton should support the weight of the patient's body as much as possible and the CoG should be on the side of the support leg so that the weight distributed on the arm does not affect the index finger when carrying out gait control.

2) Leg movement. The momentum caused by leg movement has an impact on the upper body. The upper limbs need to offset this momentum in order to maintain balance or even fail to maintain balance if the momentum is too large. These will affect the finger used to

control the gait. Therefore, the trajectory of the legs should be as smooth as possible and instantaneous change in speed should be limited.

3.6 Summary

This chapter proposed a wearable walking control interface and an electrical stimulation pattern for a paraplegic patient wearing a powered exoskeleton. The wearable walking control interface enables the patients to voluntarily control their gait, stride, and foot height by using their index finger. The electrical stimulation informs the patients about the two-dimensional correspondence of their foot position to the walking control interface.

The controllability of the wearable walking control interface was evaluated through a walking control experiment by using a robot, which was previously built by our research group, in order to simulate the walking of a paraplegic patient wearing an exoskeleton. In the experiment, the subjects controlled the movement of the robot's foot according to their own movement intention. For the electrical stimulation, we projected a sagittal plane onto an electrode array in order to provide information to the subject about their foot position. In the final target-reaching experiment, the subjects controlled the robot foot in order to reach a target position under three different feedback conditions. The experimental results revealed that the accuracy of the electrical stimulation feedback was close to that of the visual feedback, and that the electrical stimulation feedback contributed to the foot position control. These preliminary results revealed that the proposed walking control interface and the electrical stimulation feedback can be potentially applied to an exoskeleton operated by paraplegic patients.

Chapter 4

ZMP based gait modification for improving walking stability

The currently available exoskeleton for assisting the paraplegic patient in walking usually adapts a pre-programmed gait that involves the patient following an exoskeleton lead. The system allows the patient to hold a pair of canes in order to keep balance, and does not contribute to keeping balance without the patients action. This chapter introduces an algorithm based on the zero moment point (ZMP) to modify the gait generated through human walking synergy for paraplegic patients who make use of the exoskeleton system and hold their canes. The proposed ZMP will enable the paraplegic patient to keep balance during walking and also reduce the burden in maintaining balance. First, a pair of cane is used as an interface to control the user's walking and then, the synergy between legs and canes is used to synchronize the user's walking intention during the exoskeleton movement. The walking synergy is extracted from the able-bodied subject walking with a pair of canes and analyzed using principal component analysis (PCA). In order to improve the walking stability, the hip joint angle on stance leg during walking was modified based on ZMP. Furthermore, a nonlinear inverted pendulum (NIP) model was utilized in order to generate a gait with a fully stretched knee joint angle that is similar to human gait. The proposed method was verified via the Gazebo simulation using a walking robot to simulate a patient wearing an exoskeleton. The experiment results show that the walking stability was highly improved after gait modification.

4.1 Walking synergy for gait generation of exoskeleton

In recent years, research on the powered exoskeleton has become a hot topic. The rapid development of the exoskeleton has made great achievements in two aspects: (1) augmentation in human strength and durability. For example: Berkeley lower extremity exoskeleton is designed to increase human endurance and strength [85]. Quasi-passive leg utilizes only spring and damper to augment load-carrying during walking [86]. (2) restoration in the physical function of a disabled patient. For example: Roboknee determines user intent through the knee joint angle and ground reaction forces and allows the wearer to climb stairs [87]. Re-walk enables spinal cord injured patients to walk without human assistance [5]. NeuroRex uses non-invasive electroencephalography to decode a paraplegic patient motion intent and aid walking [65]. LOPES applied impedance control on joints to allow bidirectional mechanical interaction between robot and patient for gait rehabilitation [4].

Among the above-mentioned exoskeletons, exoskeletons for assisting the paraplegic patient have been widely used in scientific research, rehabilitation, and daily life. A paraplegic patient is a person who has lost the motor and sensory function of the lower body. The exoskeleton acts directly on the patient's body, supporting the user's weight and augment the strength as well as provides a high capability for the paraplegic patient to walk again. Sankai *et al*. [60] developed a well-known exoskeleton, hybrid assistive limb (HAL), to help physically challenged people to walk again. HAL uses electromyography to estimate the walking intention to support a paraplegic patient to walk. In [74], HAL detects a preliminary motion to enhance the transfer between standing and sitting for complete paraplegic patients. In [3], HAL infers the spinal cord injury patient's walking intention using the ground reaction force for gait support. In [63], HAL estimates the leg swing speed according to the walking velocity for restoring the gait of spinal cord injury patients. Besides, Ekso Bionics developed by Ekso measures the position of the user's center of gravity and estimates the walking intention of paraplegic patients by detecting the center of mass (CoM) transfer when their upper body is leaned forward [64].

All the above-mentioned exoskeletons adapt a pre-programmed joint trajectory for walk assistance. The user holds a pair of canes to keep balance which supports the exoskeleton's movements to walk. Although the start and stop of walking is controlled by the user incline the body, the user still needs to adjust the angle and fall point of the canes to cooperate with the gait of the exoskeleton. The pre-programmed trajectory method is

not the only solution to generate the exoskeleton movement. The researches about human walking synergy make non-pre-programmed trajectory generation possible.

Researches on human walking synergy have reported that human walking does not only involve a repetitive swing of legs but a highly coupled cooperative motion between upper and lower limbs. Matthew *et al.* examined the synergy between arms and legs in healthy adults by constraining one arm while walking in a treadmill [88]. Thierry *et al.* proved that the synergy between arms and legs exist not only during human walking but also in creeping and swing activities [89]. Jaclyn *et al.* studied the synergy between the arms and legs during cycling movement and stated that any contributions from the arms is functionally linked to locomotion" [90]. Volker *et al.* studied the synergy between arms and legs by measuring the electromyographic on leg and arms during walking [91]. Volker also studied the synergy between the arms and legs of patients suffering from movement disorders [92]. Besides, Principal component analysis (PCA) is often used to analyze human synergy to extract the coupling relationship between limbs. Daffertshofer *et al.* published a tutorial about how to apply PCA on moment data as feature extractor and as data-driven filter [93]. Todorov *et al.* analyzed the synergies underlying complex hand manipulation using PCA [94].

The human synergy also greatly contributed to the design and control of exoskeleton. Crocher *et al.* proposed a robot control approach that integrates an explicit model of inter-joint coordination based on a linear relationship between joint velocities [95, 96]. Liu developed a rehabilitation exoskeleton based on the postural synergy that allows the 10 degrees of freedom robot driven by only two actuators [97]. Hassan proposed an instrumented cane to help hemiplegic patients walk with the help of an exoskeleton [98–100]. Hemiplegic patients are patients who lost the motor and sensory function of half side of the body but another side remains functional. In their studies, the motion of the unaffected leg and cane were used to induce the motion of the affected leg. In our study, the target patient is paraplegic. Paraplegic patients are patients who lost the motor and sensory function of the lower body but the upper body remains functional. We researched the synergy between canes (arms) and legs and confirmed that by using the motion of canes will aid to generate the motion of legs for walking.

This chapter introduces the using of a cane as an interface to control the walk of a paraplegic patient wearing an exoskeleton. The walking synergy was extracted from a healthy subject and applied to synchronize the exoskeleton's movement with the user's intention. To improve the walking stability, the hip joint trajectory on the stance leg was modified using the zero moment point (ZMP). To generate a human-like gait, a non-linear

inverted pendulum (NIP) model was used to modify the walking trajectory generated by walking synergy. Therefore, our approach does not give additional operations to paraplegic patients. The proposed gait generation and modification method were validated by simulation using the Gazebo software. The major contribution in this paper is the gait modification method based on ZMP to improve the walking stability of a paraplegic patient wearing an exoskeleton. Using this system, the exoskeleton also contributes to the balance control, thus reduce the burden of keeping the balance of the patient while walking. The minor contribution of this paper is on the utilization of canes as an interface to synchronize the user's intention and leg motion. It is noteworthy to mention that using the cane as the interface does not increase the burden of the patients as the purpose is only to keep balance.

4.2 Gait generation based on walking synergy

The detail explanation of using principal component analysis (PCA) to analyze human walking synergy is described in [101, 102]. PCA combines the variables to derive new components and as a result produce a simpler description of the system. The matrix of the principal components (eigenvectors in descending order) is divided and rearranged to calculate the unknown variables from the known variables.

$$y = \Gamma^T x. \tag{4.1}$$

where Γ is the matrix of the eigenvectors in descending order concerning the eigenvalues. The original data x is mapped to the new data y after being multiplied by the liner transition matrix Γ^T. Since the Γ is an orthonormal matrix, then x could be rewritten as:

$$x = \Gamma y. \tag{4.2}$$

then Γ could be separated for the known variables x_1 and the unknown variables x_2:

$$x_1 = \Gamma_1 y, \quad x_2 = \Gamma_2 y. \tag{4.3}$$

where Γ_1 and Γ_2 are the separated matrix for the known and unknown variables, respectively. The unknown variables could be computed from the separated matrixes and the known variables:

$$x_2 = \Gamma_2 \Gamma_1^\sharp x_1. \tag{4.4}$$

Table 4.1: Ratio of principal components.

PC1	**PC2**	**PC3**	**PC4**	**PC5**	**PC6**
50.71%	37.74%	7.28%	2.83%	1.44%	0.01%

where $\Gamma_1^\sharp$ is the pseudo-inverse of Γ_1:

$$\Gamma_1^\sharp = (\Gamma_1^T \Gamma_1)^{-1} \Gamma_1^T. \tag{4.5}$$

In the case of a paraplegic patient, the matrix x is the data of joint angle from a subject walking with a cane, the known variable matrix x_1 is the joint angle of the upper limbs, and the unknown variable matrix x_2 is the joint trajectories of the lower limbs. Instead of applying the arm joint trajectories, the cane inclination were used as the known variable matrix x_1. In the case of this paper, the extracted synergy is contained in a 6 by 6 matrix, and each column corresponds to a principal component (PC). Each PC has a contribution ratio to the synergy, and we show the contribution ratio in Table 4.1. We chose PC1, PC2, and PC3 as the matrix Γ, where the first two rows are Γ_1 and the last four rows are Γ_2. In this way, the walking synergy was used as a gait generator, with the cane inclination angle as input, and the generator generates a joint angle of hip and knee. Therefore the x_1 and x_2 can be written as:

$$\begin{aligned} x_1 &= [\theta_l \quad \theta_r]^T, \\ x_2 &= [\theta_{sw}^h \quad \theta_{sw}^k \quad \theta_{sp}^h \quad \theta_{sp}^k]^T. \end{aligned} \tag{4.6}$$

where θ_l and θ_r are the left and right cane inclination angles. The θ_{sw}^h and θ_{sw}^k are the hip and knee joint angle of the swing leg, the θ_{sp}^h and θ_{sp}^k are the hip and knee joint angle of the support leg. The θ_{sp}^k will be replaced to improve the walking stability, and the method is introduced in following section.

Three subjects participated in this experiment and comprise of all-male, healthy, aged from 25 to 30 and without any history of movement disorder. The gait of the paraplegic patient wearing the exoskeleton was related to the degree of injury and the proficiency of exoskeleton used. A trained paraplegic patient with both unaffected arms can swing a cane and leg on the opposite side simultaneously during walking. The utilized gait is the fastest and the most efficient, therefore it becomes the target motion in this research and is used to extract the walking synergy. To mimic the walking conditions of the paraplegic patient, the subjects were asked to support the body with crutches as much as possible

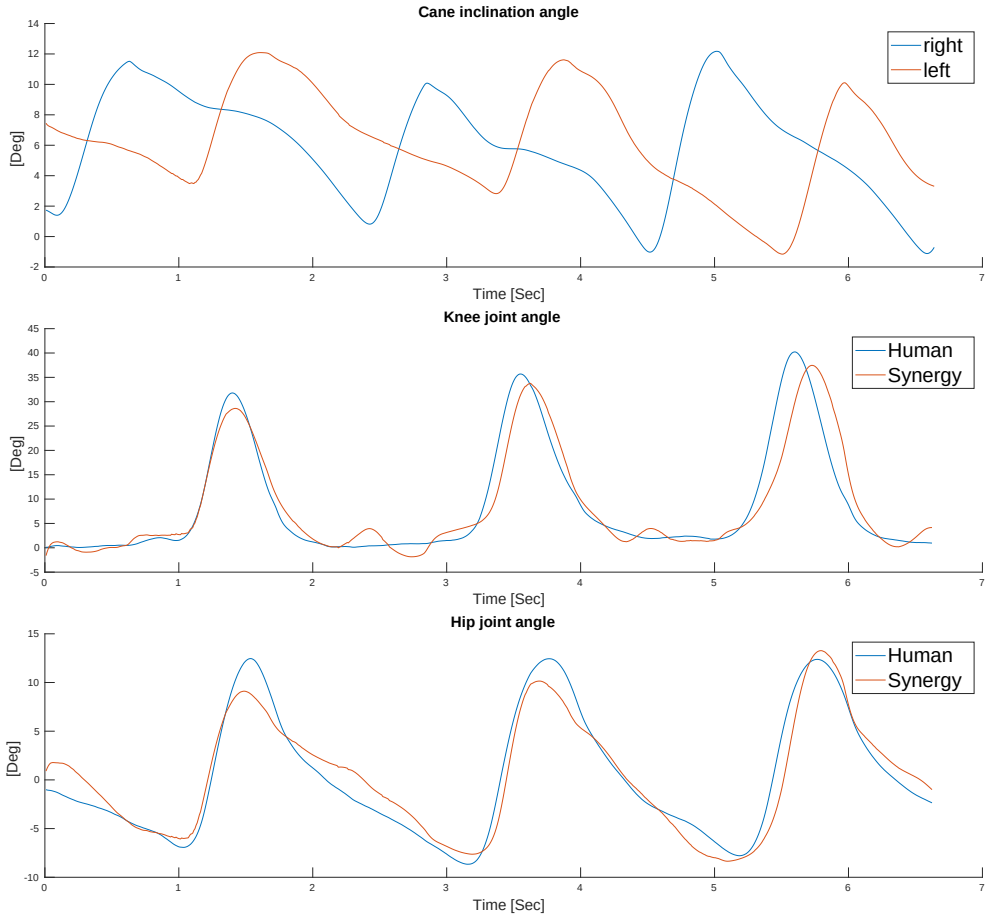

Figure 4.1: Comparison between human walking joint trajectory and walking joint angles generated using walking synergy.

during the walk while moving the cane with the leg on the opposite side simultaneously during walking.

The body kinematics was recorded using a 3D optical motion capture system (OptiTrack) at a frequency of 250 Hz. 16 infrared reactive markers were fixed on the lower body of the subject to record the walking movement and 3 markers on each cane to record the movement of canes. The 16 infrared reactive markers were fixed according to the conventional lower limb model, 2 on each foot, 1 on each ankle, 1 on each shank, 1 on each the knee, 1 on each thigh, and 4 on the waist.

Figure 4.1 shows the comparison between the joint angle of the human walk and the joint angle generated using walking synergy. For the hip joint angle, the mean error and the maximum errors are 1.51 [deg] and 5.47 [deg], respectively. In the case of the knee joint angle, the mean error and maximum errors are 2.54 [deg] and 15.96 [deg], respectively. The

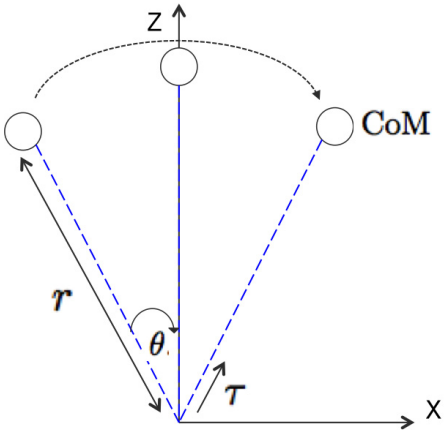

Figure 4.2: Nonlinear inverted pendulum model.

small discrepancy shows that the generated joint angle has high similarity with the joint of human walking.

4.3 Motion planning using NIP and ZMP

The ZMP is widely used for gait generation in a humanoid robot. For example, Philippe strictly defined the ZMP in [103], and Kajita used a preview control of ZMP for biped gait generation [104]. Linear inverted pendulum (LIP) model is widely used in the trajectory planning [105,106]. The LIP assumes a constant height for the center of mass (CoM) which results in a bent knee joint on the stance leg during gait. During the stance phase of the human walking the stance leg becomes fully extended, which makes the LIP model not in accordance with the natural human walking. In the present study we use a nonlinear inverted pendulum (NIP) to generate the CoM trajectory, subsequently, the leg joint angle can be obtained by solving the inverse kinematics. For the NIP, the length of the pendulum remains constant and the generated walking motion has a fully stretched knee joint on stance leg, which is similar to the human walking habit.

Figure 4.2 shows the nonlinear inverted pendulum (NIP) model. The inverted pendulum model has a constant length r, the CoM is assumed concentrated at the tip of the pendulum, and the angle between the pendulum and the vertical direction is θ. The position of the CoM can be written as follow:

$$x_M = r\ \sin(\theta),\ z_M = r\ \cos(\theta). \tag{4.7}$$

The zero moment point x_{ZMP} can be derived from this model:

$$\tau = m(g + \ddot{z}_M)(x_M - x_{ZMP}) + m\ddot{x}_M z_M. \tag{4.8}$$

where m is the mass at center, g is the gravitational acceleration, τ is the total external moment, x_M and z_M are the CoM position, $\ddot{x}_M$ and $\ddot{z}_M$ is the acceleration in the direction along the coordinate X and Z. The resultant moment τ at the zero moment point equals to zero can be written as:

$$\ddot{x}_M = \frac{\ddot{z}_M + g}{z_M}(x_M - x_{ZMP}). \tag{4.9}$$

Due to the high degree of nonlinearity, the differential equation (4.9) is difficult to find an analytical solution. Assume the Z_M is constant, this model becomes a linear inverted pendulum (LIP), and the solution can be written as:

$$\begin{aligned} x_M &= C_1 e^{\omega} + C_2 e^{-\omega} + x_{ZMP}, \\ \omega &= t/(z_M/g)^{\frac{1}{2}}. \end{aligned} \tag{4.10}$$

where z_M is a constant. Given the CoM position and walking cycle, as well as the reference ZMP, then the C_1 and C_2 can be determined, and the trajectory of CoM can be written as a function of time. From equation (4.7), we can obtain the below equation:

$$\theta = \sin^{-1}(\frac{x_M}{r}). \tag{4.11}$$

By substituting the solution (4.10) into the equation (4.11) and equation (4.7), we can get the trajectory of θ and z_M. Furthermore, by differentiating z_M we can get $\ddot{z}_M$. From equation (4.9), we can get:

$$x_{ZMP} = x_M - \frac{\ddot{x}_M z_M}{\ddot{z}_M + g}. \tag{4.12}$$

By substituting z_M and $\ddot{z}_M$ into the equation (4.12), we can get the trajectory of ZMP.

Figure 4.3 shows an example of CoM trajectory planning using a nonlinear inverted pendulum model. We calculated the difference between ZMP and reference ZMP for different pendulum lengths and step lengths. It was found that this difference is mainly related to the ratio between the step length and pendulum length. When the ratio is less than 0.5, there is almost no difference between ZMP and reference ZMP. When the ratio is above 0.5, an error is observed and the error increases with an increase in the ratio. In

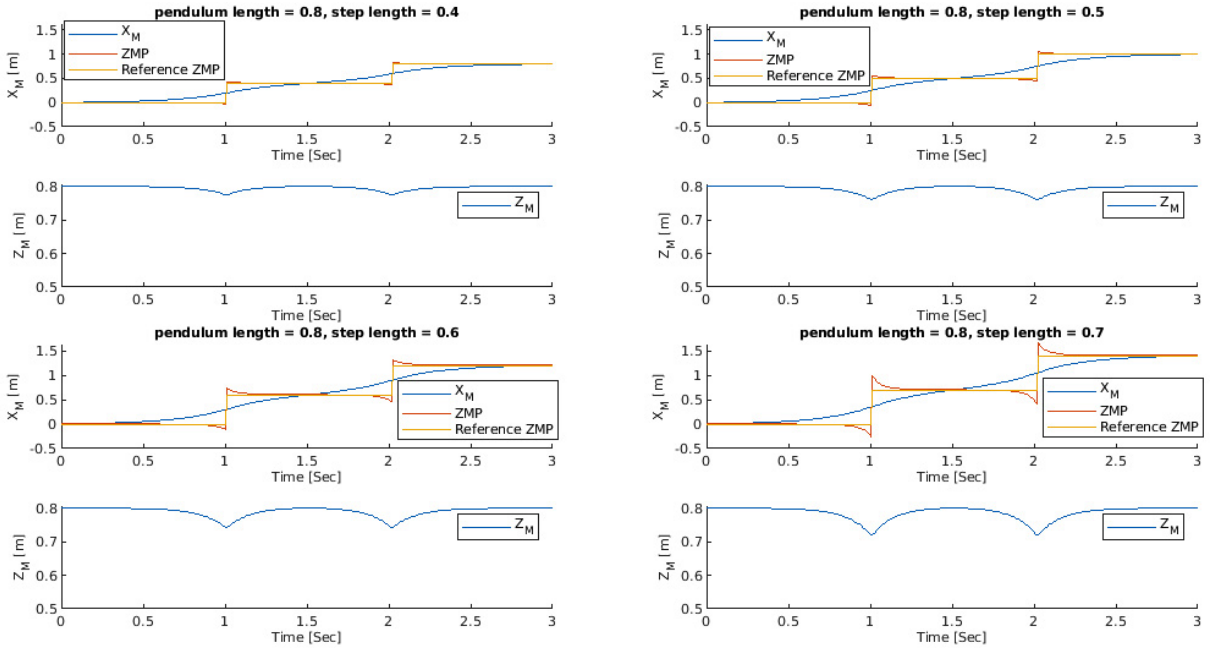

Figure 4.3: Example of ZMP planning using a nonlinear inverted pendulum model.

this case, it is necessary to judge whether the error has a significant effect on the stability of walking (i.e. whether the ZMP still falls within the supporting polygon). In this paper, the ratio is maintained at 0.5 or less.

4.4 Gait modification using NIP and ZMP

The walking gait generated from the walking synergy might not result in a fully stable walk due to the dynamic difference between the lower-limb exoskeleton and a human subject. Therefore, to make the walking synergy-based gait fits with the patient wearing the powered exoskeleton, we modified the walking gait by employing ZMP.

The walking synergy is used as a gait generator, with the motion of the cane as input and the walking synergy generates the joint angle of legs for walking. In the real case, the IMU sensor can be attached to the cane to measure its inclination. The NIP model can be used to generate a stable CoM trajectory, in which the resultant ZMP stays in the support polygon formed by the cane and foot. The key point is to use the NIP to generate a stance leg motion that is in accordance with the swing leg motion generated by walking synergy. The hip joint on stance leg is modified to improve the walking stability. We considered two points when using the ZMP to modify the walking motion: (1) The

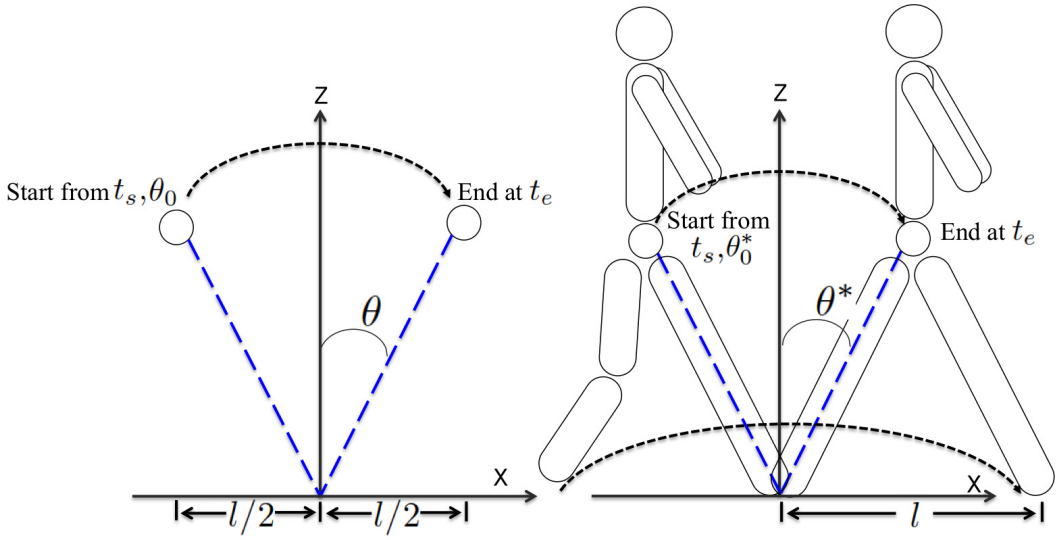

Figure 4.4: Relationship between pendulum and human walking in gait modification.

generated walking motion should have a fully stretched knee joint on stance leg which fits the human walking habit. (2) There should be no gap at the joint angle when the swing leg becomes a stance leg. When a human walks, the knee joint of stance leg is fully stretched. If the length of the NIP model equals the length of the leg when it is fully stretched, the walking motion generated using the NIP has a fully stretched knee joint on the stance leg. Given the walking cycle and step length, the hip joint trajectory of the stance leg can be generated using NIP. In addition, given the joint angle when the swing leg becomes the stance leg, the hip joint trajectory can be modified so that there exists no gap on the joint angle trajectory when the swing leg becomes the stance leg. The details can be described below.

Figure 4.4 shows the relationship between the pendulum and human walking in gait modification. The origin of the pendulum is at the contact point between the pendulum and ground while the origin of the human is at the contact point between the stance leg and ground. Assuming the step length of walking is l, and the CoM of the pendulum moves from $-l/2$ to $l/2$, the moment of the human to start a step and the pendulum to move is at time t_s, and the moment of the human to end the step and when the pendulum stops moving is at time t_e. By substituting the above-mentioned values into equation (4.10), we can get:

$$\begin{aligned} -l/2 &= C_1 a_1 + C_2 a_2 + x_{ZMP}, \\ l/2 &= C_1 a_3 + C_2 a_4 + x_{ZMP}. \end{aligned} \tag{4.13}$$

where the a_1, a_2, a_3 and a_4 are:

$$\begin{aligned} a_1 &= e^{-t_s/(z_M/g)^{\frac{1}{2}}}, \\ a_2 &= e^{t_s/(z_M/g)^{\frac{1}{2}}}, \\ a_3 &= e^{-t_e/(z_M/g)^{\frac{1}{2}}}, \\ a_4 &= e^{t_e/(z_M/g)^{\frac{1}{2}}}. \end{aligned} \tag{4.14}$$

Therefore, the parameters to determine the solution function of equation (4.10) can be obtained as follow:

$$\begin{aligned} C_1 &= \frac{a_2 l/2 + a_4 l/2}{a_1 a_4 - a_2 a_3}, \\ C_2 &= \frac{a_1 l/2 + a_3 l/2}{a_1 a_4 - a_2 a_3}. \end{aligned} \tag{4.15}$$

Using equation (4.11), we can convert the solution of equation (4.10) into an inclination angle of the pendulum θ. As shown in figure 4.4, assuming the hip joint angle on stance leg when a step is taken is θ_0^*, the inclination angle of the pendulum when it starts to move is θ_0, the modified hip joint angle trajectory of stance θ^* can be obtained by:

$$\theta^* = \theta - (\theta_0 - \theta_0^*). \tag{4.16}$$

where θ^* is used to replace the hip joint angle of support leg, θ_{sp}^h, which is mentioned in section 4.2.

Different from a fully programmed walking system, the time consumed and step length of each step are unknown in advance, and they may vary in each step. To use the ZMP to modify the hip joint trajectory on stance leg, the time consumed and the step length needs to be predicted in advance for each step.

Since walking is a highly coupled cooperative motion between upper and lower limbs, the walking cycle and step length can be related to the motion of cane. When the patient walks using a trot-like gait, the opposite leg and the cane starts and lands almost at the same time, and the relative distance between them is almost constant. In our method, the walking cycle and step length are predicted in each step using the angle change of the cane when the cane commenced moving. Walking cycle usually refers to the time consumed during walking and includes one left step and one right step. After prediction at the beginning of each step, half of the walking cycle was used as the time consumed to generate the walking motion using ZMP.

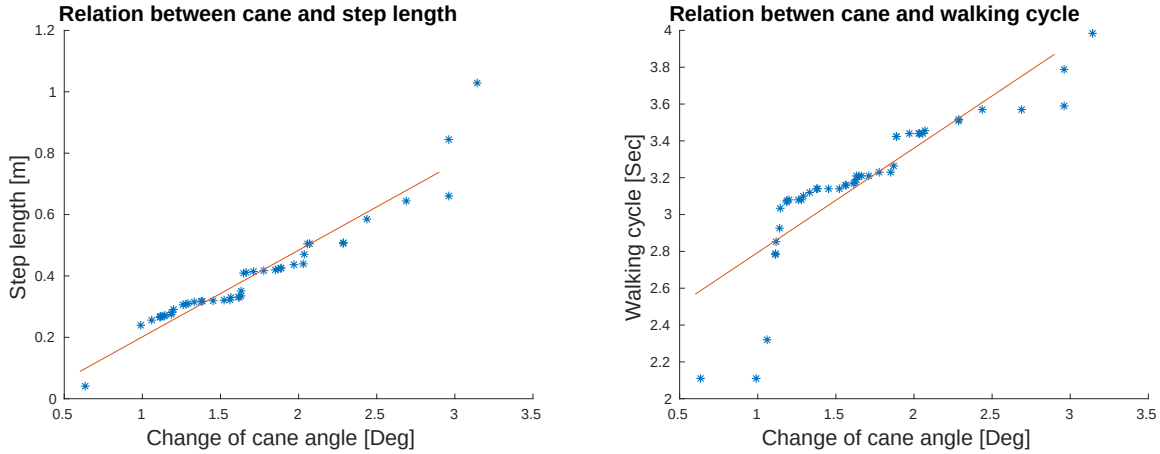

Figure 4.5: Walking cycle and step length prediction.

Figure 4.5 shows the relationship between the walking cycle and angular change of cane in 0.08 [s] as well as between step length and angular change of cane in 0.08 [s]. This Figure includes the data of 50 steps of three subjects walking with a cane. The x-axis is the angle change of the cane in 0.08 [s] after it starts to swing whereas the y-axis refers to the walking cycle and step length, respectively. The equation to predict the walking cycle and step length are obtained from this Figure and can be written as:

$$T = 0.567A_{cane} + 2.228. \tag{4.17}$$

$$S = 0.283A_{cane} - 0.081. \tag{4.18}$$

where T is the walking cycle and S is the step length, and A_{cane} is the angle change of the cane in 0.08[s] after it started to swing.

During walking, deviations between predictions and actual conditions may occur. The error of walking cycle prediction will cause the foot and the cane to land at different time. If the error is small, the stability of walking becomes unaffected. However, the error of step length prediction accumulates as the walking distance increases and needs to be corrected via compensation. To avoid the accumulation of errors, the error of the last step was compensated at the previous steps:

$$S'_K = S_K + E_{K-1}, \tag{4.19}$$

where S'_K is the step length updated in the current step, S_K is the step length predicted in the current step, E_{K-1} is the error measured in the last step.

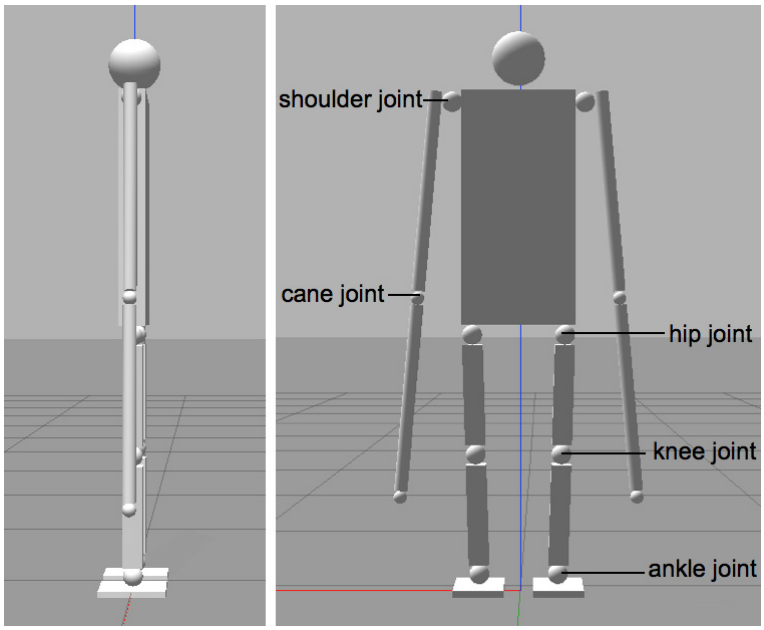

Figure 4.6: Walking robot replacing a patient for preliminary study.

Table 4.2: Parameters of walking robot.

Parameter/Part	Thigh	Lower	Foot	Body	Crutch
Mass[kg]	1.742	1.774	0.592	12.48	2.24
Length[cm]	33.3	32.75	20	73	134

4.5 Simulation and result

It is dangerous to conduct experiments with a paraplegic patient before validating the feasibility of the proposed method. Furthermore, an able-bodied subject cannot wear an exoskeleton to replace the patient used for validating experiments. Although able-bodied subjects can consciously imitate paraplegic patients and can subconsciously put force into their lower limbs to keep their balance when the risk of falling is high. Therefore, a walking robot was built to simulate a paraplegic patient wearing an exoskeleton to conduct a preliminary study for safety reasons.

Figure 4.6 shows the schematic illustrations of the walking robot. The inertia and link lengths of the lower body are shown in Table 4.2. The robot height is 180 [cm] while the width is 70 [cm]. The weight of the walking robot is 25 [kg] with 16 degrees of freedom. The movable joints are the shoulder joints, hip joints, knee joints, and ankle joints. Each

leg has six degrees of freedom, the hip has three degrees of freedom, the knee has one degree of freedom, the ankle has two degrees of freedom. The shoulder has one degree of freedom, and the crutches can be stretched and shortened meanwhile the robot can adjust its center of gravity to maintain balance. Each joint of the robot is equipped with an encoder that measures the joint angle during the experiments. To measure the ZMP during walking, a six-axis F/T sensor was installed at the ankle joint.

We performed a robot walking experiment during the simulation to verify the feasibility of the proposed method. The walking was divided into the walking phase and stance phase. The walking phase is a single-support phase while the stance leg supports the body weight and swing leg in the air for step taking. The transfer of the CoM happens at the walking phase and the stance legs aid the CoM to move forward. The stance phase is a double-support phase and both legs support the body weight. This is a transitional phase, in which the robot remains still and does not transfer its CoM. In the simulation, the stance phase takes 1 [sec] and the time consumed at the walking phase is related to the cane motion and its walking cycle.

We compared the robot walking with and without gait modification. In the case of robot walking without gait modification, the motion of the cane was extracted from a subject walking with a cane, and the gait was generated by human walking synergy using the cane motion as input. In the case of the robot walking with gait modification (modified using ZMP), the motion of the cane was extracted from a subject walking with a cane, the gait was generated by human walking synergy using the cane motion as input and was modified using ZMP.

Figure 4.7 shows the simulation scene of robot walking with gait modification. The upper image in figure 4.7 is the front view of the robot walking and the lower image in figure 4.7 is the side view of the robot walking. In a real case scenario, the exoskeleton is an under-actuated system, it has degrees of freedom in the sagittal and lateral plane, but it only provides support in the sagittal plane. In the simulation, the balance in the lateral plane was kept by the cane.

Figure 4.8 shows the ZMP measurement in sagittal direction of the walking experiment. The upper image in figure 4.8 is the ZMP of robot walking with gait modification. The lower image in figure 4.8 is the ZMP of robot walking without gait modification. In the case of robot walking with gait modification, the maximum error between ZMP and reference ZMP was 0.204 [m] with an average error of 0.028 [m]. Errors mostly occur when the robot takes a step and the ZMP gradually converges to the reference ZMP. This is mainly due to the robot change from stationary to motion, and the maintenance of balance is changed

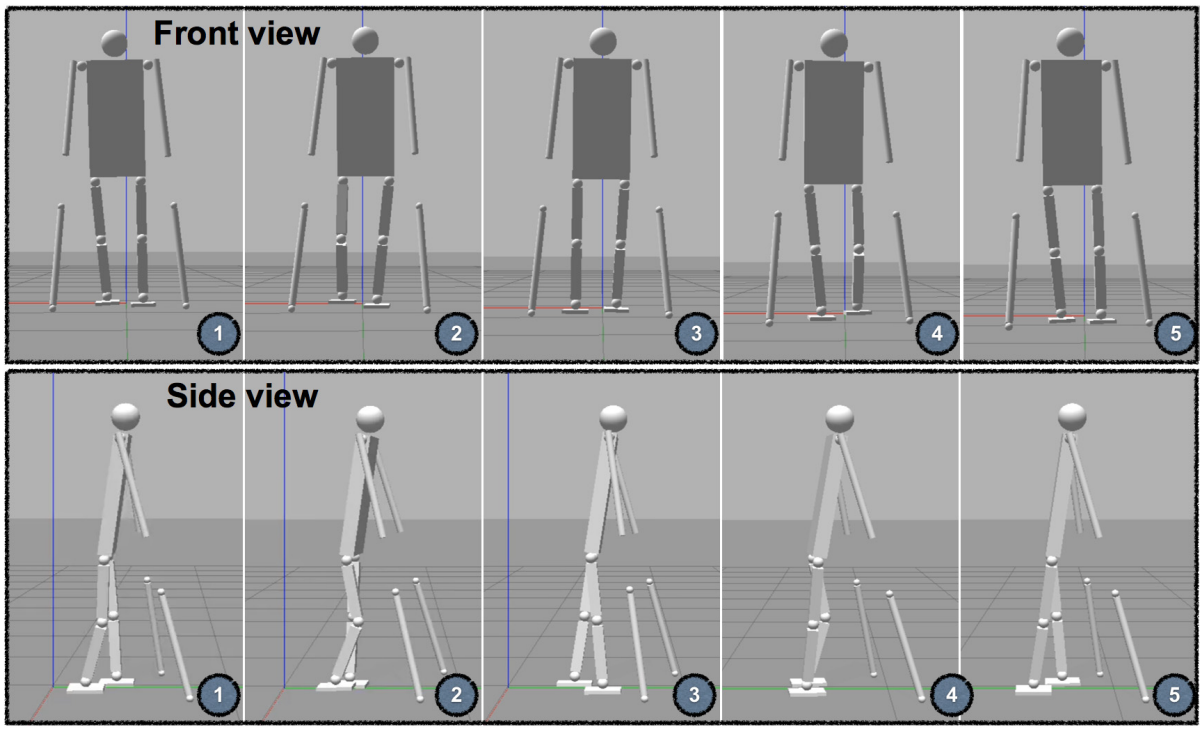

Figure 4.7: Simulation scene of robot walking.

from 4-point to 2-point support. Although there is a difference between the ZMP and the reference ZMP, the ZMP always stays in the support polygon while preventing the robot from falling. In the case of walking without gait modification, the maximum error between ZMP and reference ZMP was 0.434 [m] with an average error of 0.050 [m]. Errors mostly occur when the robot takes a step with no convergence of ZMP to the reference ZMP, leading the robot to fall within six steps. It can be seen from these experimental results that gait modification greatly improved the walking stability.

Figure 4.9 shows the ZMP measurement in lateral direction of robot walking with gait modification. Since we found in the pre-experiment that the robot usually falls in the sagittal direction, we didn't apply ZMP-based trajectory planning and gait modification in the lateral motion control. The robot uses a simple left-right-swing method to shift the center of gravity and maintain balance. As shown in Figure 4.9, the maximum error between ZMP and reference ZMP was 0.071 [m] with an average error of 0.014 [m].

Figure 4.10 shows the energy consumption of the walking experiment. The blue line represents the energy consumption of robot walking with gait modification. The red line represents the energy consumption of robot walking without gait modification. It can be

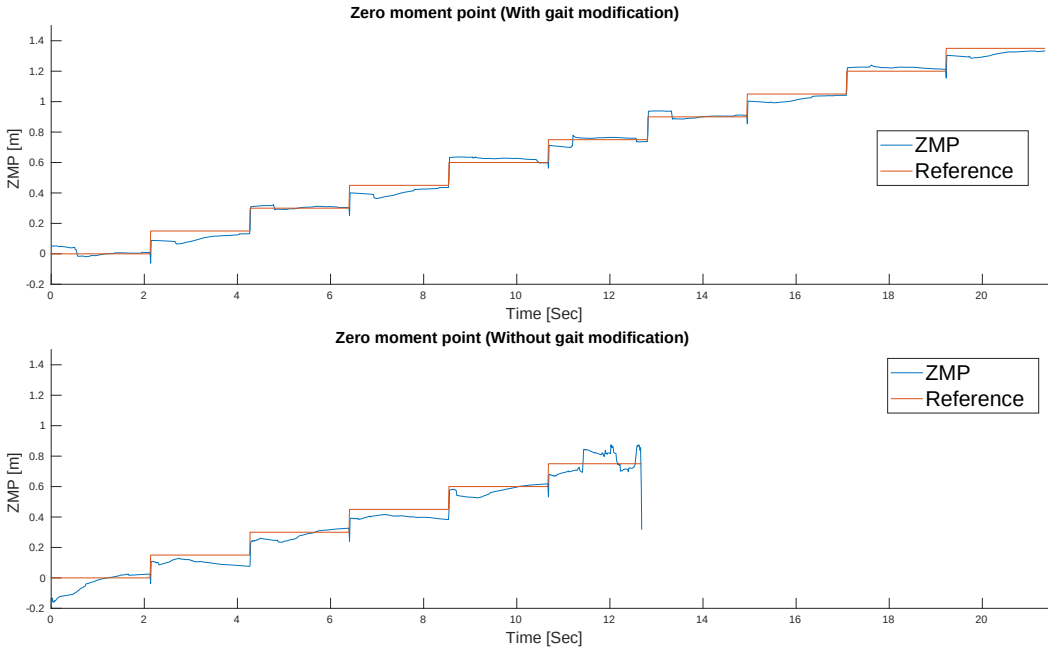

Figure 4.8: Stability comparison between robot walking with and without gait modification in sagittal direction.

seen that the energy consumption after gait correction is smaller than the energy consumption before gait correction. This is because without gait modification, the robot consumes more energy to maintain balance. Through calculation, the gait modification can save 17.46% of energy for walking on average.

Figure 4.11 shows the hip and knee joint angles during one walking cycle. From top to bottom is the inclination angle of the cane, the knee joint angle, and the hip joint angle. The blue line represents the joint trajectory extracted from human walking with a cane. The red line represents the joint trajectory generated by human walking synergy. The yellow line represents the joint trajectory generated by human walking synergy and modified using ZMP. Either the joint trajectory generated by human walking synergy or the joint trajectory modified using ZMP was close to the joint trajectory extracted from human walking with a cane.

4.6 Discussion

There are three important points for assistive control of lower-limb exoskeleton to assist a paraplegic patient during walking: (1) synchronization of exoskeleton's motion and user

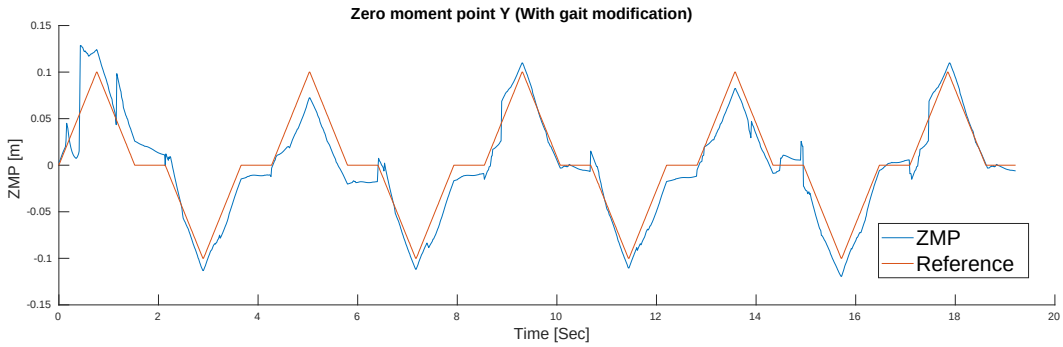

Figure 4.9: ZMP measurement in lateral direction of robot walking with gait modification.

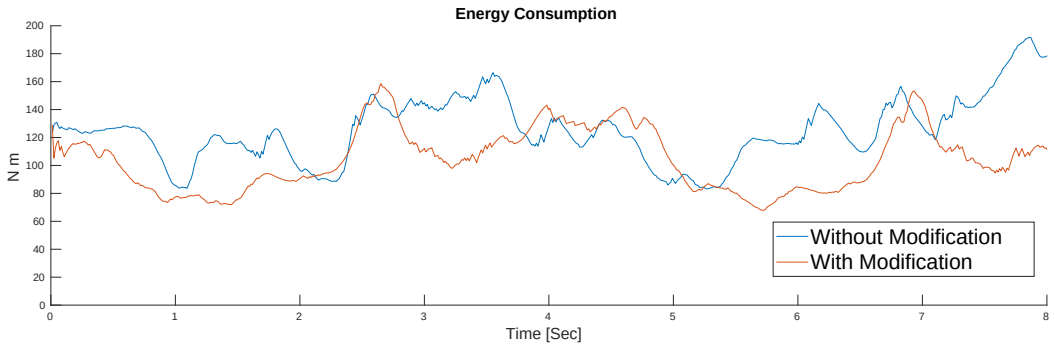

Figure 4.10: Energy consumption comparison between robot walking with and without gait modification.

walking intention, (2) human-like gait generation and (3) walking stability.

The use of human walking synergy to generate gait can solve the problems of synchronization between user intention and exoskeleton motion as well as human-like gait. Firstly, the leg motion generated by human walking synergy was completely synchronized with the motion of the cane. The motion of the cane was coupled with the motion of lower limbs, and it is controlled by the user and therefore reacts with the intention of the user. Secondly, the leg motion generated by human walking synergy is similar to the human walking motion. The walking motion generated in this way is natural and compatible.

The use of ZMP to modify the walking motion solves the stability problem. Firstly, the walking trajectory generated using ZMP becomes stable. Theoretically, The ZMP stays inside the support polygon thereby enabling the exoskeleton to keep stable during walking. Secondly, the robot is also involved in maintaining balance. In this case, the patients no longer rely solely on canes to maintain balance, as a consequence reduce the burden on

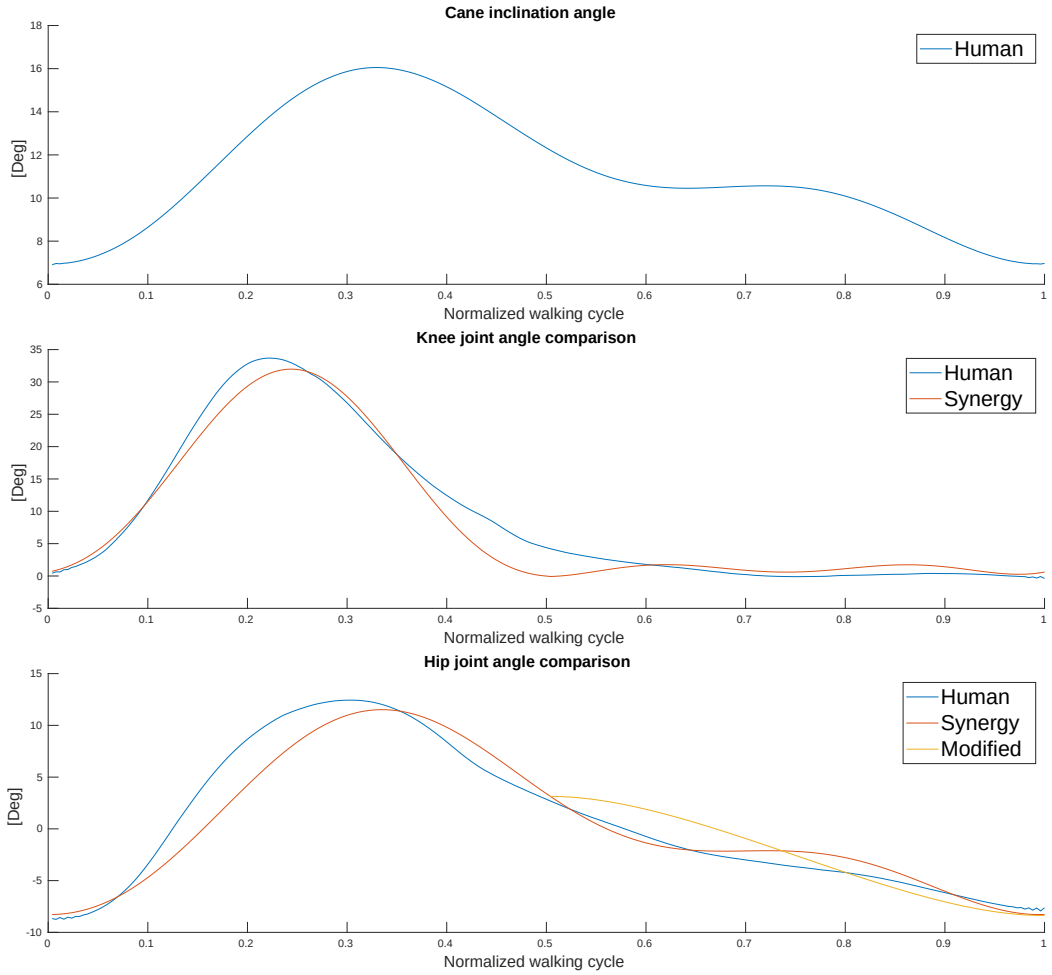

Figure 4.11: Comparison of human gait, gait generated suing synergy and modified gait.

patients.

The use of NIP ensures that the modified walking trajectory is similar to the human walking trajectory. For rapid generation and easy calculation, a combination of a linear inverted pendulum (LIP) and ZMP is often used to generate the walking trajectory in robot gait planning. However, the walking motion generated using LIP has a constant height of CoM, which is inconsistent with the walking characteristics of humans. The use of NIP makes up for this shortcoming, thereby enables the modified trajectory to conform to human walking habits.

4.7 Summary

This chapter proposes an algorithm via the modification of gait generated based on walking synergy to estimate motion intention and control powered lower-limb exoskeleton. This proposed system treats the cane as an interface between the user and the exoskeleton. The cane motion was used to generate the walking motion using walking synergy. The walking synergy was extracted from the movement trajectory of a healthy subject walking with a pair of canes. This synergy synchronizes the walking motion and the intention of user. The zero moment point (ZMP) was used to modify the walking motion to enhance the walking stability. To enable the modified walking motion in imitating the human walking habits, the nonlinear inverted pendulum model for trajectory planning was applied. Instead of a real patient wearing an exoskeleton, a cane robot was used for the Gazebo simulation. The experimental result shows that the gait modification significantly improved the walking stability, and the use of nonlinear inverted pendulum model resulted to a joint trajectory that is similar to the joint trajectory of human walking.

Chapter 5

Conclusion

Human in the loop is a popular concept appeared in recent decades. It requires sufficient feedback when a human is in charge of the movement of a robot, such as using prostheses, wearable exoskeleton, or in the case of teleoperation. The operator controls the movement of the robot at will and receives the robot's response to the environment in real-time. This study proposed the walking control interface and electrical stimulation feedback that provides a control authority and spatial location feedback to paraplegic patients for walking with the help of an exoskeleton. Besides, our work considers walking stability when synchronizing the walking motion and walking intention.

5.1 Contributions

The first contribution is the wearable walking control interface which enables the paraplegic exoskeleton user to voluntarily control the walking trajectory. The second contribution is the use of electrical stimulation to inform the user regarding the foot position. With the progressing of the research, we improved the control dimensionality as well as feedback scope and precision step by step. The third contribution is the improved walking stability while the exoskeleton motion and user walking intention are synchronized through walking synergy during walking.

In chapter two, the first generation of the wearable walking control interface and of the electrical stimulation pattern was introduced. The interface realized a one-dimensional foot position control of the walking robot, that is, controls the foot of the walking robot moves forward or backward through index fingers. Correspondingly, the electrical stimulation effects on fingertips to inform the user regarding the foot position. The electrode arrays have 22 stimulation positions. Each position that represents the foot position can evoke a

tactile sensation by electrical stimulation. The user distinguishes the stimulation position to understand the foot position. A series of robot walking experiments were implemented to validate the electrical stimulation for assisting the walking control. The experiment results show that by using electrical stimulation feedback the step length becomes more consistent compared with the case of no feedback. In addition, there is no significant difference between visual feedback to assist the waling and the electrical stimulation feedback to assist the walking.

In chapter three, the second generation of the wearable walking control interface realized a two-dimensional control. The user could control the step length and step height in real-time via the interface. It means the user is in charge of the walking trajectory and could adjust it before the foot landed on the ground. Correspondingly, the stimulation pattern also updated to convey the two-dimensional foot position for the user. Besides using the continuous stimulation, we added two another stimulation ratio to represent the foot position. The workspace of robot foot was divided into three subspaces. The three subspace was mapped to electrode array in different stimulation ratio. In this manner, one electrode array was used to represent the workspace usually represented by three electrode arrays. Each subspace was divided into 20 pieces that mapped to 20 stimulation position on the electrode array. In this manner, the workspace of the robot foot was expressed by using electrical stimulation changing stimulation ratio and stimulation position. A series of robot walking experiment was implemented to validate the interface and the cooperation between the user and the robot for walking. In addition, a series target reaching experiment was implemented to evaluate the precision of the electrical stimulation to assist the foot position control.

In chapter four, the walking motion was generated based on human walking synergy which synchronized the walking motion and walking intention. Our method does not only consider the synchronization between exoskeleton walking motion and user walking intention, but also the stability while walking. The trajectory generated using synergy is updated by a trajectory optimization method basing on zero moment point and a nonlinear inverted pendulum model. In this manner, the robot also takes part of the responsibility of balance keeping while walking. This greatly reduces the patient's burden when walking.

5.2 Remaining issues

For walking control interface and electro-tactile feedback: During the walking controlled by the interface, the can keep still until a step is taken. This walking method has a good

balance, but walking is not continuous, and walking speed is slow. When the cane and legs move at the same time, whether the balance can still be kept without affecting the use of the interface is a subject that needs to be explored.

For ZMP-based gait modification: The traditional lower extremity exoskeleton uses a pre-planned walking trajectory. Its walking can be controlled in terms of when to start and stop, and the walking speed. Walking with a pre-planned trajectory is continuous. However in our method, it is necessary to predict the landing point and walking cycle of each step before lifting the foot, the walking action generated by the proposed method is step-by-step. This step-by-step walking may make the paraplegic patient feel safe to use the exoskeleton at the early stage of rehabilitation, but for patients who are familiar with the exoskeleton, walking might feel unnatural.

All verification experiments in this work are done using walking robots or in a simulation environment. Although the robot is designed according to the proportion of the human body and the weight distribution of the human body, there are still some differences between its parameters and the actual patient. There are also certain differences between the verification experiment using robots and the actual walking of patients wearing exoskeletons, For example, the human body has a certain elasticity, and the robot is a rigid body, and each step of contact with the ground is hard. Therefore, it is necessary to use exoskeletons and patients for trials in the future

5.3 Future directions

In summary, the future research direction is dedicated to solving the following problems:

(1) Continuity of walking should be improved to better conform to the walking habits of humans. At the same time, the increase in walking speed should not affect the stability of walking and the use of control interfaces and the reception of feedback information.

(2) The experiment in simulation or with a simulator is different from a real situation, experiment implementation with a paraplegic patient wearing the exoskeleton should be carried out to further investigate the feasibility of using a control interface with electrotactile feedback for gait control, and the gait modification method.

Bibliography

[1] https://www.christopherreeve.org/living-with-paralysis/stats-about-paralysis/.

[2] https://www.spinalcure.org.au/research/sci-facts/.

[3] A. Tsukahara, Y. Hasegawa, K. Eguchi, and Y. Sankai, "Restoration of gait for spinal cord injury patients using hal with intention estimator for preferable swing speed," *IEEE Transactions on neural systems and rehabilitation engineering*, vol. 23, no. 2, pp. 308–318, 2015.

[4] J. F. Veneman, R. Kruidhof, E. E. Hekman, R. Ekkelenkamp, E. H. Van Asseldonk, and H. Van Der Kooij, "Design and evaluation of the lopes exoskeleton robot for interactive gait rehabilitation," *IEEE Transactions on Neural Systems and Rehabilitation Engineering*, vol. 15, no. 3, pp. 379–386, 2007.

[5] A. Esquenazi, M. Talaty, A. Packel, and M. Saulino, "The rewalk powered exoskeleton to restore ambulatory function to individuals with thoracic-level motor-complete spinal cord injury," *American journal of physical medicine & rehabilitation*, vol. 91, no. 11, pp. 911–921, 2012.

[6] Y. Mao and S. K. Agrawal, "Design of a cable-driven arm exoskeleton (carex) for neural rehabilitation," *IEEE Transactions on Robotics*, vol. 28, pp. 922–931, Aug 2012.

[7] J. C. Perry, J. Rosen, and S. Burns, "Upper-limb powered exoskeleton design," *IEEE/ASME transactions on mechatronics*, vol. 12, no. 4, pp. 408–417, 2007.

[8] T. Nef, V. Klamroth-Marganska, U. Keller, and R. Riener, "Three-dimensional multi-degree-of-freedom arm therapy robot (armin)," in *Neurorehabilitation technology*, pp. 351–374, Springer, 2016.

[9] T. Nef, M. Mihelj, G. Colombo, and R. Riener, "Armin-robot for rehabilitation of the upper extremities," in *Proceedings 2006 IEEE International Conference on Robotics and Automation, 2006. ICRA 2006.*, pp. 3152–3157, IEEE, 2006.

[10] M. Mihelj, T. Nef, and R. Riener, "Armin-toward a six dof upper limb rehabilitation robot," in *The First IEEE/RAS-EMBS International Conference on Biomedical Robotics and Biomechatronics, 2006. BioRob 2006.*, pp. 1154–1159, IEEE, 2006.

[11] M. Mihelj, T. Nef, and R. Riener, "Armin ii-7 dof rehabilitation robot: mechanics and kinematics," in *Proceedings 2007 IEEE International Conference on Robotics and Automation*, pp. 4120–4125, IEEE, 2007.

[12] T. Nef, M. Guidali, and R. Riener, "Armin iii–arm therapy exoskeleton with an ergonomic shoulder actuation," *Applied Bionics and Biomechanics*, vol. 6, no. 2, pp. 127–142, 2009.

[13] A. Frisoli, F. Rocchi, S. Marcheschi, A. Dettori, F. Salsedo, and M. Bergamasco, "A new force-feedback arm exoskeleton for haptic interaction in virtual environments," in *First Joint Eurohaptics Conference and Symposium on Haptic Interfaces for Virtual Environment and Teleoperator Systems. World Haptics Conference*, pp. 195–201, IEEE, 2005.

[14] A. Ruiz, A. Forner-Cordero, E. Rocon, and J. L. Pons, "Exoskeletons for rehabilitation and motor control," in *The First IEEE/RAS-EMBS International Conference on Biomedical Robotics and Biomechatronics, 2006. BioRob 2006.*, pp. 601–606, IEEE, 2006.

[15] E. Rocon, A. Ruiz, J. L. Pons, J. M. Belda-Lois, and J. Sánchez-Lacuesta, "Rehabilitation robotics: a wearable exo-skeleton for tremor assessment and suppression," in *Proceedings of the 2005 IEEE International Conference on Robotics and Automation*, pp. 2271–2276, IEEE, 2005.

[16] T. Lenzi, S. De Rossi, N. Vitiello, A. Chiri, S. Roccella, F. Giovacchini, F. Vecchi, and M. C. Carrozza, "The neuro-robotics paradigm: Neurarm, neuroexos, handexos," in *2009 Annual International Conference of the IEEE Engineering in Medicine and Biology Society*, pp. 2430–2433, IEEE, 2009.

[17] N. Vitiello, T. Lenzi, S. Roccella, S. M. M. De Rossi, E. Cattin, F. Giovacchini, F. Vecchi, and M. C. Carrozza, "Neuroexos: A powered elbow exoskeleton for physical rehabilitation," *IEEE Transactions on Robotics*, vol. 29, no. 1, pp. 220–235, 2012.

[18] H. Kazerooni, J.-L. Racine, L. Huang, and R. Steger, "On the control of the berkeley lower extremity exoskeleton (bleex)," in *Proceedings of the 2005 IEEE international conference on robotics and automation*, pp. 4353–4360, IEEE, 2005.

[19] A. B. Zoss, H. Kazerooni, and A. Chu, "Biomechanical design of the berkeley lower extremity exoskeleton (bleex)," *IEEE/ASME Transactions on mechatronics*, vol. 11, no. 2, pp. 128–138, 2006.

[20] K. Suzuki, G. Mito, H. Kawamoto, Y. Hasegawa, and Y. Sankai, "Intention-based walking support for paraplegia patients with robot suit hal," *Advanced Robotics*, vol. 21, no. 12, pp. 1441–1469, 2007.

[21] Y. Sankai, "Hal: Hybrid assistive limb based on cybernics," in *Robotics research*, pp. 25–34, Springer, 2010.

[22] A. Esquenazi, M. Talaty, A. Packel, and M. Saulino, "The rewalk powered exoskeleton to restore ambulatory function to individuals with thoracic-level motor-complete spinal cord injury," *American journal of physical medicine & rehabilitation*, vol. 91, no. 11, pp. 911–921, 2012.

[23] M. Talaty, A. Esquenazi, and J. E. Briceno, "Differentiating ability in users of the rewalk tm powered exoskeleton: An analysis of walking kinematics," in *2013 IEEE 13th international conference on rehabilitation robotics (ICORR)*, pp. 1–5, IEEE, 2013.

[24] K. A. Strausser and H. Kazerooni, "The development and testing of a human machine interface for a mobile medical exoskeleton," in *2011 IEEE/RSJ International Conference on Intelligent Robots and Systems*, pp. 4911–4916, IEEE, 2011.

[25] A. T. Asbeck, R. J. Dyer, A. F. Larusson, and C. J. Walsh, "Biologically-inspired soft exosuit," in *2013 IEEE 13th International Conference on Rehabilitation Robotics (ICORR)*, pp. 1–8, IEEE, 2013.

[26] A. T. Asbeck, S. M. De Rossi, K. G. Holt, and C. J. Walsh, "A biologically inspired soft exosuit for walking assistance," *The International Journal of Robotics Research*, vol. 34, no. 6, pp. 744–762, 2015.

[27] H. K. Kwa, J. H. Noorden, M. Missel, T. Craig, J. E. Pratt, and P. D. Neuhaus, "Development of the ihmc mobility assist exoskeleton," in *2009 IEEE International Conference on Robotics and Automation*, pp. 2556–2562, IEEE, 2009.

[28] P. D. Neuhaus, J. H. Noorden, T. J. Craig, T. Torres, J. Kirschbaum, and J. E. Pratt, "Design and evaluation of mina: A robotic orthosis for paraplegics," in *2011 IEEE International Conference on Rehabilitation Robotics*, pp. 1–8, IEEE, 2011.

[29] G. A. Pratt and M. M. Williamson, "Series elastic actuators," in *Proceedings 1995 IEEE/RSJ International Conference on Intelligent Robots and Systems. Human Robot Interaction and Cooperative Robots*, vol. 1, pp. 399–406, IEEE, 1995.

[30] T. Yan, M. Cempini, C. M. Oddo, and N. Vitiello, "Review of assistive strategies in powered lower-limb orthoses and exoskeletons," *Robotics and Autonomous Systems*, vol. 64, pp. 120–136, 2015.

[31] Y. Yu, W. Liang, and Y. Ge, "Jacobian analysis for parallel mechanism using on human walking power assisting," in *2011 IEEE International Conference on Mechatronics and Automation*, pp. 282–288, IEEE, 2011.

[32] Y. Yu, D. Yoshimitsu, S. Tsujio, and R. Hayashi, "Power assist system with power-damped operation information feedbacking," in *2007 IEEE International Conference on Robotics and Biomimetics (ROBIO)*, pp. 1709–1714, IEEE, 2007.

[33] G. Aguirre-Ollinger, J. E. Colgate, M. A. Peshkin, and A. Goswami, "Inertia compensation control of a one-degree-of-freedom exoskeleton for lower-limb assistance: Initial experiments," *IEEE Transactions on Neural Systems and Rehabilitation Engineering*, vol. 20, no. 1, pp. 68–77, 2012.

[34] J. E. Pratt, B. T. Krupp, C. J. Morse, and S. H. Collins, "The roboknee: an exoskeleton for enhancing strength and endurance during walking," in *IEEE International Conference on Robotics and Automation, 2004. Proceedings. ICRA'04. 2004*, vol. 3, pp. 2430–2435, IEEE, 2004.

[35] A. Polinkovsky, R. J. Bachmann, N. I. Kern, and R. D. Quinn, "An ankle foot orthosis with insertion point eccentricity control," in *2012 IEEE/RSJ International Conference on Intelligent Robots and Systems*, pp. 1603–1608, IEEE, 2012.

[36] A. Gams, T. Petrič, T. Debevec, and J. Babič, "Effects of robotic knee exoskeleton on human energy expenditure," *IEEE Transactions on Biomedical Engineering*, vol. 60, no. 6, pp. 1636–1644, 2013.

[37] H. Takemura, T. Onodera, D. Ming, and H. Mizoguchi, "Design and control of a wearable stewart platform-type ankle-foot assistive device," *International Journal of Advanced Robotic Systems*, vol. 9, no. 5, p. 202, 2012.

[38] B. G. Do Nascimento, C. B. S. Vimieiro, D. A. P. Nagem, and M. Pinotti, "Hip orthosis powered by pneumatic artificial muscle: Voluntary activation in absence of myoelectrical signal," *Artificial organs*, vol. 32, no. 4, pp. 317–322, 2008.

[39] C. L. Lewis and D. P. Ferris, "Invariant hip moment pattern while walking with a robotic hip exoskeleton," *Journal of biomechanics*, vol. 44, no. 5, pp. 789–793, 2011.

[40] W.-Y. Lai, H. Ma, W.-H. Liao, D. T.-P. Fong, and K.-M. Chan, "Hip-knee control for gait assistance with powered knee orthosis," in *2013 IEEE International Conference on Robotics and Biomimetics (ROBIO)*, pp. 762–767, IEEE, 2013.

[41] A. N. Spring, J. Kofman, and E. D. Lemaire, "Design and evaluation of an orthotic knee-extension assist," *IEEE Transactions on Neural Systems and Rehabilitation Engineering*, vol. 20, no. 5, pp. 678–687, 2012.

[42] K. Kim, C.-H. Yu, G.-Y. Jeong, M. Heo, and T.-K. Kwon, "Analysis of the assistance characteristics for the knee extension motion of knee orthosis using muscular stiffness force feedback," *Journal of Mechanical Science and Technology*, vol. 27, no. 10, pp. 3161–3169, 2013.

[43] N. Karavas, A. Ajoudani, N. Tsagarakis, J. Saglia, A. Bicchi, and D. Caldwell, "Tele-impedance based stiffness and motion augmentation for a knee exoskeleton device," in *2013 IEEE International Conference on Robotics and Automation*, pp. 2194–2200, IEEE, 2013.

[44] C. Fleischer and G. Hommel, "A human–exoskeleton interface utilizing electromyography," *IEEE Transactions on Robotics*, vol. 24, no. 4, pp. 872–882, 2008.

[45] K. Kiguchi, T. Tanaka, and T. Fukuda, "Neuro-fuzzy control of a robotic exoskeleton with emg signals," *IEEE Transactions on fuzzy systems*, vol. 12, no. 4, pp. 481–490, 2004.

[46] Y. H. Yin, Y. J. Fan, and L. D. Xu, "Emg and epp-integrated human–machine interface between the paralyzed and rehabilitation exoskeleton," *IEEE Transactions on Information Technology in Biomedicine*, vol. 16, no. 4, pp. 542–549, 2012.

[47] Y. Nam, B. Koo, A. Cichocki, and S. Choi, "Gom-face: Gkp, eog, and emg-based multimodal interface with application to humanoid robot control," *IEEE Transactions on Biomedical Engineering*, vol. 61, no. 2, pp. 453–462, 2014.

[48] D. P. McMullen, G. Hotson, K. D. Katyal, B. A. Wester, M. S. Fifer, T. G. McGee, A. Harris, M. S. Johannes, R. J. Vogelstein, A. D. Ravitz, *et al.*, "Demonstration of a semi-autonomous hybrid brain–machine interface using human intracranial eeg, eye tracking, and computer vision to control a robotic upper limb prosthetic," *IEEE Transactions on Neural Systems and Rehabilitation Engineering*, vol. 22, no. 4, pp. 784–796, 2014.

[49] J. Ma, Y. Zhang, A. Cichocki, and F. Matsuno, "A novel eog/eeg hybrid human–machine interface adopting eye movements and erps: Application to robot control," *IEEE Transactions on Biomedical Engineering*, vol. 62, no. 3, pp. 876–889, 2015.

[50] K. A. Kaczmarek, J. G. Webster, P. Bach-y Rita, and W. J. Tompkins, "Electrotactile and vibrotactile displays for sensory substitution systems," *IEEE Transactions on Biomedical Engineering*, vol. 38, no. 1, pp. 1–16, 1991.

[51] D. Pamungkas and K. Ward, "Electro-tactile feedback system to enhance virtual reality experience," 2016.

[52] D. S. Pamungkas and K. Ward, "Tele-operation of a robot arm with electro tactile feedback," in *2013 IEEE/ASME International Conference on Advanced Intelligent Mechatronics*, pp. 704–709, IEEE, 2013.

[53] D. Pamungkas and K. Ward, "Immersive teleoperation of a robot arm using electro-tactile feedback," in *2015 6th International Conference on Automation, Robotics and Applications (ICARA)*, pp. 300–305, IEEE, 2015.

[54] D. Pamungkas and K. Ward, "Tactile sensing system using electro-tactile feedback," in *2015 6th International Conference on Automation, Robotics and Applications (ICARA)*, pp. 295–299, IEEE, 2015.

[55] H. A. Alejandro, R. Kato, H. Yokoi, T. Arai, and T. Ohnishi, "An fmri study on the effects of electrical stimulation as biofeedback," in *Intelligent Robots and Systems, 2006 IEEE/RSJ International Conference on*, pp. 4336–4342, IEEE, 2006.

[56] A. H. Arieta, H. Yokoi, T. Arai, and W. Yu, "Study on the effects of electrical stimulation on the pattern recognition for an emg prosthetic application," in *Engineering in Medicine and Biology Society, 2005. IEEE-EMBS 2005. 27th Annual International Conference of the*, pp. 6919–6922, IEEE, 2006.

[57] R. E. Fan, M. O. Culjat, C.-H. King, M. L. Franco, R. Boryk, J. W. Bisley, E. Dutson, and W. S. Grundfest, "A haptic feedback system for lower-limb prostheses," *IEEE Transactions on Neural Systems and Rehabilitation Engineering*, vol. 16, no. 3, pp. 270–277, 2008.

[58] N. Gurari, K. Smith, M. Madhav, and A. M. Okamura, "Environment discrimination with vibration feedback to the foot, arm, and fingertip," in *Rehabilitation Robotics, 2009. ICORR 2009. IEEE International Conference on*, pp. 343–348, IEEE, 2009.

[59] A. Cheng, K. A. Nichols, H. M. Weeks, N. Gurari, and A. M. Okamura, "Conveying the configuration of a virtual human hand using vibrotactile feedback," in *Haptics Symposium (HAPTICS), 2012 IEEE*, pp. 155–162, IEEE, 2012.

[60] A. Tsukahara, R. Kawanishi, Y. Hasegawa, and Y. Sankai, "Sit-to-stand and stand-to-sit transfer support for complete paraplegic patients with robot suit hal," *Advanced robotics*, vol. 24, no. 11, pp. 1615–1638, 2010.

[61] Y. Hasegawa and K. Nakayama, "Finger-mounted walk controller of powered exoskeleton for paraplegic patient's walk," in *World Automation Congress (WAC), 2014*, pp. 400–405, IEEE, 2014.

[62] A. B. Zoss, H. Kazerooni, and A. Chu, "Biomechanical design of the berkeley lower extremity exoskeleton (bleex)," *IEEE/ASME Transactions On Mechatronics*, vol. 11, no. 2, pp. 128–138, 2006.

[63] K. Suzuki, G. Mito, H. Kawamoto, Y. Hasegawa, and Y. Sankai, "Intention-based walking support for paraplegia patients with robot suit hal," *Advanced Robotics*, vol. 21, no. 12, pp. 1441–1469, 2007.

[64] E. Strickland, "Good-bye, wheelchair," *IEEE Spectrum*, vol. 49, no. 1, 2012.

[65] A. Kilicarslan, S. Prasad, R. G. Grossman, and J. L. Contreras-Vidal, "High accuracy decoding of user intentions using eeg to control a lower-body exoskeleton," in *Engineering in medicine and biology society (EMBC), 2013 35th annual international conference of the IEEE*, pp. 5606–5609, IEEE, 2013.

[66] T. Kagawa and Y. Uno, "Gait pattern generation for a power-assist device of paraplegic gait," in *Robot and Human Interactive Communication, 2009. RO-MAN 2009. The 18th IEEE International Symposium on*, pp. 633–638, IEEE, 2009.

[67] K. A. Strausser and H. Kazerooni, "The development and testing of a human machine interface for a mobile medical exoskeleton," in *Intelligent Robots and Systems (IROS), 2011 IEEE/RSJ International Conference on*, pp. 4911–4916, IEEE, 2011.

[68] R. Steger, S. H. Kim, and H. Kazerooni, "Control scheme and networked control architecture for the berkeley lower extremity exoskeleton (bleex)," in *Robotics and Automation, 2006. ICRA 2006. Proceedings 2006 IEEE International Conference on*, pp. 3469–3476, IEEE, 2006.

[69] Y. H. Yin, Y. J. Fan, and L. D. Xu, "Emg and epp-integrated human–machine interface between the paralyzed and rehabilitation exoskeleton," *IEEE Transactions on Information Technology in Biomedicine*, vol. 16, no. 4, pp. 542–549, 2012.

[70] D. P. McMullen, G. Hotson, K. D. Katyal, B. A. Wester, M. S. Fifer, T. G. McGee, A. Harris, M. S. Johannes, R. J. Vogelstein, A. D. Ravitz, *et al.*, "Demonstration of a semi-autonomous hybrid brain–machine interface using human intracranial eeg, eye tracking, and computer vision to control a robotic upper limb prosthetic," *IEEE Transactions on Neural Systems and Rehabilitation Engineering*, vol. 22, no. 4, pp. 784–796, 2014.

[71] Y. Nam, B. Koo, A. Cichocki, and S. Choi, "Gom-face: Gkp, eog, and emg-based multimodal interface with application to humanoid robot control," *IEEE Transactions on Biomedical Engineering*, vol. 61, no. 2, pp. 453–462, 2014.

[72] J. Ma, Y. Zhang, A. Cichocki, and F. Matsuno, "A novel eog/eeg hybrid human–machine interface adopting eye movements and erps: Application to robot control," *IEEE Transactions on Biomedical Engineering*, vol. 62, no. 3, pp. 876–889, 2015.

[73] E. Hortal, D. Planelles, A. Costa, E. Iáñez, A. Úbeda, J. M. Azorín, and E. Fernández, "Svm-based brain–machine interface for controlling a robot arm through four mental tasks," *Neurocomputing*, vol. 151, pp. 116–121, 2015.

[74] A. Tsukahara, Y. Hasegawa, and Y. Sankai, "Gait support for complete spinal cord injury patient by synchronized leg-swing with hal," in *Intelligent Robots and Systems (IROS), 2011 IEEE/RSJ International Conference on*, pp. 1737–1742, IEEE, 2011.

[75] C.-Y. Shing, C.-P. Fung, T.-Y. Chuang, I.-W. Penn, and J.-L. Doong, "The study of auditory and haptic signals in a virtual reality-based hand rehabilitation system," *Robotica*, vol. 21, no. 2, pp. 211–218, 2003.

[76] K. A. Kaczmarek, J. G. Webster, P. Bach-y Rita, and W. J. Tompkins, "Electrotactile and vibrotactile displays for sensory substitution systems," *IEEE Transactions on Biomedical Engineering*, vol. 38, no. 1, pp. 1–16, 1991.

[77] Y. Hasegawa, M. Sasaki, and A. Tsukahara, "Pseudo-proprioceptive motion feedback by electric stimulation," in *Micro-NanoMechatronics and Human Science (MHS), 2012 International Symposium on*, pp. 409–414, IEEE, 2012.

[78] Y. Hasegawa and K. Ozawa, "Pseudo-somatosensory feedback about joint's angle using electrode array," in *System Integration (SII), 2014 IEEE/SICE International Symposium on*, pp. 644–649, IEEE, 2014.

[79] Y. Hasegawa and K. Nakayama, "Gait control of powered exoskeleton with finger-mounted walk controller for paraplegic patient," in *Micro-NanoMechatronics and Human Science (MHS), 2014 International Symposium on*, pp. 1–3, IEEE, 2014.

[80] Y. Hasegawa, K. Nakayama, K. Ozawa, and M. Li, "Electric stimulation feedback for gait control of walking robot," in *Intelligent Robots and Systems (IROS), 2015 IEEE/RSJ International Conference on*, pp. 14–19, IEEE, 2015.

[81] E. Hortal, D. Planelles, A. Costa, E. Iáñez, A. Úbeda, J. M. Azorín, and E. Fernández, "Svm-based brain–machine interface for controlling a robot arm through four mental tasks," *Neurocomputing*, vol. 151, pp. 116–121, 2015.

[82] A. Cheng, K. A. Nichols, H. M. Weeks, N. Gurari, and A. M. Okamura, "Conveying the configuration of a virtual human hand using vibrotactile feedback," in *Haptics Symposium (HAPTICS), 2012 IEEE*, pp. 155–162, IEEE, 2012.

[83] M. Li, Z. Yuan, X. Wang, and Y. Hasegawa, "Electric stimulation and cooperative control for paraplegic patient wearing an exoskeleton," *Robotics and Autonomous Systems*, vol. 98, pp. 204–212, 2017.

[84] S. R. Buss, "Introduction to inverse kinematics with jacobian transpose, pseudoinverse and damped least squares methods," *IEEE Journal of Robotics and Automation*, vol. 17, no. 1-19, p. 16, 2004.

[85] A. B. Zoss, H. Kazerooni, and A. Chu, "Biomechanical design of the berkeley lower extremity exoskeleton (bleex)," *IEEE/ASME Transactions On Mechatronics*, vol. 11, no. 2, pp. 128–138, 2006.

[86] C. J. Walsh, K. Endo, and H. Herr, "A quasi-passive leg exoskeleton for load-carrying augmentation," *International Journal of Humanoid Robotics*, vol. 4, no. 03, pp. 487–506, 2007.

[87] J. E. Pratt, B. T. Krupp, C. J. Morse, and S. H. Collins, "The roboknee: an exoskeleton for enhancing strength and endurance during walking," in *Robotics and Automation, 2004. Proceedings. ICRA'04. 2004 IEEE International Conference on*, vol. 3, pp. 2430–2435, IEEE, 2004.

[88] M. P. Ford, R. C. Wagenaar, and K. M. Newell, "Arm constraint and walking in healthy adults," *Gait & posture*, vol. 26, no. 1, pp. 135–141, 2007.

[89] T. Wannier, C. Bastiaanse, G. Colombo, and V. Dietz, "Arm to leg coordination in humans during walking, creeping and swimming activities," *Experimental brain research*, vol. 141, no. 3, pp. 375–379, 2001.

[90] J. E. Balter and E. P. Zehr, "Neural coupling between the arms and legs during rhythmic locomotor-like cycling movement," *Journal of neurophysiology*, vol. 97, no. 2, pp. 1809–1818, 2007.

[91] V. Dietz, K. Fouad, and C. Bastiaanse, "Neuronal coordination of arm and leg movements during human locomotion," *European Journal of Neuroscience*, vol. 14, no. 11, pp. 1906–1914, 2001.

[92] V. Dietz, "Quadrupedal coordination of bipedal gait: implications for movement disorders," *Journal of neurology*, vol. 258, no. 8, p. 1406, 2011.

[93] A. Daffertshofer, C. J. Lamoth, O. G. Meijer, and P. J. Beek, "Pca in studying coordination and variability: a tutorial," *Clinical biomechanics*, vol. 19, no. 4, pp. 415–428, 2004.

[94] E. Todorov and Z. Ghahramani, "Analysis of the synergies underlying complex hand manipulation," in *The 26th Annual International Conference of the IEEE Engineering in Medicine and Biology Society*, vol. 2, pp. 4637–4640, IEEE, 2004.

[95] V. Crocher, A. Sahbani, J. Robertson, A. Roby-Brami, and G. Morel, "Constraining upper limb synergies of hemiparetic patients using a robotic exoskeleton in the perspective of neuro-rehabilitation," *IEEE Transactions on Neural Systems and Rehabilitation Engineering*, vol. 20, no. 3, pp. 247–257, 2012.

[96] V. Crocher, N. Jarrassé, A. Sahbani, A. Roby-Brami, and G. Morel, "Changing human upper-limb synergies with an exoskeleton using viscous fields," in *2011 IEEE International Conference on Robotics and Automation*, pp. 4657–4663, IEEE, 2011.

[97] K. Liu and C. Xiong, "A novel 10-dof exoskeleton rehabilitation robot based on the postural synergies of upper extremity movements," in *International Conference on Intelligent Robotics and Applications*, pp. 363–372, Springer, 2013.

[98] M. Hassan, H. Kadone, K. Suzuki, and Y. Sankai, "Exoskeleton robot control based on cane and body joint synergies," in *Proceeding of IEEE International Conference on Intelligent Robots and Systems*, pp. 1609–1614, IEEE, 2012.

[99] M. Hassan, H. Kadone, K. Suzuki, and Y. Sankai, "Wearable gait measurement system with an instrumented cane for exoskeleton control," *Sensors*, vol. 14, no. 1, pp. 1705–1722, 2014.

[100] M. Hassan, H. Kadone, T. Ueno, K. Suzuki, and Y. Sankai, "Feasibility study of wearable robot control based on upper and lower limbs synergies," in *Proceeding of International Symposium on Micro-NanoMechatronics and Human Science*, pp. 1–6, IEEE, 2015.

[101] H. Vallery, E. H. Van Asseldonk, M. Buss, and H. Van Der Kooij, "Reference trajectory generation for rehabilitation robots: complementary limb motion estimation," *IEEE transactions on neural systems and rehabilitation engineering*, vol. 17, no. 1, pp. 23–30, 2008.

[102] H. Vallery and M. Buss, "Complementary limb motion estimation based on interjoint coordination using principal components analysis," in *Proceeding of IEEE Conference on Computer Aided Control System Design, Proceeding of IEEE International Conference on Control Applications, Proceeding of IEEE International Symposium on Intelligent Control*, pp. 933–938, IEEE, 2006.

[103] P. Sardain and G. Bessonnet, "Forces acting on a biped robot. center of pressure-zero moment point," *IEEE Transactions on Systems, Man, and Cybernetics-Part A: Systems and Humans*, vol. 34, no. 5, pp. 630–637, 2004.

[104] S. Kajita, F. Kanehiro, K. Kaneko, K. Fujiwara, K. Harada, K. Yokoi, and Hirukawa, "Biped walking pattern generation by using preview control of zero-moment point,"

[105] J. H. Park and K. D. Kim, "Biped robot walking using gravity-compensated inverted pendulum mode and computed torque control," in *Proceedings of IEEE International Conference on Robotics and Automation*, vol. 4, pp. 3528–3533, IEEE, 1998.

[106] T. Sugihara, Y. Nakamura, and H. Inoue, "Real-time humanoid motion generation through zmp manipulation based on inverted pendulum control," in *Proceedings of IEEE International Conference on Robotics and Automation*, vol. 2, pp. 1404–1409, IEEE, 2002.

List of Publications

(1) Journal

[1] Mengze Li, Zhaofan Yuan, Xufeng Wang, and Yasuhisa Hasegawa. "Electric stimulation and cooperative control for paraplegic patient wearing an exoskeleton." Robotics and Autonomous Systems 98 (2017): 204-212.

[2] Mengze Li, Zhaofan Yuan, Tadayoshi Aoyama, and Yasuhisa Hasegawa. "Precise Foot Positioning of Walking Robot for Paraplegic Patient Wearing Exoskeleton by Using Electrical Stimulation Feedback." Journal of Mechanisms and Robotics 10, no. 4 (2018).

[3] Mengze Li, Tadayoshi Aoyama, and Yasuhisa Hasegawa. "Gait Modification for Improving Walking Stability of Exoskeleton Assisted Paraplegic Patient." ROBOMECH Journal 7 (2020): 1-12.

(2) International Conference

[1] Yasuhisa Hasegawa, Keisuke Nakayama, Kohei Ozawa, and Mengze Li. "Electric stimulation feedback for gait control of walking robot." 2015 IEEE/RSJ International Conference on Intelligent Robots and Systems (IROS), pp. 14-19. IEEE, 2015.

[2]Xufeng Wang, Mengze Li, and Yasuhisa Hasegawa. "Electric stimulation feedback system for lower limb exoskeleton Evaluation of reaction time to abnormal situation of lower-limb." 2016 International Symposium on Micro-NanoMechatronics and Human Science (MHS), pp. 1-3. IEEE, 2016.

[3] Mengze Li, Zhaofan Yuan, Tadayoshi Aoyama, and Yasuhisa Hasegawa. "Electrical stimulation feedback for gait control of walking simulator." 2017 IEEE-RAS 17th International Conference on Humanoid Robotics (Humanoids), pp. 797-802. IEEE, 2017.

[4] Mengze Li, Tadayoshi Aoyama, and Yasuhisa Hasegawa. "Electrical stimulation for compensation of impaired lower limb sensation." 2017 International Symposium on Micro-NanoMechatronics and Human Science (MHS), pp. 1-3. IEEE, 2017.

[5] Mengze Li, Xufeng Wang, Tadayoshi Aoyama, and Yasuhisa Hasegawa. "Electric Stimulation based Weight Discrimination for Paraplegic Wearing Exoskeleton." 2018 IEEE International Conference on Intelligence and Safety for Robotics (ISR), pp. 261-266. IEEE, 2018.

(3) Domestic Conference

[1] Kun Liu, Yasuhisa Hasegawa, Segura Meraz Noel, Mengze Li. Development of MRI Compatible Tapping Assistive Robot. The Robotics and Mechatronics Conference (ROBOMECH) 2017.

[2] Zhaofan Yuan, Mengze Li and Yasuhisa Hasegawa. Electric Stimulation and Gait Control for Assisting Paraplegic Walk. International Sessions, the 34th Annual Conference of the Robotics Society of Japan (RSJ) 2017.

[3] Mengze Li, Tadayoshi Aoyama and Yasuhisa Hasegawa. Gait Generation Based on Human Walking Synergy for Paraplegic Patient with Canes. International Sessions, the 36th Annual Conference of the Robotics Society of Japan (RSJ) 2019.